

A NETWORK APPROACH FOR THERMO-ELECTRICAL MODELLING: FROM IC INTERCONNECTS TO TEXTILE COMPOSITES

by

CHIUN-SHEN LIAO

B.Sc., Chung Cheng Institute of Technology, Taiwan, 1990
M.Sc., Lehigh University, PA, United States, 1996

A THESIS SUBMITTED IN PARTIAL FULFILLMENT OF
THE REQUIREMENTS FOR THE DEGREE OF

MASTER OF APPLIED SCIENCE

in

The College of Graduate Studies
(Electrical and Computer Engineering)

THE UNIVERSITY OF BRITISH COLUMBIA
(OKANAGAN)

August 2010

© Chiun-Shen Liao, 2010

Abstract

Simulations of the temperature distribution in regular IC interconnect networks and textile composites are achieved by means of an analytical-symbolic approach. Analytical heating solutions along each interconnect can provide accurate solutions with far fewer nodes than numerical solutions. To simulate the case of textile composite, the textile composite is modelled by a network of interconnects. The necessary input information is contained in netlist files, similar to the SPICE (Simulation Program with Integrated Circuit Emphasis) input format. Analytical solutions to the heat equation along each interconnect can provide accuracy and require the minimum number of symbolic network nodes. The LU decomposition of the symbolic network scales as the cube of the number of nodes. Multiple evaluations, including iterating temperature-dependent thermal conductivity to achieve a self-consistent solution, scale linearly with the number of nodes and hardly affect the total solution time. Memory consumption, CPU time, and solutions of the new network calculation method compare favorably to a finite element analysis using ABAQUS.

Table of Contents

| | |
|---|------|
| Abstract | ii |
| Table of Contents | iii |
| List of Tables | vi |
| List of Figures | vii |
| List of Acronyms | xi |
| Acknowledgments | xiii |
| Dedication | xiv |
| 1 Introduction | 1 |
| 1.1 Background and Motivation | 1 |
| 1.2 Literature Review | 4 |
| 1.3 Summary of Research Goals | 9 |
| 1.4 Thesis Organization | 10 |
| 2 Network-Based Simulation | 11 |
| 2.1 Basic Physical Model | 11 |
| 2.1.1 Thermal Model | 12 |
| 2.1.2 Electrical Analogy for Thermal Conduction | 14 |
| 2.2 Interconnect Model | 16 |

| | | |
|----------|--|-----------|
| 2.2.1 | Textile Fibre Model | 19 |
| 2.3 | Network-Based Simulation Concept | 21 |
| 2.4 | Summary | 22 |
| 3 | Therminator3D | 23 |
| 3.1 | The Analytical Solution of Networked Elements | 23 |
| 3.1.1 | Resistor-Capacitor Network | 23 |
| 3.1.2 | The Format of Input Files | 25 |
| 3.2 | Symbolic Network Analysis Solution | 28 |
| 3.3 | Iterative and Multiphysics Evaluation | 32 |
| 3.3.1 | On Convergence of Non-linear Problems in Therminator3D | 35 |
| 3.4 | Summary | 40 |
| 4 | Finite Element Analysis | 41 |
| 4.1 | Basic Physical Model of Finite Element Analysis | 41 |
| 4.1.1 | Mesh Method | 42 |
| 4.2 | Simulation with ABAQUS | 43 |
| 4.3 | Summary | 47 |
| 5 | Applications and Comparisons | 48 |
| 5.1 | Basic Layout Examples: Verification of Therminator3D | 48 |
| 5.2 | IC Interconnects Network | 52 |
| 5.3 | Non-Crimp Fabric Network | 58 |
| 5.4 | Woven Fabric Composite Network | 65 |
| 5.5 | Large-Scale Network Simulation | 71 |
| 5.6 | Evaluation of Effective Thermal Conductivity | 80 |
| 5.7 | Summary | 81 |

Table of Contents

| | | |
|-----------------------|---|-----|
| 6 | Conclusions | 83 |
| 6.1 | Summary of Contributions | 83 |
| 6.2 | Future Work | 84 |
| | Bibliography | 86 |
| Appendices | | |
| A | The Input Parameters of Weave Program | 96 |
| B | Modified Netlist and Coupling Data for Simulations | 99 |
| C | Using DOE in the Evaluation of Effective Thermal Conductivity of the Fabric with T3D | 102 |

List of Tables

| | | |
|-----|---|-----|
| 3.1 | Therminator3D input file format and typical values. | 27 |
| 5.1 | Material properties used in simulations adjusted by narrow-line effects. | 52 |
| 5.2 | Material properties used in simulations. | 52 |
| 5.3 | Comparison of CPU time and memory required by Therminator3D and ABAQUS | 57 |
| 5.4 | Comparison of Therminator3D and ABAQUS CPU times for the heat analysis of a 4x4 metal non-crimp structure. | 65 |
| 5.5 | Comparison of CPU time and memory required by Therminator3D and ABAQUS on woven fabric materials. | 70 |
| 5.6 | Comparison of CPU time required by Therminator3D and ABAQUS on Large Scale network. | 75 |
| C.1 | Study factors and their levels. | 104 |
| C.2 | ANOVA results and effect estimates from minitab. | 104 |

List of Figures

| | | |
|------|--|----|
| 1.1 | An example of temperature-aware ASIC design flow. | 5 |
| 2.1 | Heat Transfer along a bar | 13 |
| 2.2 | Diagrams of thermal resistance. (a) Series thermal resistance (b) Parallel thermal resistance | 15 |
| 2.3 | Resistor segment of interconnects | 17 |
| 2.4 | Heat conservation model and capacitances | 20 |
| 3.1 | A net-based interconnect model with vias shown with an ‘X’. | 24 |
| 3.2 | A two-layer interconnect grid with vias showing approximate segmentation to connected resistors. | 24 |
| 3.3 | EMR methodology diagrams. | 26 |
| 3.4 | Typical lateral thermal conductance model in IC Interconnects. | 28 |
| 3.5 | Lateral thermal conductance for woven case (shown by the capacitor symbols) . | 29 |
| 3.6 | The distribution of problem matrix A (the 20 columns and 20 rows case with via between each row and column). | 31 |
| 3.7 | The flowchart of Therminator3D thermo-electrical simulation | 34 |
| 3.8 | Fixed point iteration for a general function $g(x)$ for the four cases of interest. . | 36 |
| 3.9 | Sample circuit 1 for Therminator3D convergence verification | 37 |
| 3.10 | Sample circuit 2 for Therminator3D convergence verification with infinitely-long resistors and substrate. | 39 |

List of Figures

| | | |
|------|--|----|
| 4.1 | Typical models of Finite Element Method (a) stitched unit cell of a NCF, (b) a closed-form RVE of the same fabric. | 43 |
| 4.2 | Typical finite element shapes and mesh points in one through three dimensions. | 44 |
| 4.3 | Comparison between the finite element and experimental results in a coupled thermo-electrical problem | 47 |
| 5.1 | The layout of one wire simulation. | 50 |
| 5.2 | The temperature distribution of one wire simulation. | 50 |
| 5.3 | The layout of three-wire simulation | 51 |
| 5.4 | The temperature distribution of three-wire simulation. | 51 |
| 5.5 | Four-by-four, two-layer grid with vias showing approximate segmentation into connected resistors. | 54 |
| 5.6 | Boundary conditions achieved by equivalent circuit source and resistors. | 55 |
| 5.7 | Temperature-dependent thermal and electrical conductivities of copper. | 55 |
| 5.8 | Interconnect temperature distribution for the network shown in Figure 5.5 | 56 |
| 5.9 | Comparison of column 3 temperature distribution in Figure 5.5, calculated by Therminator3D and ABAQUS. | 58 |
| 5.10 | Interconnect temperature distribution for the network shown in Figure 5.5 with vias removed | 59 |
| 5.11 | Comparison of column 3 temperatures shown in Figure 5.5 with vias removed . . | 60 |
| 5.12 | Comparison of column 4 temperature distribution in Figure 5.5 with vias removed, calculated by Therminator3D and ABAQUS. | 60 |
| 5.13 | An NCF represented by a two-layer interconnect grid with vias showing approximate segmentation into connected resistors. | 62 |
| 5.14 | Interconnect temperature distribution for the network shown in Figure 5.13 . . . | 63 |
| 5.15 | The row 3 temperature trajectory for the network in Figure 5.13 | 64 |
| 5.16 | A two-layer interconnect grid layout with vias and Joule heat generated on interconnect 7. | 66 |

List of Figures

| | | |
|------|--|-----|
| 5.17 | T3D implementation of NCF layout in Figure 5.16 | 67 |
| 5.18 | ABAQUS implementation of NCF layout in Figure 5.16 | 67 |
| 5.19 | The comparison of all 8 wires between ABAQUS and Therminator3D with vias and heated wire 7 | 68 |
| 5.20 | A woven fabric composites represented by a two-layer interconnect grid with vias showing approximate segmentation into connected resistors. | 70 |
| 5.21 | Yarn temperature distribution for the network shown in Figure 5.20, computed by Therminator3D. | 71 |
| 5.22 | Yarn temperature distribution for the network shown in Figure 5.20, computed by ABAQUS. | 72 |
| 5.23 | The comparison of all 8 yarns between ABAQUS and Therminator3D on wo- ven case without vias and with heated yarn 5 | 73 |
| 5.24 | The comparison of all 8 yarns between ABAQUS and Therminator3D on wo- ven case without vias and with heated yarn 7. | 74 |
| 5.25 | The layout of a 20 (columns) by 20 (rows) large scale network with vias (X) with a heated wire (red line). | 76 |
| 5.26 | The layout of a 20 (columns) by 20 (rows) large scale network without vias and with a heated wire. | 77 |
| 5.27 | The simulation results of Therminator3D for a 20x20 net. (a) Layout as Figure 5.25. (b) Layout as Figure 5.26. | 78 |
| 5.28 | The simulation results of ABAQUS for a 20x20 net. (a) Layout as Figure 5.25. (b) Layout as Figure 5.26. | 79 |
| 5.29 | The multiple boundary condition simulation results by Therminator3D for a 18x18 net. | 80 |
| 5.30 | Cause-effect diagram used in the DOE study. | 81 |
| C.1 | The layout used in the DOE study. | 103 |
| C.2 | Main effects plot for K_{eff} | 105 |

List of Figures

C.3 Interaction effects plot for K_{eff} 106

List of Acronyms

| Acronyms | Definitions |
|-----------------|---|
| 3D | Three-Dimensional |
| 3DIC | Three-dimensional Integrated Circuit |
| ANOVA | Analysis of Variance |
| ASIC | Application-Specific Integrated Circuit |
| BC | Boundary Condition |
| CIR | Channel Impulse Response |
| CAD | Computer-Aided Design |
| DC | Direct Current |
| DOE | Design of Experiment |
| EMR | Electromigration Reliability |
| FE | Finite-Element |
| FEA | Finite-Element Analysis |
| FEM | Finite Element Method |
| IC | Integrated Circuit |
| ITRS | International Technology Roadmap for Semiconductors |
| MTTF | Mean Time to Failure |
| NCF | Non-Crimp Fabric |
| PCB | Printed Circuit Boards |
| RC | Resistor-Capacitance |
| RVE | Representative Volume Element |

List of Acronyms

| | |
|-------|---|
| CFD | Computational Fluid Dynamics |
| SPICE | Simulation Program with Integrated Circuit Emphasis |
| TCAD | Technology CAD |
| T3D | Therminator3D |
| VLSI | Very-Large-Scale Integration |
| ULSI | Ultra-Large-Scale Integration |

Acknowledgments

I am deeply grateful to many individuals and organizations. Without their support, this project could not be completed.

First and the most, I would like to thank my supervisors, Dr. Andrew H. Labun and Dr. Abbas S. Milani, for their understanding, encouragement, support, enthusiasm, and guidance. Their helpful suggestions and patient conduction have gone through all my works in the past two years and made this thesis possible. I will continue to be influenced by their rigorous scholarship, clarity in thinking, and professional integrity.

I would also like to express my thanks to Dr. Deborah Roberts and the following advisory committee members: Dr. Peter Hallschmid, and Dr. Ahmad Rteil. Thanks also go to Dr. Edmond Cretu for his willingness to serve as my external examiner. I highly appreciate their valuable time and constructive comments on my thesis.

I would like to thank my dear peers Nick Kuan-Hsiang Huang, Xian Jin, Xuegui Song, Ning Wang, and Yeyuan Xiao for all of their assistance, insight, encouragement and support during my two-year studied at the University of British Columbia Okanagan.

Finally, special thanks go to my mother and my family for their patience, understanding and support over all these years. In particular, I wish to acknowledge my dear wife, Wei-Wei Yu, for giving invaluable and heartfelt support. Without their constant support and encouragement, all my achievements would not be possible.

Dedication

*This thesis is dedicated to my family . . .
for all of their love and endless support.*

Chapter 1

Introduction

In this chapter, background and thesis organization will be presented. The first part of this chapter introduces the background and motivation. Related literature papers are reviewed in the second part. The third part illustrates the research goals of this study. The scope and organization of the thesis are described in the final section of the chapter.

1.1 Background and Motivation

This thesis applies a new fast network-based simulation methodology to solve coupled thermo-electrical problems. The solution algorithm was originally developed to calculate the temperature distributions of interconnects due to Joule heating in microchips. This algorithm demonstrates a very fast calculation on large scale layouts. To extend the benefit of this algorithm, this thesis proposes to use the same algorithm to textile composite materials whose geometry is also network-based. The following paragraphs will illustrate the background and motivation of this research starting from interconnects of microchips to textile composite materials. Also, each chapter in this thesis is roughly divided into two applications: interconnects and textile composite materials.

The International Technology Roadmap for Semiconductors (ITRS) illustrates that modeling and control of thermal reliability mechanisms in circuit interconnects is one of the difficult challenges in the semiconductor industry for the next decade [1]. The 2007 International Technology Roadmap calls for new computer-aided design (CAD) tools that would be used as inputs to predict interconnect resistance as it increases due to temperature variation based

on wire length/current, and “to calculate local operating temperature, [including] the effects of Joule heating in the circuit and elsewhere” [[1] p. 39]. Since the interconnects are the major components to connect with other components in a circuit, accurate temperature estimation of interconnect is very important in CAD verification of circuit behaviour and reliability.

Previous studies on interconnects have focused on the electromigration reliability (EMR) verification fields with specific technologies. Electromigration verification is a prediction and functional evaluation on integrated circuit (IC). In the worst case, the electromigration effect could cause the connection to eventually disconnect and result in failure of IC. In the real world, ICs rarely fail due to electromigration since all designs and simulations are made using worst-case temperature assumptions. Those temperature assumptions prevent and reduce the possibilities of failure due to electromigration effects. This kind of design is called “electromigration-aware design”. To evaluate the electromigration reliability of a wire, the following Black equation [2] is used to estimate the “Mean Time to Failure (MTTF)” of wires,

$$MTTF = A(J^{-n})e^{E_a/kT}, \quad (1.1)$$

where A is a constant based on the cross-sectional area of the interconnect, J is the current density (amperes per square meter), n is a scaling factor, E_a is the activation energy in eV, k is the Boltzmann’s constant ($\text{eV } K^{-1}$), and T is the absolute temperature in K.

It states that current density and temperature are the main factors that affect electromigration. The temperature is changing during operation of systems. It is a challenge to precisely predict the temperature distributions and effects of MTTF on electromigration. Most electromigration verification studies on the reliability of a specific interconnect technology (e.g., [3, 4]) are based on uniform temperature experiments. The temperatures of interconnects are of concern because of the low-thermal-conductivity dielectric, high-resistivity conductor, and high interconnects stacks. All these factors tend to increase the temperatures of interconnects. Electromigration reliability verification of high-performance integrated circuits requires a detailed interconnect temperature simulation capability to accurately identify problematic interconnect

layout configurations and operating conditions. Those new CAD tools developed on the 2007 ITRS Roadmap could precisely predict the current behaviours and EMR reliability with the temperature increased by the Joule heating. There is no need for worst case assumptions on the temperature after the components of interconnect temperature simulations have been added properly. This thesis proposes a rapid symbolic, analytical, and network based approach for full-chip interconnects reliability verification that calculates the detailed temperature distribution along each interconnect. This very fast simulation tool is called “Therminator3D” (T3D).

Most of the layouts of textile composite materials are similar to the layouts of interconnects in integrated circuits, except for those angular woven materials. I could apply the fast speed simulation and network-based idea of “Therminator3D” into the simulations of textile composite materials starting from temperature estimations. Therminator3D has the potential to extend to different mechanical properties.

For textile material applications, composite materials are used widely in a broad range of industries to improve design properties such as lower density with higher stiffness and strength, lower effective thermal conductivities to block the heat, higher effective thermal conductivities to detect the real temperature instantly, etc. Composite materials can reach the desired mechanical properties by changing the reinforcement layouts, reducing the need for extra materials and fabrications.

In textile materials which can be knitted, woven or braided, the fibre yarns and matrix materials are consolidated during manufacturing. A number of composite components in the aerospace, automotive, marine and construction industries are built of woven textile preforms. They can give excellent mechanical properties with very low weights, but their complex weaving fabrication processes occasionally make them expensive for particular composite manufacturers. As an alternative, non-crimp fabrics (NCFs) have proven to provide fairly good mechanical properties while maintaining low weight and providing cost effective solutions through their simplified fabrication processes. NCF composites are fabricated from preforms with multiple layers of straight fibre bundles that can be oriented in different directions and

stitched together by a (warp) knitting procedure. The previous study by Dransfield et al. (1998) showed that out-of-plane fracture toughness and damage tolerance properties of these materials are also improved through the stitching process [5].

The layout of NCF materials is similar to that of printed circuit boards (PCB). The architecture is layer by layer and wire-crossed fabrication. For woven materials, the layout is not identical but similar to printed circuit boards. The woven structure can be interpreted into the same layouts of interconnects with suitable twisted (angular) coupling values. The simulation of full-layout textile material properties in commercial CAD/FEM tools including the layout drawing, CPU time, and memories consumes several resources. The proposed method here is to employ “Therminator3D” for textile materials to reach more rapid multi-physics simulations with low CPU time and memory.

1.2 Literature Review

Consideration of a complete physical interconnect model includes the configuration, such as the set of layouts and materials, their microstructure and interfaces (e.g. Cu, Ta, and SiNx), and the dimensions of interconnects; and operating conditions, such as local temperature, driving currents, heat and electrical flux, and stress, etc. This complexity and the specific characteristics of individual process technologies require detailed Technology CAD (TCAD), including Finite Element Analysis (FEA), to predict reliability for specific interconnect configurations [6]. For circuit design, however, it is necessary to have a CAD solution, and it can be analyzed based on a network representation extracted from layout and process technology information. There are several models to predict the temperature of interconnects and apply the result to System-on-Chip in order to obtain more precise simulation results.

Huang et al. (2004) proposed a “compact thermal modeling for temperature-aware design” model [7]. They used the idea of “temperature-aware design” with a model reduction concept applied on every step of the application-specific integrated circuit (ASIC) design flow, as shown

in Figure 1.1. This design reveals the importance of temperature estimates on every stage of CAD design. Without temperature evaluation on each stage, the function of ASIC will not perform as designed due to dubious temperatures. For thermal estimation of interconnects, they used a compact thermal model to estimate the temperature of each node in the RC circuit that corresponds to a block. Then they treated the heat dissipation of each block as a current source, “hotspot”, connected to the corresponding node. This model shows good benefits for a wide range of applications on the temperature simulation and model reduction evaluations.

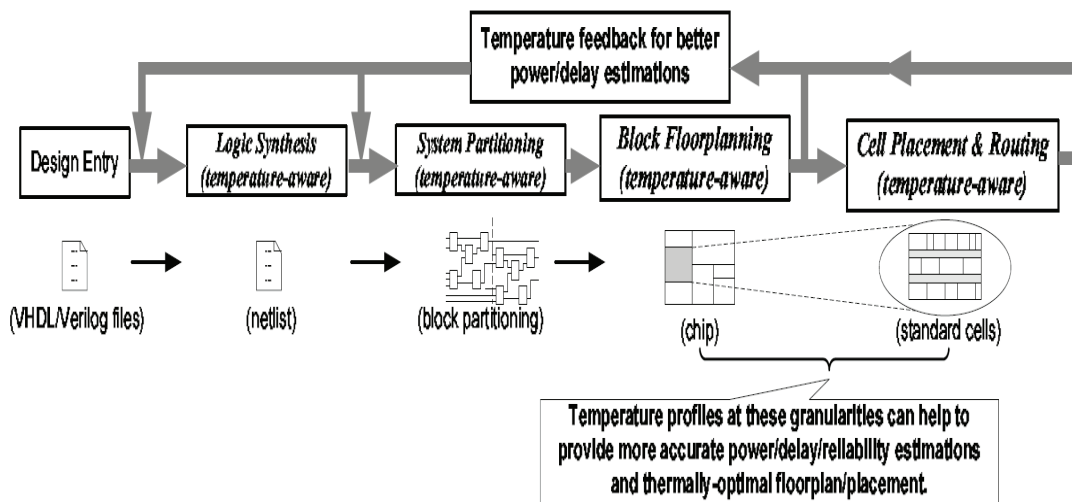


Figure 1.1: An example of temperature-aware ASIC design flow (Cited from [7]).

Franzon et al. (2008) presented a CAD tool for a three-dimensional IC (3DIC) [8]. They developed a thermal extraction and modeling flow which provide sufficient solutions for 3D IC design. The thermal model included a factor for the effect of local metallization, that can modify the thermal conductivity and anisotropic thermal conductivity. They also used model reduction to determine the interest ports of their model. After modeling the layout, they extracted the thermal information of the layout, then exported the extracted data to third-party thermal analysis software such as Pro-ENGINEER Mechanical. The third-party thermal analysis software performs the steady state thermal analysis. Their concepts of model reduction and layout extraction are similar to the ones used in this study and very efficient for performing the

thermal analysis. However, they did not develop an integrated simulation program to avoid the migration inconsistency between extraction softwares, circuit analysis software and thermal analysis software and, thus, to attain a faster and more practical simulation tool.

Alam et al. (2003) proposed that operating conditions may be determined by rapid circuit simulation and that a reliable prediction based on prior and detailed TCAD analysis can then be made by combining configuration and operating information using a simpler, parameterized model [9–11]. They used their SySRel, a CAD tool, for interconnect tree-based reliability assessment and thermal-aware cell-based extraction. However, they also use third-party thermal analysis software - ANSYS, a Finite Element Analysis solver, to verify and simulate the three-dimensional full-chip steady state and transient thermal behaviours. It could have some data inconsistency as the previous CAD tool.

Walkey et al. (2004) used controlled sources to simulate a compact, netlist-based representation of the thermal coupling problem [12]. In these two technologies of controlled source, sub-circuits separated self-heating and coupling effects or terms from the original circuits, to avoid a complex systems solution.

There are several studies that used netlist-based methods to extract thermal and electrical netlists and then performed thermo-electrical temperature simulation, including self-heating [13, 14]. Székely et al. (1997) used a relaxation method with coupled thermal and electrical solvers [15]. They extracted a thermal and electrical netlists based on layout information of the circuit. Once the electrical and thermal netlists were extracted, their self-consistent electro-thermal simulation was executed. This concept of coupled thermal and electrical simulation is similar to the implementation of Therminator3D. However, their simulation required longer run time and computing resources, and was economically expensive since they used simulator for integrated semiconductor structures by simultaneous iteration (SISSSI) under Cadence DFVII. Most small- and medium-size companies could not afford to use this system.

Joule heating is the heat generated by current in IC circuits. It could cause the failure of circuits without treating. Shen (1999) studied the analysis of Joule heating in multilevel

interconnects with two dimensional six-level interconnect stack. He did not mention the simulation method. However, he pointed out the interconnect of Joule heating became a reliability problem [16].

This research applies a new network approach, Terminator3D, to interconnect temperature estimation [17]. This research compares the relative accuracy, speed, and memory requirements of T3D to the ABAQUS FEA software, and demonstrates the feasibility of this CAD method for thermal and reliability analysis of large circuits. I also extend the concept of interconnect simulation to the thermal properties of textile composites materials. In this thesis, I only apply this algorithm to fully coupled thermo-electrical simulations and the future goal is to initiate other applications such as estimating mechanical properties using the same algorithm.

There are numerous works that are dedicated to mechanical, thermal and other physical properties of woven and non-woven fabrics. Bibo, Hogg and Kemp (1997) studied the elastic properties of several non-crimp fabric materials under tension and compression [18]. They compared the elastic properties of four kinds of uni-directional composite materials and found the NCF materials could provide competitive advantages. Drapier and Wisnom (1999) investigated the interlaminar shear behaviour of non-crimp-fabric-based composites [19]. Tessitore and Riccio (2006) performed Finite Element Method (FEM) modelling for biaxial extension of non-crimp fabric composite materials [20]. Hind, Robitaille and Raizenne (2006) conducted numerical studies on the effective thermal conductivity of a plain weave [21]. Nordlund et al. (2004) [22] and Lundstrom (2006) [23] have performed both numerical and experiential studies on the permeability of NCFs. Ning and Chou (1995), using a closed-form representation of the transverse thermal conductivity, derived a thermal resistance network [24]; Xu and Wirtz (2002), employing a simple-to-fabricate woven mesh, described the in-plane effective thermal conductivity of two-dimensional bonded-laminate plain-weave screen laminates [25]. Peng, Lu and Balendra (2004) studied the FE simulation of the blanking of electrically heated engineering materials [26]. They also used thermo-electrical simulation with FEA implementation

scheme.

Tiwari, Basu and Biswas (2009) employed a new simulation of thermal and electric field evolution during spark plasma sintering [27]. They conducted a different thermal conductivity powder compact on the die and punch surface of spark plasma sintering by a fully coupled thermo-electrical finite element analysis using ABAQUS and MATLAB. Their simulation results from ABAQUS revealed that maximum surface temperature is attained at the punch region. It indicates that a good finite element analysis could help users to find the critical points.

Ishikawa and Chou (1982) studied stiffness and strength behaviour of woven fabric composites [28]. Peng and Cao (2005) studied a continuum mechanics-based non-orthogonal constitutive model for woven composite fabrics [29]. Li et al. (2007) proposed a finite element model of woven fabric composite PCB to predict the bending behaviours of PCB [30]. They built four shell-element layers in ABAQUS. Then they used the stiffness factors, such as Young's modulus, Poisson's ratios, and shear modulus into non-linear equation systems and performed the numerical simulation for a three-point bending test. They compared and verified the results of experiments with the results of ABAQUS simulation. They concluded that the high fibre bundles in the filling direction of woven fibres could enhance the stiffness of the multi-layer PCBs .

The majority of the numerical studies on the mechanical and/or thermal analysis of fabrics have been based on the meso-level FEA analysis of unit cells representing repetitive (network) patterns in the fabrics. In practice, however, fabric unit cells are not perfectly repetitive, owing to uncertainties during fabric fabrication processes and/or unsymmetrical loading conditions for a given problem. They can require performing analyses on larger representative volumes. As the size of the problem scales, the solution complexity and the simulation run time can pose a problem. In addition, the selection of the position of a unit cell and the associated boundary conditions can become highly important. (Therminator3D is capable of simulating temperature distributions of an entire thermal network rapidly and accurately, without relying on the simplified unit cell descriptions.) Therminator3D applies network simulation concepts

with technological parameters extracted from CAD layout descriptions to the entire network (similar to FE models). A detailed description of the method in its original format for thermo-electrical analysis is presented in Chapter 3.

1.3 Summary of Research Goals

In this work, I propose not only to perform IC interconnects temperature estimation, but also to treat thermal problems of NCFs and woven materials using the same concept of net-based calculations by Therminator3D which was originally developed for IC interconnect systems. An auxiliary program is used to create netlist files to describe the thermal (resistor) network properties of biaxial NCFs and woven fabrics, including the thermal conductance of fabric segments. It will also create additional, virtual segments around the edges of the fabric to impose appropriate boundary conditions.

The eventual benefit of my study is to use the same modified interconnect net-based method to rapidly estimate the temperature distribution on big complicated IC interconnects, as well as the textile materials including NCF and woven types. Another major benefit of the method will be that it relies on a symbolic, semi-analytical, and net-based approach that can reduce the computational time and enhance the accuracy of the results at full resolution. Comparative studies with a commercial finite element software (ABAQUS) will be conducted.

My contributions of this study are:

1. Simulative results of Therminator3D are comparative to those of ABAQUS.
2. Application of textile materials.
3. Description of additional heat conduction behaviour, G_{twist}^{lat} , for woven materials.
4. Demonstration of Large-scale network simulations using Therminator3D.
5. Three-dimensional model could be easily represented by one-dimensional model with corresponded lateral thermal conductance.

1.4 Thesis Organization

This thesis consists of six chapters. Chapter 2 starts from the thermo-electrical modelling theory with a basic physical model and introduces the network based simulation. In Chapter 3, a new network calculation method “Therminator3D” is presented with detailed algorithms and solvers. Chapter 4 discusses the finite element analysis and describes the calculation of thermo-electrical simulations. Chapter 5 presents applications and comparisons on IC interconnects and textile composites in Manhattan layout. Computational cost and accuracy are compared to FE approach in the last section of this chapter. Chapter 6 concludes the thesis and lists my main contributions and results. In addition, some future work is proposed for further applications of the method to other mechanical properties.

Chapter 2

Network-Based Simulation

In this chapter, the fundamental concept of network-based simulation is presented. The first part of this chapter emphasizes the basic physical model and describes the supported theorems. The second part of this chapter introduces the interconnect model, and textile fabric model in interconnect form. The detailed network-Based Simulation is introduced in the third part of the chapter. A summary is given in the last section of the chapter.

2.1 Basic Physical Model

Operating temperature is an important issue in both IC interconnects and textile material components. One of the greatest challenges of the temperature calculation is the quick and full-scale simulation.

In ICs, the temperature calculation is involved in all levels. The temperature is varied from the interaction of Joule heating, thermal conduction, and the coupling of thermal and electrical effects. The purpose of temperature prediction for integrated circuits is to find the operating temperature of a whole system, perform the simulation closest to real situation, and prohibit the failure of the system. In a circuit, embedded thermal and electrical conductive interconnects are not only to provide low power consumption but also to conduct the heat out to the environment. A good layout of interconnects will maintain the temperature close to the designated operating temperature in order to keep the system functioning normally.

For textile materials, the same issues are expressed, but the applications are not limited to lower temperature under critical failure temperature. There are several different purposes

using textile materials compared to IC interconnects. For example, with so called “electrical textile materials” in medical applications, the embedded wires could transfer accurate real-time temperature data to the control unit and /or keep the body warm in a critical circumstance by changing the thermal conductivity. For earth friendly design, it could keep the temperature of a living space within comfortable level without the use of air-conditioning by blocking loss of heat by designing with low-thermal-conductivity matrix materials.

In this thesis, I focus on the electro-thermal application only. Thus, the basic physical models in my application include thermal conduction, Joule self-heating, thermal resistors, and the coupling of electrical and thermal effects as discussed below.

2.1.1 Thermal Model

Heat transfer processes are classified into three types: heat conduction, heat convection, and heat radiation. Heat convection is a heat transfer problem due to a flowing fluid or gas. Since this research is focused on the IC interconnect and textile materials below their melting points, I do not include the effect of heat convection. Heat radiation is the emission of energy through an external space, material or source. In this research, heat radiation is not directly considered, however it can be conveniently modelled as an arbitrary input (boundary condition) flux. Heat conduction is the interaction of energy within the materials. The heat transfer rate can be dependent on the thermal property of the material which is called “thermal conductivity”. Fourier’s law is the main concept of heat conduction. This is the main effect that I discuss and simulate in this research.

A general form of the heat equation is [31]:

$$\frac{1}{\alpha} \frac{\partial T}{\partial t} = \nabla^2 T + \frac{q}{k}, \quad (2.1)$$

where the thermal diffusivity $\alpha = k/\rho C_p$ (m^2/s), T is temperature function (Kelvin $^\circ\text{K}$), k is thermal conductivity ($\text{W}/\text{m}\cdot\text{K}$), ρ is mass density (kg/m^3), q is the volume heat flux (W/m^3),

and C_p is the specific heat (J/Kg-K).

Basically, the function of temperature in a material has two factors – position with coordinates and time (t). For steady state, the thermal system is balanced. The temperature does not change while time is changing. For a one-dimensional problem, I consider the heat flow along a bar with two different temperatures on the ends: T_a and T_b as shown in Figure 2.1, the total heat transfer rate Q (W) could be described as the following equation:

$$Q = -kA \frac{(T_b - T_a)}{L} = -kA \frac{dT}{dx}, \quad (2.2)$$

where k is the thermal conductivity (W/m-K), the negative sign indicates that the direction of the heat flux is opposite to the temperature gradient, T is temperature in Kelvin (K), and A is the area of bar cross-section.

The heat transfer per unit area could be defined as $q_A = Q/A$ (W/m²), then the one-dimensional steady-state heat transfer conduction equation becomes:

$$q_A = -k \frac{dT}{dx}, \quad (2.3)$$

where q_A is the surface heat flux, which is the heat transfer rate from a high temperature region to a low temperature region. The unit of q_A is W/m²

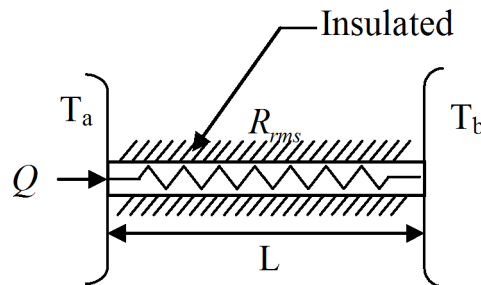


Figure 2.1: Heat Transfer along a bar

2.1.2 Electrical Analogy for Thermal Conduction

For the electrical analog with heat conduction, the thermal conduction could be addressed as a current flow driven by the difference of voltages with thermal resistance. For a homogeneous bar, the analog of Q is the current I , and the voltage difference is analogous to the temperature difference ($T_b - T_a$):

$$Q = \frac{(T_b - T_a)}{R_{eq}}, \quad (2.4)$$

where R_{eq} is the thermal resistance to the conduction through the bar, and is equal to $L/(kA)$.

For the series thermal resistance such as two different material bars connected along their lengths, shown in Figure 2.2 (a), the total heat transfer rate is given by:

$$Q = \frac{(T_b - T_a)}{R_{eq}} = \frac{(T_b - T_a)}{R_1 + R_2}. \quad (2.5)$$

For the parallel thermal resistance such as a square bar surrounded with resin (matrix) material, shown in Figure 2.2 (b), the heat transfer rate is given by:

$$Q = \frac{(T_b - T_a)}{R_{eq}}, \quad \frac{1}{R_{eq}} = \frac{1}{R_1} + \frac{1}{R_2}. \quad (2.6)$$

In electrical circuits, Ohm's law states that the current is directly proportional to the potential difference across the two points, and inversely proportional to the resistance between them. The equation is

$$I = \frac{V}{R}, \quad (2.7)$$

where V is the relative voltage across the conductance and its unit is volts; I is the current through the conductance in units of amperes, and R is the resistance of the conductor in units of ohms and the inverse of electrical conductance. Ohm's law also states that the R is independent of the current. Equation (2.7) appears in a form similar to equation (2.4). Because I want to extract the thermal and electrical netlist information with a layout extraction tool which cannot

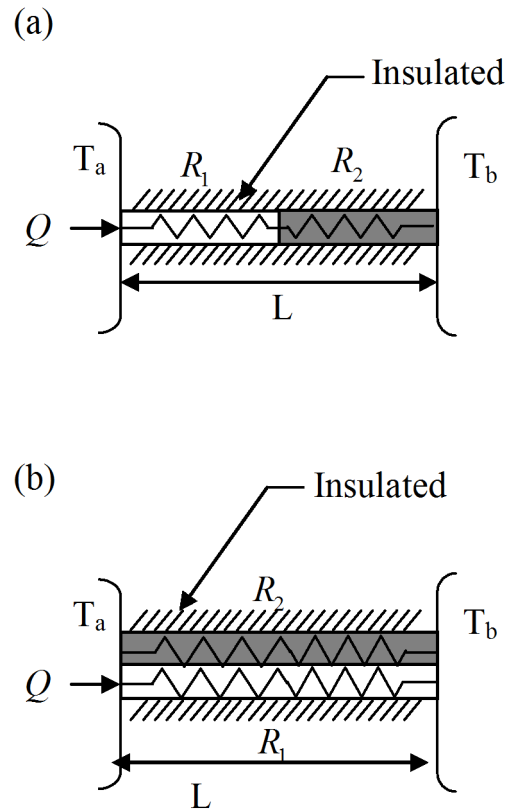


Figure 2.2: Diagrams of thermal resistance. (a) Series thermal resistance (b) Parallel thermal resistance

undergo thermal extraction, I need to interpret the relationship between thermal and electrical fields by the concept of resistors. While I consider the Joule heating, described below, the thermal and electrical properties of materials will be changed corresponding to temperature.

In electrical components, there is heat generation in a resistor due to the current Joule self-heating. The Joule heating equation for a uniform bar/wire can be expressed as

$$\Phi_l = I_{rms}^2 R_l, \quad (2.8)$$

Φ_l is the Joule heat per unit length, R_l is the electrical resistance of the bar per unit length, I_{rms} is the time-averaged root mean square (rms) current.

The longitudinal thermal conductivity k^{long} can be related to the electrical conductivity σ and temperature, as stated by the well-known Wiedemann-Franz law:

$$k^{long} = \lambda T \sigma \Rightarrow \lambda = k^{long} / (T \sigma). \quad (2.9)$$

where λ is a Lorenz constant, σ is electrical conductivity, and T is the absolute temperature of the resistor [32]. The Wiedemann-Franz law is named after Gustav Wiedemann and Rudolph Franz. In 1853, they reported that different metals have approximately the same value of k^{long} / σ at the same temperature. In 1872, Ludvig Lorenz discovered the λ which is the proportionality of k^{long} / σ with temperature. By applying the Wiedemann-Franz law with Lorenz's constant, I can derive the value of thermal conductivity from the electrical conductivity extracted by TCAD tools. The material used in interconnects and textile layout in this thesis is copper. The Lorenz constant is $2.23 \times 10^{-8} (W - \Omega - K^{-2})$ for copper at $0^\circ C$ [33].

2.2 Interconnect Model

Considering the interconnects of Very-Large-Scale Integration (VLSI) devices, the temperature distribution of interconnects is a subject of interest as VLSI devices become denser and low-

thermal-conductivity dielectrics with reduced thermal conductivity are introduced. In current CMOS technologies, estimating interconnects temperature from the layout and a model of the switching behaviour of the circuits has become an important part of electromigration reliability verification. For detailed temperature estimation of interconnects, interconnect is divided into rectangular “resistor” segments (Figure 2.3) paired with capacitance by a layout extraction tool. The layout extraction tool extracts the information of net topology, resistance and capacitance information, and coordinates of interconnects. This extracted information of nets from a layout is then relabeled to match the electrical circuit. The extraction method may merge the resistors to an order-reduced model. For example, Clement et al. extracted the information of resistors and capacitors from layout using CAD tools (e.g., REX) [34] [35]. The capacitors then are replaced by corresponding current sources which are set to capacitances multiplied by voltage swing divided by the cycle time. This strategy could directly solve the node voltages and branch currents by standard nodal analysis technologies [36]. I used the concept of RC network with extraction information in my interconnect simulations by the Therminator3D program.

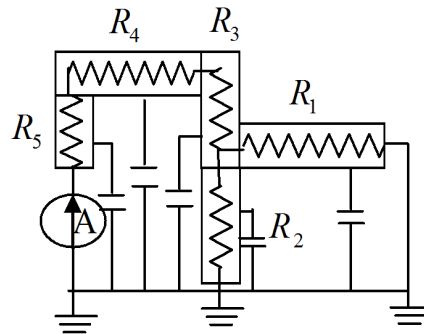


Figure 2.3: Resistor segment of interconnects

In a general interconnect layout, segmentation occurs at vias and at changes in width, junctions, and corners. Each segment has a resistance R_n given by the following formula:

$$R_n = L_n / k_n A_n \quad , \quad (2.10)$$

where L is its length (m), k is its conductivity ($\Omega - m$), and A is its cross-sectional area (m^2).

Consider a segment of length Δx on the thermal resistor network as shown in Figure 2.4. Its heat conservation can be written [17]

$$mC_p \frac{\partial T}{\partial t} = Q(x + \Delta x) - Q(x) + \Phi_l(x)\Delta x - f(x)\Delta x. \quad (2.11)$$

The longitudinal heat transfer rate, Q , is opposite to the increasing direction- x and obeys Equation (2.2); G^{long} is a longitudinal thermal conductance found by integrating thermal conductivity k^{long} over the resistor cross-section. The lateral heat rate per unit length (W/m) is written as $f(x) = G^{lat}(T(x) - T^{ref})$ with the lateral thermal conductance G^{lat} representing the diffusion of heat flux from the sides of the resistor with unit length, through a dielectric with thermal conductivity k^{lat} , to a uniform reference temperature T^{ref} . Parasitic interconnect capacitance C is analogous to G^{lat} and both may be calculated using the same technique. The segment mass is m and C_p denotes the specific heat. The Joule self-heat per unit length Φ_l (W/m) generated by a current in the circuit is $\Phi_l = I_{rms}^2 R_l$.

In a steady-state case, $T(x, t)$ is a function of x only, and when $\Delta x \rightarrow 0$, Equation (2.11) becomes a second order ordinary differential equation:

$$\Phi_l = -G^{long} d^2 T / dx^2 + G^{lat} (T - T^{ref}). \quad (2.12)$$

The solution on each resistor segment with boundary conditions $T(x = 0) = T_0$ and $T(x = L) = T_L$, and defining a constant term

$$T^\infty = \frac{\Phi_l}{G^{lat}} + T^{ref}, \quad (2.13)$$

is then given by [17]

$$T(x) = \left(\frac{T_L - T^\infty - (T_0 - T^\infty) \cosh(\xi L)}{\sinh(\xi L)} \right) \sinh(\xi x) + (T_0 - T^\infty) \cosh(\xi x) + T^\infty, \quad (2.14)$$

where $\xi = \sqrt{G^{lat}/G^{long}}$. For specific resistors such as vias for which $G^{lat}=0$, the solution becomes

$$T(x) = -\frac{I_{rms}^2 R x^2}{2G^{long}} + \left(\frac{T_L - T_0}{L} + \frac{\Phi_l L}{2G^{long}} \right) x + T_0. \quad (2.15)$$

Equation (2.14) and (2.15) have been applied to thermal estimation of multilevel interconnects [37]. In Therminator3D, electrical and thermal resistances are taken as constants within a resistor given a temperature. However, each resistor has its own values, depending on its average temperature.

The network numerical solutions are iterated over temperature and current until a self-consistent state (equilibrium) is achieved.

2.2.1 Textile Fibre Model

For the analysis of textile material, the solutions of the one-dimensional heat equation are derived on fibre segment resistors and on vias that represent the contact of overlapping fibres. The networks that are formed by these resistors and vias are treated in the same way as the electrical resistors that are used in metal interconnect EMR analysis [34].

The textile fibre model can be interpreted as an equivalent interconnect RC model. The starting point for the textile fibre model examples will be a steady-state and a NCF fabric with no heat source. Thus, the following assumptions are made: (a) steady state: $\partial T / \partial t = 0$; (b) one dimensionality: the heat is flowing in only one coordinate direction along the length of the resistor. (c) no heat source: there are no heat sources within the system. Then equation (2.1)

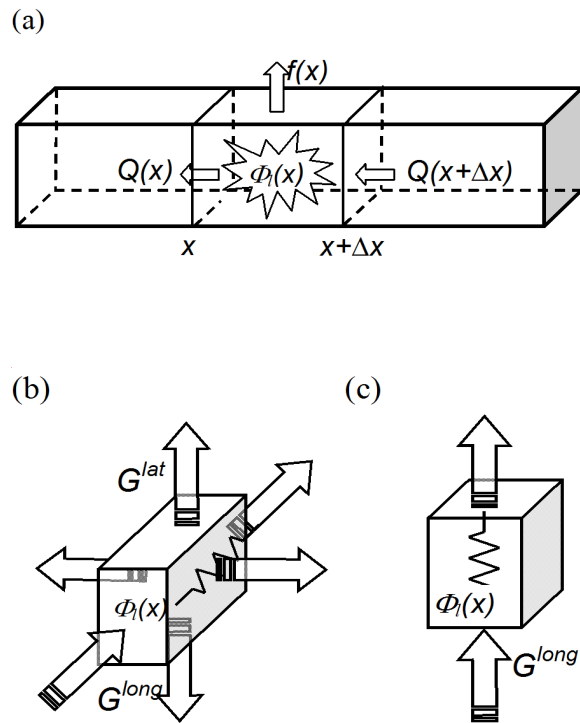


Figure 2.4: Heat conservation model and capacitances (a) Heat conservation within a differential slice of a one-dimensional thermal resistor accounts for longitudinal flux, lateral flux, and Joule self-heat. (b) Horizontal resistors have G^{lat} and G^{long} , while (c) via resistors only have G^{long} .

turns to:

$$\frac{\partial^2 T}{\partial x^2} = 0, \quad (2.16)$$

and

$$T(x) = (T_l - T_0) \frac{x}{L} + T_0. \quad (2.17)$$

Results of simulation for this case with a fixed temperature boundary conditions will be shown as the first example in Section 5.3.

The second step was to apply heat source to a specific wire and consider a model in steady-state. Such, the whole model of NCF material will look like the interconnect model presented in Section 2.2. Results of simulation for this case will be shown as the second example in Section 5.3.

Finally, I will continue to perform simulation problems for a woven pattern based on a network-based model.

2.3 Network-Based Simulation Concept

Network-based simulation is an approach based on the information of the whole network. It has a concept of network calculation on nodes and corresponding connections of the entire network. Each node has detailed information between adjacent nodes and itself. For IC interconnect simulations, there are netlist files describing the coordinates of components, the values of capacitance and resistance, and the properties of materials. The list of a net provides detailed data including the values of resistors, properties of materials and the information of adjacent nodes (e.g., the net-list format of SPICE). The net-based simulation can be composed of several nets. Those nets may be coupled. By the net-based approach, each net is solved individually then the nets are assembled from the layout database to form the entire network. Using the

net-based approach, the total calculation time does not increase with the entire model size, but rather with the size of each net, and the number of nets. Some earlier works introduced a “Model Reduction” concept (for relatively coarse computational grids) to minimize the time of simulation in temperature prediction of interconnects [38–41], but they lost the details of information of temperature distribution for the whole system.

As described in Section 2.2, I adopt a modified RC network with thermal module from the electrical module [37, 42, 43]. Using this modified RC network, the net-based approach can demonstrate resistor-level accuracy of the full-chip temperature estimation.

2.4 Summary

In the chapter, I introduced “Network-Based Simulation” for temperature estimation of IC interconnects and textile fabrics along with underlying theories. I discussed an analogy between thermal and electrical problems. Based on those, I proposed a RC network model from the concept of electromigration in circuits. With the RC network, I can simulate large networks with full-chip calculations without losing the detailed information on each component and the accuracy of temperature distribution. Moreover, this method can be conveniently adapted to textile materials. The program implementation will be described in the next chapter.

Chapter 3

Therminator3D

This chapter introduces the Therminator3D network-based calculation method. The first part begins with background and input formats of this program. The symbolic network analysis solution is shown in the second part. The third part demonstrates the iterative and multiphysics evaluation procedure. Finally, a summary of the Therminator3D is presented in the end of the chapter.

3.1 The Analytical Solution of Networked Elements

In this section, the analytical solutions of the one-dimensional heat equation are summarized for fibre segment resistors and vias that represent the contact of overlapping fibres. A typical interconnect network with vias is shown in Figure 3.1. The network formed by such resistors and vias is often treated in metal interconnect electromigration reliability (EMR) problems [34]. An equivalent multilevel Manhattan interconnect model of the net-based interconnects with vias is shown in Figure 3.2. The interconnect columns (1-4) and rows (5-8) are embedded in dielectric and divided into rectangular segments (“resistors”).

3.1.1 Resistor-Capacitor Network

The electric current in each resistor can be found by DC analysis of the interconnect RC network, which is described as equivalent pi-networks that consist of resistors and current sources proportional to interconnect parasitic capacitance as shown in Figure 3.3. This equivalent network is commonly used for electromigration analysis [6]. The network nodes correspond to

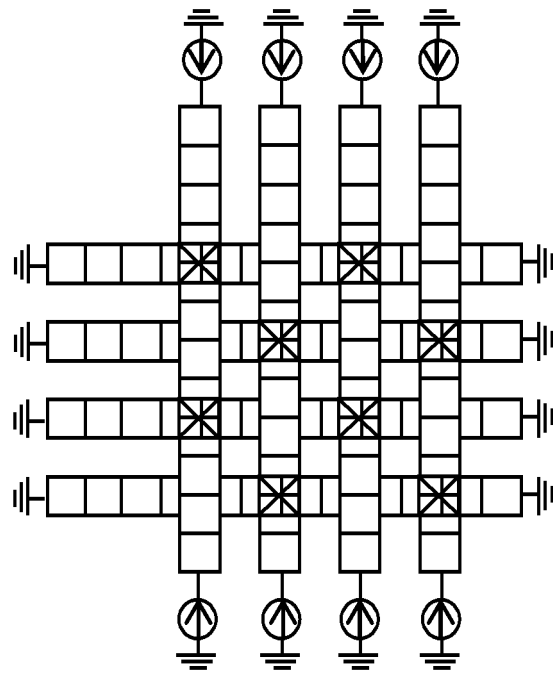


Figure 3.1: A net-based interconnect model with vias shown with an 'X'.

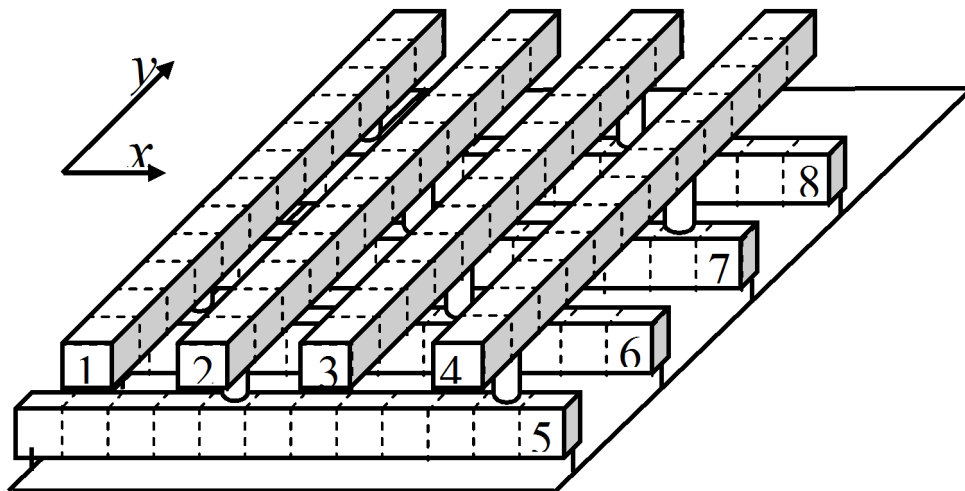


Figure 3.2: A two-layer interconnect grid with vias showing approximate segmentation to connected resistors.

the resistor endpoints. The system of analytical boundary value equations (2.14) and (2.15) can be evaluated over the same RC network by assigning the appropriate values to the circuit symbols in Figure 3.3. From equation (2.14) and (2.15), for interconnect resistors, the equivalent quantities are:

$$\alpha = G^{long} \xi / \sinh(\xi L), \quad (3.1)$$

$$\psi = 2\Phi_l (\cosh(\xi L) - 1) / (\xi \sinh(\xi L)) \quad (3.2)$$

$$\beta = \alpha (\cosh(\xi L) - 1). \quad (3.3)$$

For vias:

$$\alpha = G^{long} / L, \quad (3.4)$$

$$\psi = \Phi_l L. \quad (3.5)$$

Connected resistors have common temperatures at their junctions and heat flux along their length is conserved. Analytical trajectories of equation (2.14) have been previously applied to study thermal scaling of interconnect architectures [44].

3.1.2 The Format of Input Files

The two input files for Therminator3D are the netlist file and the coupling file. The formats of these two files are shown in Table 3.1. The netlist file is formed by the resistor and node numbers, the coordinates, length, and thermal resistance values. Every line in the coupling file consists “CAP”, the resistor number, the “coupled to” resistor number, capacitance value, and the value of lateral thermal conductance G^{lat} .

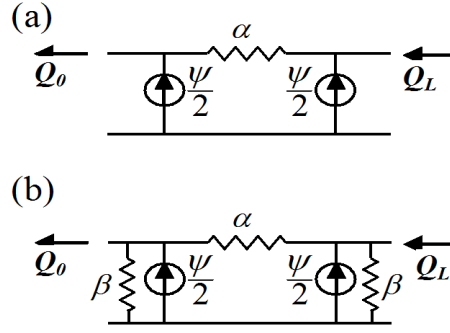


Figure 3.3: EMR methodology diagrams. Typical EMR methodology, each of the resistors that form a net is represented by the equivalent pi network. In the EMR methodology network (a) is used for via resistors and network (b) for other resistors, but with conductance $\beta = 0$ in electrical analysis and $\beta > 0$ in thermal analysis.

The coupling file presents the heat conductance to the neighbouring dielectric, substrate, and resistors. The pair-wise G^{lat} through the dielectric between each resistor and its neighbouring resistors (analogous to their coupling capacitance) can be extracted from the layout by a parasitic capacitance extractor and summed to form the total G^{lat} for that resistor, as shown in Figure 3.4. The equations for $K_{in-plane}$ and $K_{cross-plane}$ are [45]:

$$K_{in-plane} = \frac{1}{(1-r)(k_v P + k_f(1-P))^{-1} + \frac{Pr}{k_v} + \frac{(1-P)r}{k_f}} \quad (3.6)$$

$$K_{cross-plane} = (1-r)\left(\frac{P}{k_v} + \frac{P}{k_f}\right)^{-1} + (k_v - k_f)Pr + k_f r \quad (3.7)$$

where P is the porosity of the dielectric/matrix, k_v is the thermal conductivity of the inclusion medium, k_f is the thermal conductivity of the host medium, r is the ratio of the parallel component area to the total area.

Although a simple area model is used in this study, the more sophisticated coupling models found in most capacitance extractors could potentially be used for more accurate results if supplied with appropriate thermal conductivity parameters.

For example, in application to woven materials (Figure 3.5), the simple area model is not

appropriate to describe the G^{lat} to represent the phenomenon. Currently, there are no experimental data to achieve the formulization of G^{lat} as related to the woven structures and coupling areas, and the matrix between the fibres. In this research, I initially estimate G^{lat} by the simple area model in Figure 3.5 then calibrate the values of G^{lat} with the result of ABAQUS's simulation. The G^{lat} for the twist part with angular section coupled to wire 3, G_{twist}^{lat} , is around 0.15 of $K_{cross-plane}w/2h$. Then the result of Therminator3D simulation is closest to the result of ABAQUS simulation. That is because the angular section enhances the coupling effects to adjacent wires as the distant between wires changes.

Table 3.1: Therminator3D input file format and typical values.

| |
|---|
| <p>netlist file (resistor node0 nodeL R # $x_{lowerleft}y_{lowerleft}x_{upperright}y_{upperright}LR^{long}$) (current_source node0 nodeL I_{rms})</p> |
| <p>..... RES27 25 26 83.046936 # 40 -20 40 -10 10.000000 3433.110212 RES28 26 27 83.046936 # 40 -10 40 0 10.000000 3433.110212 AMP1 0 23 0.000000 RESAMP1 0 23 3.000000 # 35 -45 45 -35 1.000000 0.0001 RES4-27 4 27 3.000000 # 35 -5 45 5 1.000000 0.001 </p> |
| <p>coupling file (CAP RESISTOR {RESISTOR 0(SUBSTRATE)} c # G^{lat})</p> |
| <p>..... CAP RES27 0 12.666667 # 0.00000040086361458 CAP RES28 0 6.333333 # 0.00000020043180686 CAP RES28 RES4 9.500000 # 0.00000030064771072 CAP RES28 RES5 9.500000 # 0.00000030064771072 </p> |

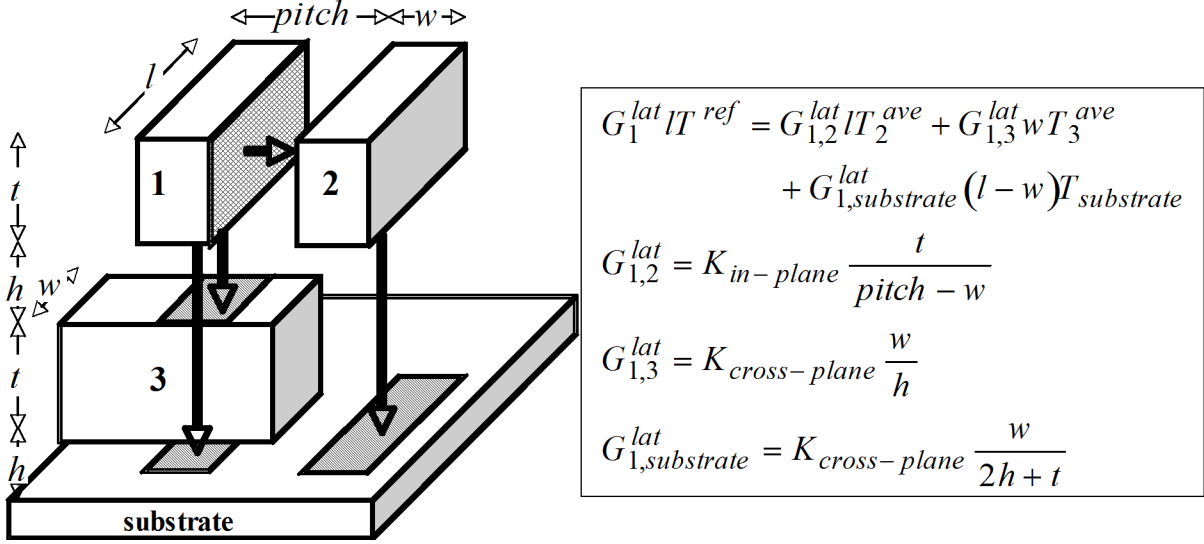


Figure 3.4: Typical Lateral thermal conductance model in IC Interconnects. Lateral thermal conductance G^{lat} between each resistor and its assumed uniform background temperature T^{ref} is the weighted average of temperatures to neighbouring resistors and the substrate, using simple area models of conductance. Anisotropic thermal conductance is indicated by $K_{in-plane}$ and $K_{cross-plane}$ values. [46]

3.2 Symbolic Network Analysis Solution

The sparse $N \times N$ system of linear algebraic equations

$$Az = b, \quad (3.8)$$

can be decomposed to lower and upper triangular matrices L and U with order $O(N^3)$ operations by the Crout algorithm. The system can then be evaluated for z by two consecutive back-substitution operations ($O(N)$ if null operations are not performed):

$$A = LU \quad (3.9)$$

$$Az = (LU)z = L(Uz) = b \quad (3.10)$$

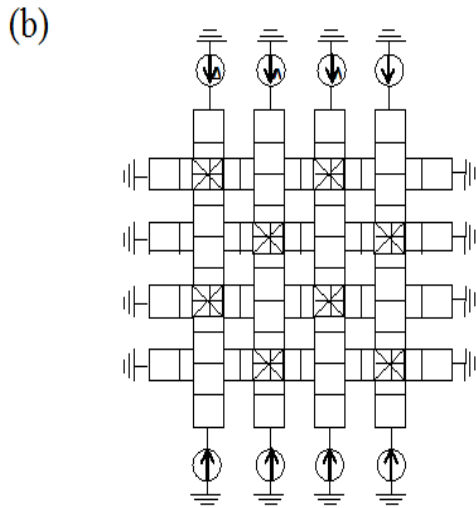
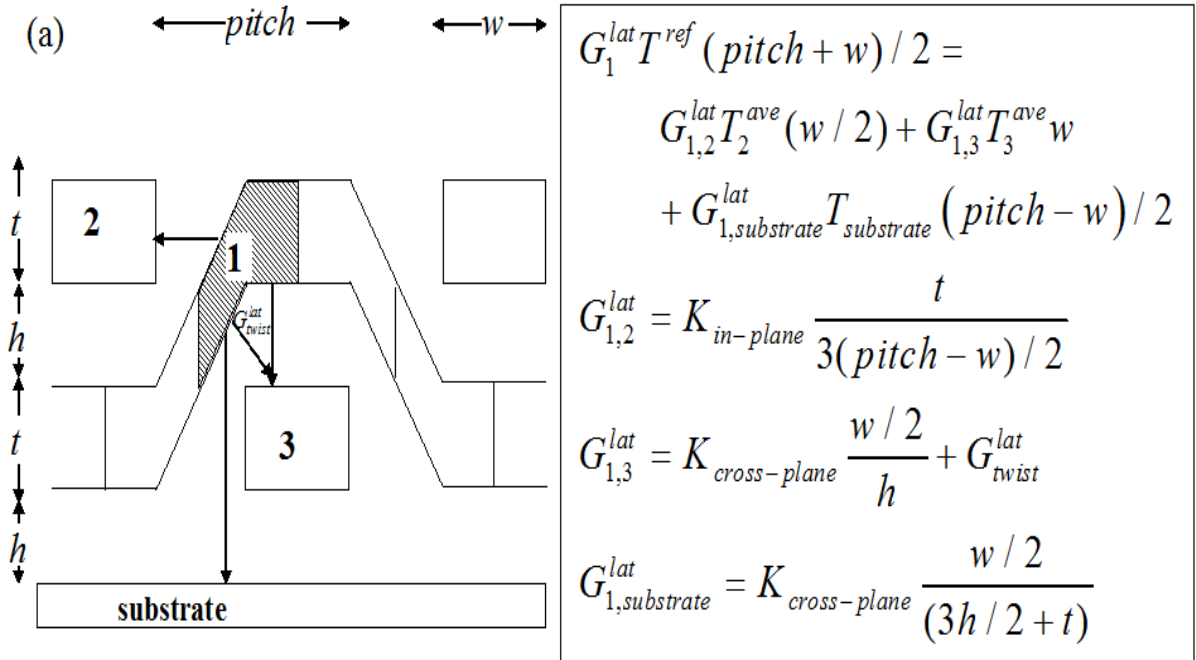


Figure 3.5: Lateral thermal conductance for woven case (shown by the capacitor symbols) (a) Lateral thermal conductance G^{lat} between each resistor in woven case. (b) Equivalent layout in T3D. The value of multi-directional coupling G_1^{lat} is calibrated by the results of ABAQUS FEA.

$$Ly = b \quad (3.11)$$

$$Uz = y \quad (3.12)$$

The elements l_{ij} and u_{ij} of L and U can be found by equations (3.13), (3.14), and (3.15) over the elements a_{ij} of A [47, 48].

$$l_{ij} = 0, \text{ for } i < j, u_{ij} = 1 \text{ for } 1 \leq i \leq N, \text{ and } u_{ij} = 0, \text{ for } i > j, \text{ where } 1 \leq i, j \leq N \quad (3.13)$$

$$l_{im} = a_{im} - \sum_{\mu=1}^{m-1} l_{i\mu} u_{\mu m}, \quad i = m, m+1, \dots, N \quad (3.14)$$

$$u_{mj} = \frac{1}{l_{mm}} \left(a_{mj} - \sum_{\mu=1}^{m-1} l_{m\mu} u_{\mu j} \right), \quad j = m+1, m+2, \dots, N. \quad (3.15)$$

Therminator3D, a C language program, applies dynamic storage allocation and data structures to store the symbolic structure of the solution. Each resistor in the net-list file is given a data structure containing all numerical data and results for the problem to be solved. All the resistor structures are referenced through ‘hash’ tables. The problem matrix A is represented by a linked list of $O(N)$ non-null elements of A . Figure 3.6 shows the distribution of elements in A . The cross marks represent the non-zero values. The distribution of Figure 3.6 is the least-sparse case with all vias between columns and rows. The vector b consists of links to heat source elements and boundary conditions. Matrix A is decomposed to the L and U linked lists by the Crout factorization formulas. Vectors z and y are constructed as linked lists pointing to components of L , U , and b . After the entire system of linked lists has been created, it is straightforward to evaluate the specific physical problem (mechanical, thermal, electrical, etc). For thermal problems, the temperature trajectories $T(x)$ are determined after the z vector (the

temperature of each node) has been found. Average and maximum values are stored in the data structure for convenience. The $O(N)$ evaluation can be iterated for nonlinear problems (for example when k^{long} is temperature-dependent) or for multiphysics problems.

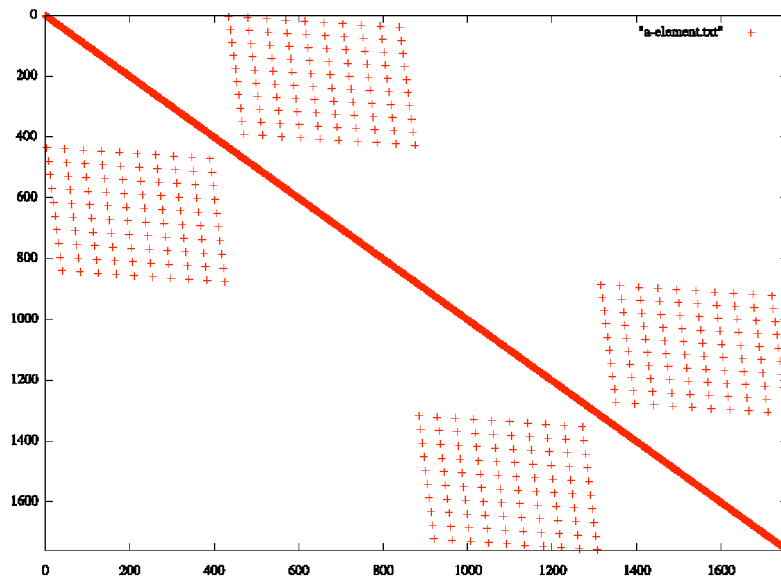


Figure 3.6: The distribution of problem matrix A (the 20 columns and 20 rows case with via between each row and column).

Consider the Joule self-heat generated by an electric current flowing through a resistive conductor. In an IC, multiple active devices (e.g. transistors) are connected electrically by a metal interconnect network, or “net” of uniform-width resistor segments connected at their endpoints, or “nodes” that may be “extracted” to a file. Any system of 1-D boundary value equations, such as the steady-state heat conduction, can be solved over the entire net by connecting the individual solutions in each resistor segment. As mentioned earlier, Terminator3D applies the Crout algorithm for LU decomposition and back-substitution to the system and records only the non-null operations, thus forming a generic symbolic solution for the entire net. This symbolic solution is then evaluated with electrical parameters to solve the electrical problem first, and then evaluated again with thermal parameters to solve the resulting Joule heat problem. The resistance of each resistor can increase with the increasing temperature. The final resistance and temperature is therefore found iteratively. Also, thermal conductance

through the insulator between adjacent resistors on different nets may be extracted in the same way as capacitive coupling for IC interconnect. By composing the ambient, reference temperature for each resistor from temperatures of resistors to which it couples through the dielectric, it is possible to iteratively couple separate nets' temperature trajectories. To form the symbolic solution requires $O(N^3)$ operations, but for a sparse system such as an interconnect network there are only $O(N)$ non-null operations (where N is the number of nodes). Thus, the electrical and thermal evaluations require only $O(N)$ operations. Therminator3D requires a database that contains network information, such as the nodal relationships, coupling between resistors, input sources, and boundary conditions. A netlist file extracted from IC layout with a standard CAD tool would be the most common source of this information.

3.3 Iterative and Multiphysics Evaluation

The analytical solution procedure involves the coupling of thermal and electrical calculation until the convergence of temperature solution for steady-state is reached. After the symbolic solution is done, the L and U matrices in linked-list forms pass to the analytical solution loop.

For the electrical problem, the pi equivalent network values α , β , and Ψ are considered from electrical circuit values for each resistor as described in Section 3.1.1. In IC interconnects, the electrical conductivity of dielectric is almost zero, so $\beta = 0$. The value of non-zero a_{ij} is the sum of the α field of linked resistors. The elements of y matrix and z matrix are calculated by the back-substitution.

For the thermal problem, the pi equivalent network values α , β , and Ψ are considered from thermal and electrical current values for each resistor using (3.1), (3.2), and (3.3) and the evaluation procedure is repeated. The z array (nodal temperature in the thermal problem) is then found. The temperature of resistors are updated and coupled to form the T^{ref} (uniform

thermal reference):

$$G_{n_m}^{lat}(T_{n_m} - T_{n_m}^{ref}) = \sum_{v=0}^N \sum_{\mu=1}^{M_v} G_{n_m v_\mu}^{lat} (T_{n_m} - \overline{T_{v_\mu}}) (n \neq v), \quad (3.16)$$

$$T_{n_m}^{ref} = \frac{\sum_{v=0}^N \sum_{\mu=1}^{M_v} G_{n_m v_\mu}^{lat} \overline{T_{v_\mu}}}{G_{n_m}^{lat}}, \quad (3.17)$$

where

$$\overline{T} = \frac{1}{L} \int_{x=0}^L T(x) dx \text{ for each resistor.} \quad (3.18)$$

The temperature at each junction between resistors is stored. The temperature of each resistor is updated from equation (3.18) and the values of I_{rms} and T^{ref} .

Since T^{ref} is also updated, the temperatures of nodes of the entire net have to be recalculated through electrical and thermal solutions until convergence is reached. Figure 3.7 shows the flow chart of Therminator3D. There are several published reports that present different schemes of thermo-electrical coupling calculation [49–51]. These reports calculate the Joule heating first, then pass and couple the electrical results to an additional thermal calculation package, then return the calculations of thermal problem for post-processing. The procedure is repeated until convergence is reached. This type of thermo-electrical coupling calculation could lose some consistency of data due to interpretations between different packages. Therminator3D program uses one package to calculate both electrical and thermal problems using the same symbolic solution procedure. Hence, the Therminator3D analytical approach may be more suitable for large systems by making only minor modifications from the EMR verification methodology [34, 52]. The modified RC-network model describes all possible properties of a resistor or component. Additional coupling data represent that the behaviour of thermal coupling could also represent other mechanical coupling properties. This gives Therminator3D a potential to solve large networks of multi-physics problems with high speed and accuracy.

3.3. Iterative and Multiphysics Evaluation

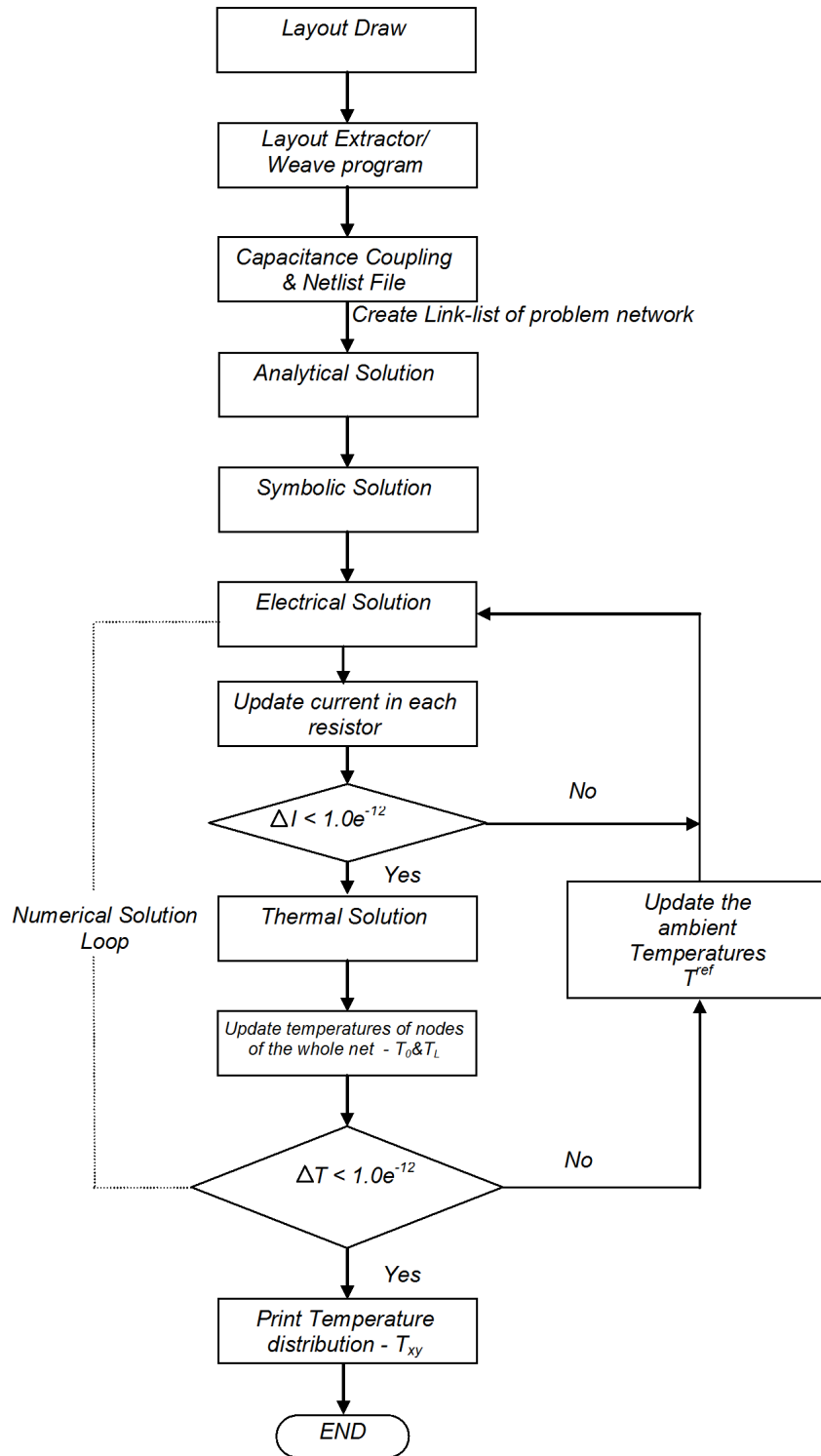


Figure 3.7: The flowchart of Therminator3D thermo-electrical simulation

3.3.1 On Convergence of Non-linear Problems in Therminator3D

In Therminator3D, as described in Section 3.2, the symbolic solution of $Az = b$ is reformed using the following steps:

1. Construct the matrices L and U .
2. Solve $Ly = b$ for y using forward substitution.
3. Solve $Uz = y$ for z using back substitution.

If the matrix A is not constant, the system becomes non-linear and to find the solution the program use an iterative method. There are several iterative methods available in the literature.

Examples include:

- Fixed-point method,
- Newton-Raphson method,
- Quasi-Newton method,
- Dynamical relaxation method, and
- Continuation or Arc-length methods

The algorithm used in Therminator3D for iterations is “Fixed-point method”. A general fixed-point problem is defined as the follows [53]:

Definition

Solve the non – linear fixed point system of

$$\vec{z}_k = \vec{g}(\vec{z}_{k-1}) \quad (3.19)$$

given one initial value \vec{P}_0 and generating a sequence \vec{P}_k which converges to the final solution \vec{P} where

$$\vec{G}(\vec{P}_k) = \vec{P} \quad (3.20)$$

For the case of this research, the sequence for solving the non-linear system $A(z)z = b$ using the fixed-point method is as follows (here I assume the load vector b is constant):

1. $A_{z_{k-1}} z_k = b$
2. $z_k = A_{z_{k-1}}^{-1} b$
3. $z_k = g(z_{k-1})$ where $k = 1, 2, \dots$ (iteration number)

The convergence criteria of fixed-point algorithm is proven to be $|dg/dz| < 1$ [53]. Figure 3.8 shows this criterion in one dimensional case.

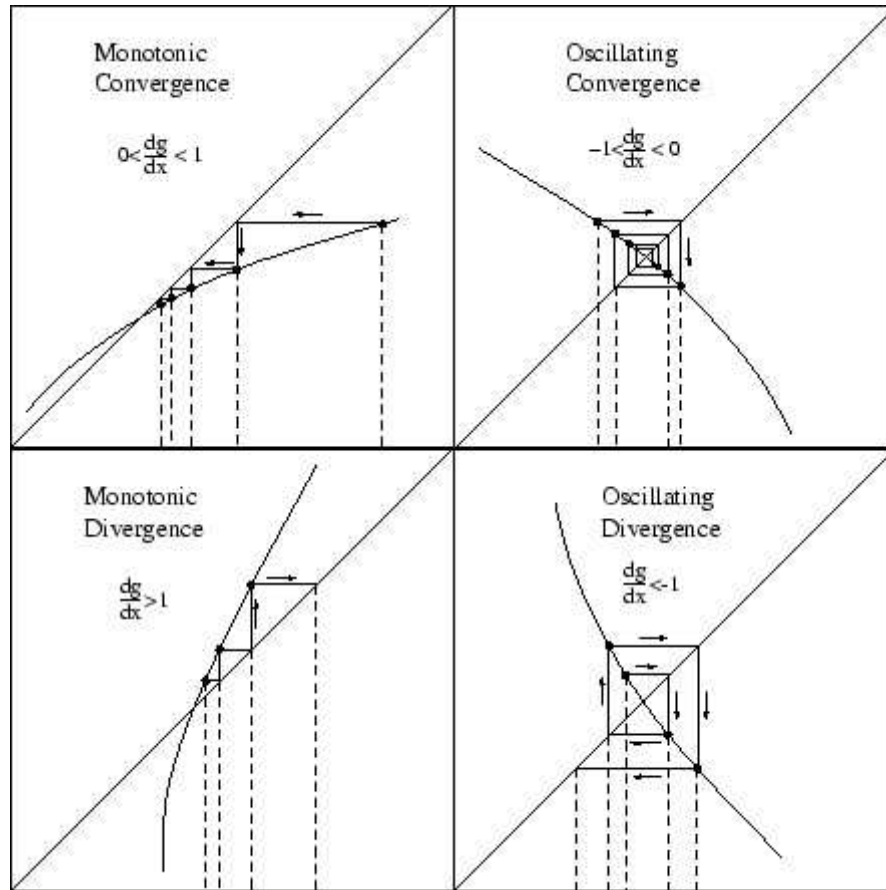


Figure 3.8: Fixed point iteration for a general function $g(x)$ for the four cases of interest. (Cited from [54])

Let us consider a sample non-linear heat problem shown in Figure 3.9

Assume $T_3 = 0$, thus

$$\begin{bmatrix} \frac{1}{R_1} & 0 \\ \frac{-1}{R_2} & \frac{1}{R_2} \end{bmatrix} \begin{bmatrix} T_1 \\ T_2 \end{bmatrix} = \begin{bmatrix} Q \\ Q \end{bmatrix} \quad (3.21)$$

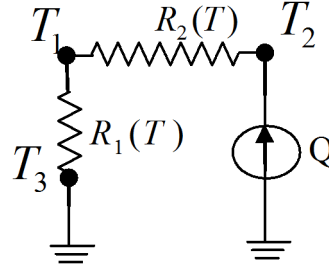


Figure 3.9: Sample circuit 1 for Therminator3D convergence verification

Also assume $\frac{\Delta R}{R_0} = \alpha_0 \Delta T$ where R_0 is a constant resistance at initial temperature T_0 , and α_0 is a temperature-dependent coefficient.

$$R_1 = R_0[1 + \alpha_0(T_1 - T_0)] \quad (3.22)$$

$$R_2 = R_0[1 + \alpha_0(T_2 - T_0)] \quad (3.23)$$

Using (3.22) and (3.23) in (3.21), I have:

$$\begin{bmatrix} \frac{1}{R_0[1 + \alpha_0(T_1 - T_0)]} & 0 \\ \frac{-1}{R_0[1 + \alpha_0(T_2 - T_0)]} & \frac{1}{R_0[1 + \alpha_0(T_2 - T_0)]} \end{bmatrix} \begin{bmatrix} T_1 \\ T_2 \end{bmatrix} = \begin{bmatrix} Q \\ Q \end{bmatrix} \quad (3.24)$$

Hence, the temperature solution will follow:

$$T_1 = QR_0[1 + \alpha_0(T_1 - T_0)] \quad (3.25)$$

$$T_2 = QR_0[1 + \alpha_0(T_2 - T_0)] \quad (3.26)$$

Or in a general form, for both temperature solutions:

$$T = QR_0[1 + \alpha_0(T - T_0)] \quad (3.27)$$

Using the fixed-point iteration method to solve equation (3.27) results in

$$T = g(T) = QR_0[1 + \alpha_0(T - T_0)] \quad (3.28)$$

For convergence, I should have $\left| \frac{\partial g}{\partial T} \right| < 1 \Rightarrow |QR_0\alpha_0| < 1$. For example, using values of the netlist in Table 3.1, assumed $\alpha_0 \sim 0.33\%$ for copper, its thermal resistant is 3433.110 (K/W) for a $10 \mu\text{m} \times 10 \mu\text{m} \times 40 \mu\text{m}$ (WxDxL) brick resistor, and its electrical resistant is 83.047 Ω . To ensure the above convergence, I_{rms} should be smaller than 3.26×10^{-2} Amp for a range of $Q < 1.063 \times 10^{-3}$.

As a second example, to evaluate Therminator3D in a small case with G^{lat} , consider a system containing two infinitely-long, coupled nets, each with one resistor (Figure 3.10), coupled by the $G_{1,2}^{lat}$ and couplings $G_{1,subst}^{lat}$ and $G_{2,subst}^{lat}$ (all positive) to the substrate. Also assume temperature of substrate, $T_{subst} = 0$. From equation (3.16), the overall lateral thermal conductance of a given resistor is the sum of all conductances to neighbouring resistors and the substrate:

$$G_{n_m}^{lat} = \sum_{v=0}^N \sum_{\mu=1}^{M_v} G_{n_m v \mu}^{lat} (n \neq v), \quad (3.29)$$

For the infinitely-long nets, note $T_i^\infty = \bar{T}_i = T_i$.

From equation (3.17), I have

$$\begin{aligned} T_1^{ref} &= \frac{G_{1,2}^{lat} \bar{T}_2}{G_{1,2}^{lat} + G_{1,subst}^{lat}} \\ &= \frac{G_{1,2}^{lat}}{G_1^{lat}} T_2 \end{aligned} \quad (3.30)$$

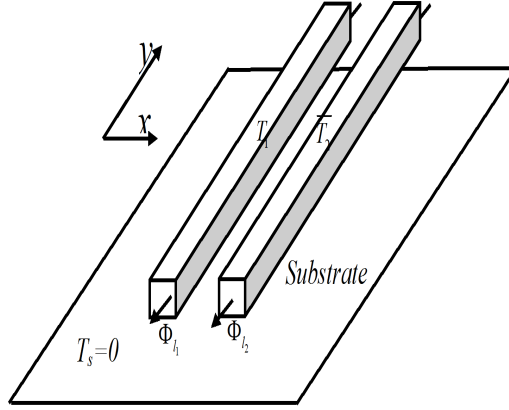


Figure 3.10: Sample circuit 2 for Therminator3D convergence verification with infinitely-long resistors and substrate.

$$\begin{aligned}
 T_2^{ref} &= \frac{G_{1,2}^{lat} \bar{T}_1}{G_{1,2}^{lat} + G_{2,subst}^{lat}} \\
 &= \frac{G_{1,2}^{lat}}{G_2^{lat}} T_1
 \end{aligned} \tag{3.31}$$

The temperature of each wire is given by equation (2.13), and thus

$$\begin{aligned}
 T_1 &= \frac{\Phi_{l1}}{G_1^{lat}} + T_1^{ref} \\
 &= \frac{\Phi_{l1}}{G_1^{lat}} + \frac{G_{1,2}^{lat}}{G_1^{lat}} T_2 \\
 &= \frac{\Phi_{l1}}{G_1^{lat}} + \frac{G_{1,2}^{lat}}{G_1^{lat}} \left(\frac{\Phi_{l2}}{G_2^{lat}} + T_2^{ref} \right) \\
 &= \frac{\Phi_{l1}}{G_1^{lat}} + \frac{G_{1,2}^{lat}}{G_1^{lat}} \frac{\Phi_{l1}}{G_2^{lat}} + \frac{G_{1,2}^{lat}}{G_1^{lat}} \frac{G_{1,2}^{lat}}{G_2^{lat}} T_1 \\
 &= g(T_1)
 \end{aligned} \tag{3.32}$$

Although for temperature-independent case, equation (3.32) can be solved in closed-form, for the general case solved by Therminator3D a fixed-point iteration scheme is used (e.g., when

R and thus Φ is a function of T). The convergence condition of a one-dimensional fixed-point iteration scheme, $0 < \left| \frac{dg(x)}{dx} \right| < 1$, yields

$$\frac{dg(T_1)}{dT_1} = \frac{(G_{1,2}^{lat})^2}{G_1^{lat} G_2^{lat}} < 1 \quad (3.33)$$

Thus, it is proven that fixed-point iteration of the simple system described will always converge. However, coupling of more segments, with more complex formula for T given above, does not change the argument given here. So the general case must also converge. Also, the nearer the derivative is to unity, the more rapid the convergence. Thus, when coupling between nets becomes weaker relative to coupling to the substrate, say because the nets are moved further apart, more iterations will be required for convergence.

3.4 Summary

Therminator3D, a network-based integrated simulation tool, was introduced in this chapter. Therminator3D applies network topology to the solution of fully-coupled electric and thermal problems. This program derives a modified RC model from EMR and has the ability to simulate multi-physics problems. It can also deal with textile materials by changing the physical properties of columns and vias to represent the fibre yarns and conditions. The matrix between yarns is analogous to the dielectric between wires in Therminator3D. The porosity of dielectric can be interpreted to the properties of matrix by coupling effects. Those interpretations show that Therminator3D can simulate textile materials with a network-based topology. Chapter 5 will demonstrate results of several examples of temperature distributions in IC interconnects and textile materials.

Chapter 4

Finite Element Analysis

This chapter describes details of the finite element analysis (FEA) used in this work and introduces the well-known FEA software - ABAQUS. The first part of the chapter discusses the basic simulation model using FEA. The second section describes the concept of mesh methods. Different mesh methods applied on shapes of objects can affect the accuracy of simulation results. The third section shows that the FEA software, ABAQUS, is capable of conducting the thermo-electrical stimulations and can be successfully used for comparison with Terminator3D. The last part of this chapter is a summary of the FEA using in this work.

4.1 Basic Physical Model of Finite Element Analysis

The finite element method (FEM) is a numerical procedure for solving physical problems by a series of ordinary and partial differential equations. This method was originally developed to solve stress and strain mechanical analysis. Today, it has numerous of applications such as heat transfer analysis, thermo-electrical analysis, fluid mechanical analysis, etc. The classical FEA approach includes a series of equations to represent the continuity of physical behaviours, transferring the solution domain to a finite element mesh (such as the interpolation of shape functions), assembling equations of elements, applying the boundary conditions, and computing the solutions of system equations. There are numerous articles and books on FEA. The FEM handbook by Kardestuncer (1987) has described most of these applications [55]. For the application of this research, I focus on the heat transfer and coupled electro-thermal problems of IC interconnects and textile materials. Before solving these problems, the FEM has to form

a CAD model to represent the layout pattern. There are two common (often interchangeable) ways, unit-cell and Representative Volume Element (RVE) modeling, used for this purpose in the literature.

Unit-cell is a concept from the material crystal structure. In crystallography, crystal structure is a unique arrangement of atoms in a crystalline solid or liquid with symmetrical pattern. The symmetrical pattern in a given lattice is called a “Unit-cell”. Unit cells can be stacked to form a model which represent the meso or macro-level problem that I want to solve. Figure 4.1 (a) shows a typical unit cell that emphasizes the opening between fibres of a non-crimp fabrics [56].

Representative Volume Element (RVE) is an effective volume contained a set of microstructure elements. It has to be smaller than the original sample. W.J. Drugan and J. R. Willis [57] has a definition of RVE – “the smallest material volume element of the composite for which the usual spatially constant “overall modules” macroscopic constitutive representative is a sufficiently accurate model to represent mean constitutive response”. They pointed out the importance meaning of “mean constitutive response”. It expresses that the RVE has to be small enough to represent the mean of surrounding materials. Figure 4.1(b) shows a typical RVE. The spaces beside the wire/yarn could be filled with a matrix material. The sum of all properties of materials in the square would be replaced by the effective volume of each mechanical property. It is very difficult to get a good representative cell. This concept has extracted many articles which propose their research in finding the best fitted RVE that is suitable to their specific application [58–60].

4.1.1 Mesh Method

To successfully implement a FEA, the meshing methodology is important to locate joint points (nodes) and continuous elements over the modelled object. There are several meshing methods such as lines for one-dimensional models, triangles and quadrilaterals for two-dimensional models, and tetrahedral, triangular prisms and hexahedra for three-dimensional models. Fig-

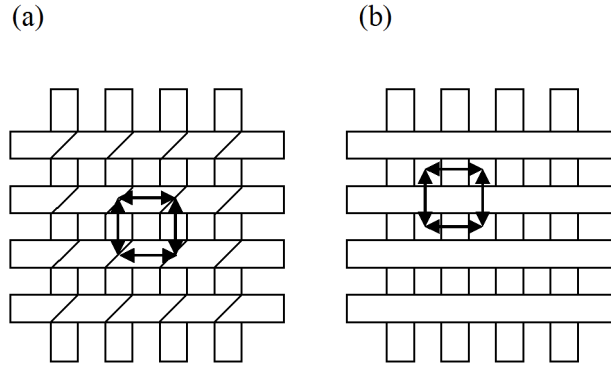


Figure 4.1: Typical models of Finite Element Method (a) stitched unit cell of a NCF, (b) a closed-form RVE of the same fabric.

Figure 4.2 exhibits samples of these mesh methods and typical elements shapes in them. FEA accuracy can be improved when more elements and correct mesh methods are used. However, the simulation will then spend much more computing resources, as more elements and meshes mean larger numbers of equations to be solved.

4.2 Simulation with ABAQUS

ABAQUS is a well-known commercial FEA software originally developed by HKS, USA, and now is under SIMULIA of Dassault Systemes. It has a full capability of performing coupled thermo-electrical analysis as described in its documentation. In ABAQUS, while coupling, electrical conductivity can be temperature-dependent, and the internal heat can also be a function of electrical current. Theories of thermo-electrical applications in ABAQUS are such that the solver of electrical problem is based on Ohm's law equation for the flow of the electrical current, then it derives the amount of thermal energy generated by electrical current (Joule heating); the solver of thermal part is essentially based on heat conduction; however, it could be extended to heat convection and radiation from its library [61].

The coupled thermo-electrical problem is an unsymmetrical problem. It is impossible to

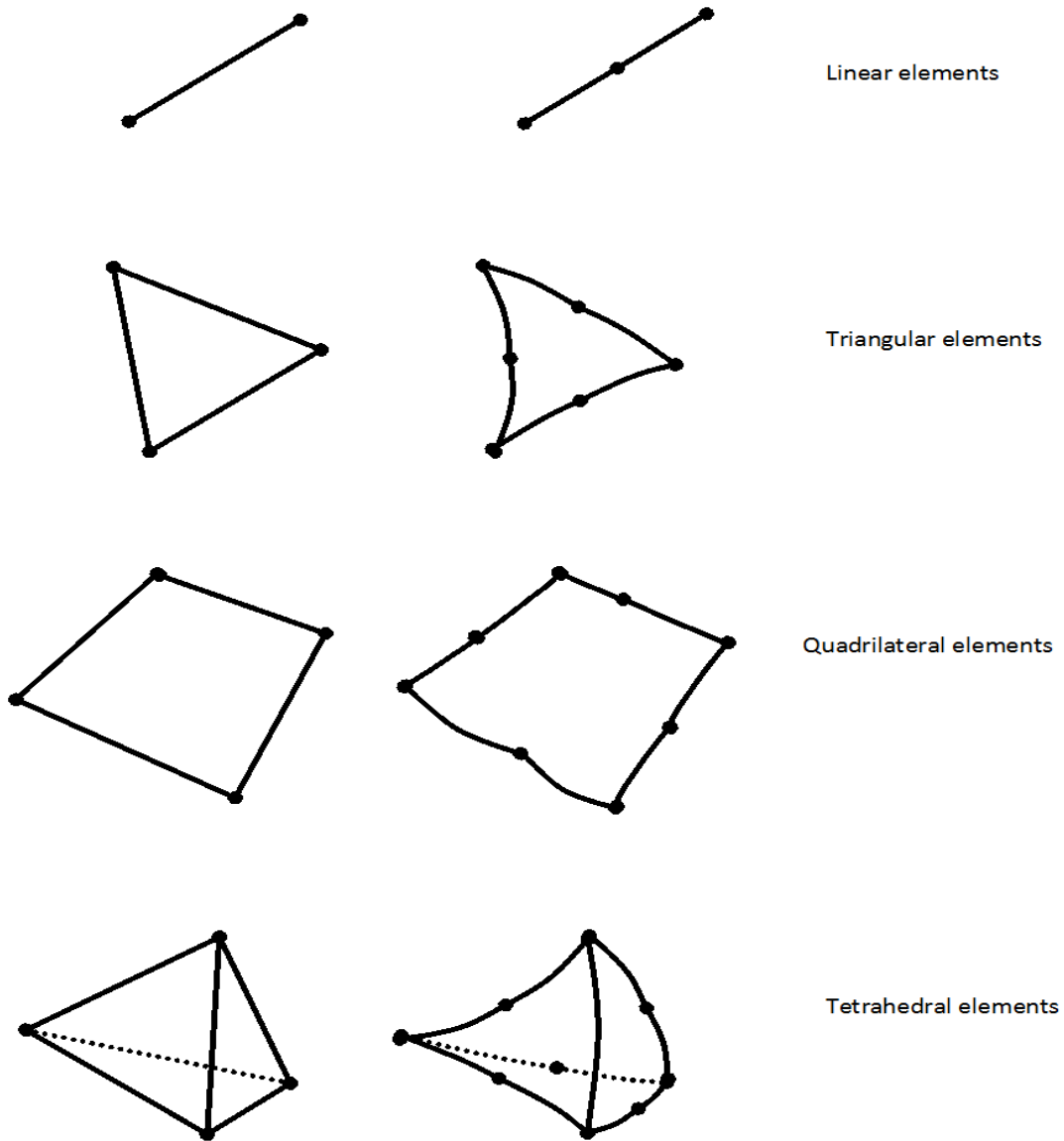


Figure 4.2: Typical finite element shapes and mesh points in one through three dimensions.

calculate thermal and electrical evaluations simultaneously. It has to first reach the convergence of either the thermal or the electrical solution, then couples the solution of the first solver to the other solver, reaches the convergence of the new problem and couples back to the first solver, and so on, until both solvers are convergent and the system equilibrium is reached. There are two types of coupled thermo-electrical analysis in ABAQUS - exact and approximate Newton's methods.

The exact implementation has a non-symmetric Jacobian matrix to represent the coupled equations:

$$\begin{bmatrix} K_{VV} & K_{VT} \\ K_{TV} & K_{TT} \end{bmatrix} \begin{Bmatrix} \Delta V \\ \Delta T \end{Bmatrix} = \begin{Bmatrix} R_V \\ R_T \end{Bmatrix} \quad (4.1)$$

where ΔV and ΔT are the respective corrections to the incremental electrical potential and temperature. K_{ij} are submatrices of the fully coupled Jacobian matrix, and R_V and R_T are the electrical and thermal residual vectors, respectively.

The coupled thermo-electrical analysis will be quadratically convergent when the solution estimate is within the radius of convergence of the algorithm.

For problems with weak coupling between thermal and electrical solutions, ABAQUS uses the approximate implementation. The K_{VT} and K_{TV} are assumed to be relatively small to the components K_{VV} and K_{TT} . Equation 4.1 is turned to equation 4.2. The rate of convergence is not quadratic any more and depends strongly on the magnitude of the neglected coupling effect. This approximate method generally needs more iterations to achieve equilibrium, compared to the exact implementation of Newton's method.

$$\begin{bmatrix} K_{VV} & 0 \\ 0 & K_{TT} \end{bmatrix} \begin{Bmatrix} \Delta V \\ \Delta T \end{Bmatrix} = \begin{Bmatrix} R_V \\ R_T \end{Bmatrix} \quad (4.2)$$

In the implementations of this research, I use the exact implementation of Newton's method to execute the coupling thermo-electrical simulation.

The electrical and thermal conductivity value can be temperature dependent in particular applications. Applying the temperature dependence makes the problem complicated and increases the cost of calculations significantly. There are numerous articles using the results of ABAQUS simulation to compare them to experiments. To know the capability and accuracy of coupled thermal- electrical stimulation of ABAQUS, Wang and Hilali (1995) ran a comparison with an experiment in automotive electrical fuse [62]. They reported that the finite element analysis results are in some agreement with experimental results. The differences between the simulations in ABAQUS and experiments may be due to the type of model chosen, overestimated infrared temperature measurement, etc. Zhang, Zavaliangos, and Groza (2003) also reported that their electrical-thermal prediction using ABAQUS mostly match the experimentally observed values [63]. There are other papers that have used the coupled thermo-electrical simulation of ABAQUS in different areas such as in the powder compact/die/punch assembly during the spark plasma sintering process [27], or in blanking of electrically heated engineering materials [26].

For textile material analysis, ABAQUS/CAE has predicted the thermal transport behaviour of woven ceramic matrix composites with unit cell FE modeling [56], and tension and strain on meso-scale with representative volume element [64]. In ABAQUS, to draw a layout of a textile pattern is always a challenge. The difficulties are not only modelling in shapes of fabrics but also planning designated contacts and boundary conditions. These reported woven models for simulations on mechanical properties in ABAQUS or other FEA tools chose Unit-Cell or RVE and expand the successful results to larger networks by uniform behaviour assumptions.

ABAQUS has capabilities of solving highly non-linear problems in various fields. The coupled electrical-thermal problem may not be as difficult as other coupling mechanical applications such as fluid-solid interactions. However, time and memory consumption are very large while applying the simulations to a larger networks even for thermo-electrical problems.

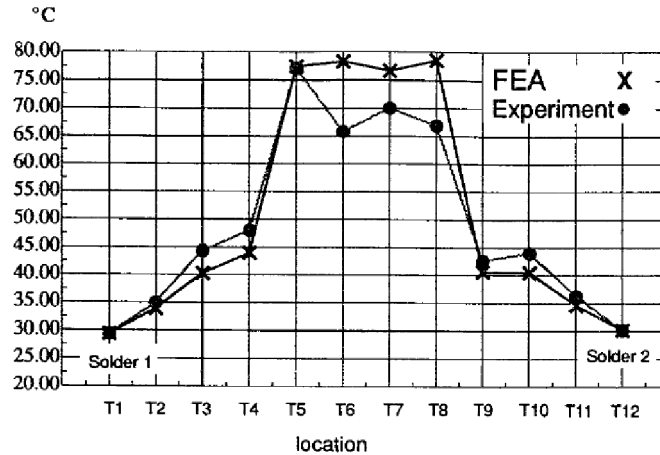


Figure 4.3: Comparison between the finite element and experimental results in a coupled thermo-electrical problem (cited from Wang and Hilali [62])

4.3 Summary

In summary, thermo-electrical simulation using ABAQUS is a convenient and efficient tool for design, specially when there are no or limited experimental data. The more the elements or meshes included in a model, the more the accurate results would be in a simulation. The main reason that ABAQUS was chosen in this study to compare with Therminator3D program is that there are several published papers comparing their experimental results with simulations of ABAQUS based on finite element method [26][27][56][62][63][64]. Reports show that the results from ABAQUS have been reasonably accurate. I use ABAQUS to build the layouts of IC interconnects and textile composite models, run the simulations of thermal and/or electrical problems, and post-process the results. The next chapter will illustrate several examples of Therminator3D and ABAQUS and compare the results using the two programs. The main point of interest is to evaluate how Therminator3D (network-based approach) compared to ABAQUS (finite element method) under computation time and CPU memory criteria.

Chapter 5

Applications and Comparisons

In this chapter, the results of thermo-electrical simulations from Therminator3D will be compared with those of ABAQUS in different examples. For all simulations, I have used an identical MacBook machine, which has MAC OSX 10.5 OS, 4G RAM, Intel Core 2 Duo 2.4 GHz. The compiler for Therminator3D is gcc version 4.3. ABAQUS is installed in windows XP pro system VMFUSE virtual machine in the same MacBook. While performing the simulations of ABAQUS, I disable unnecessary running programs in MACOSX system and allow ABAQUS software in the VMFUSE could take as many resources of the MACOSX system as possible. In the first section, I verify the solutions of Therminator3D by basic layout examples. The following sections in this chapter present results of thermal simulations of Manhattan layout of IC interconnects with/without current, non-crimp fabric composites with temperature boundary conditions and with/without a body heat flux (current), woven fabric composites and 20 by 20 large network results. Finally, a large-scale model with multiple boundary conditions is demonstrated. The comparison of computation cost for each example case is shown in the end of the example. A summary of performance of Therminator3D is given in the last part of the chapter.

5.1 Basic Layout Examples: Verification of Therminator3D

It is first necessary to verify the accuracy of solution of Therminator3D in basic problems before I continue my simulations in more complex problems. Let us start with a single wire (with dielectric) simulation which has a current of 0.001 A in the wire. The size of wire is

$10\mu m \times 10\mu m \times 400\mu m$ (width x depth x length). The layout is shown in Figure 5.1. Results of this thermo-electrical simulation are shown in Figure 5.2. Materials of the wire and dielectric are given in Table 5.1. The results of the exact calculation from Equations (2.14) and (2.15), Therminator3D, and ABAQUS are well matched. For example, on node ($x=22.5\mu m$), the temperature calculated using ABAQUS was $10.674200^\circ C$, the exact calculation from Excel resulted was a temperature of $10.673000^\circ C$, and for Therminator3D the temperature was $10.672037^\circ C$. The percentage of difference of exact calculation and Therminator3D simulation is 0.01%. The total number of nodes and elements in Therminator3D were 11 and 12, respectively. I minimized the meshes of ABAQUS to 10 elements which formed 44 nodes to make it close to Therminator3D. The percentage of difference of exact calculation and ABAQUS simulation is 0.0112%. The percentage of difference of Therminator3D and ABAQUS simulation is 0.02%.

The next basic example is a layout of three wires with the same size. The system was heated in the middle wire by an electrical current (0.001 A). The layout is shown in Figure 5.3 and the comparison of results is included in Figure 5.4. There is no exact calculation for this case because of the complexity of coupling behaviour among the three wires. However, I can compare the results between ABAQUS and Therminator3D. For the node position $x=22.5\mu m$ on the middle wire, the temperature calculated using ABAQUS was $9.107710^\circ C$, and for Therminator3D the temperature was $9.087000^\circ C$. The percentage of difference is 0.0227 %, which is slightly higher than the previous example with one-wire.

Results of these two simple layouts suggest that Therminator3D can perform thermo-electrical simulations as accurate as ABAQUS. Next, I move forward to more complicated simulation cases in IC interconnects, textile materials and finally large-scale networks. I will compare results from the two programs with respect to their simulation time and the CPU/memory used.

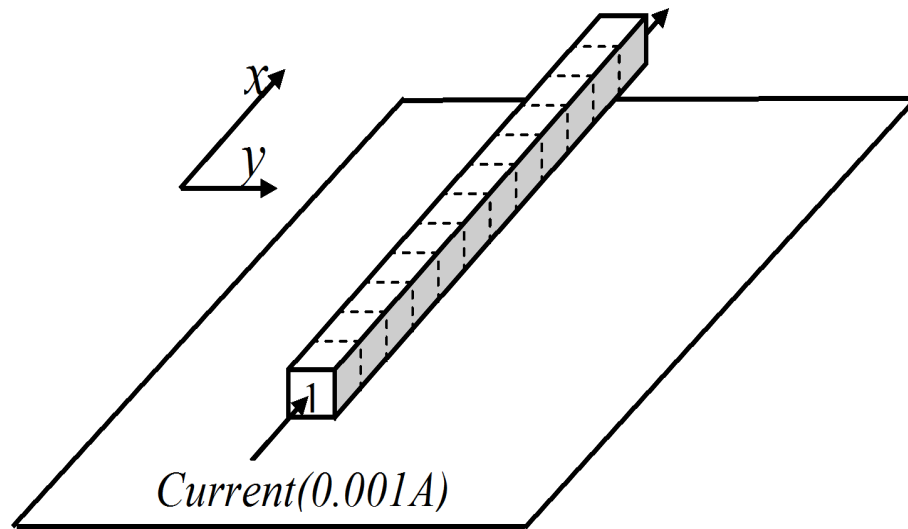


Figure 5.1: The layout of one wire simulation.

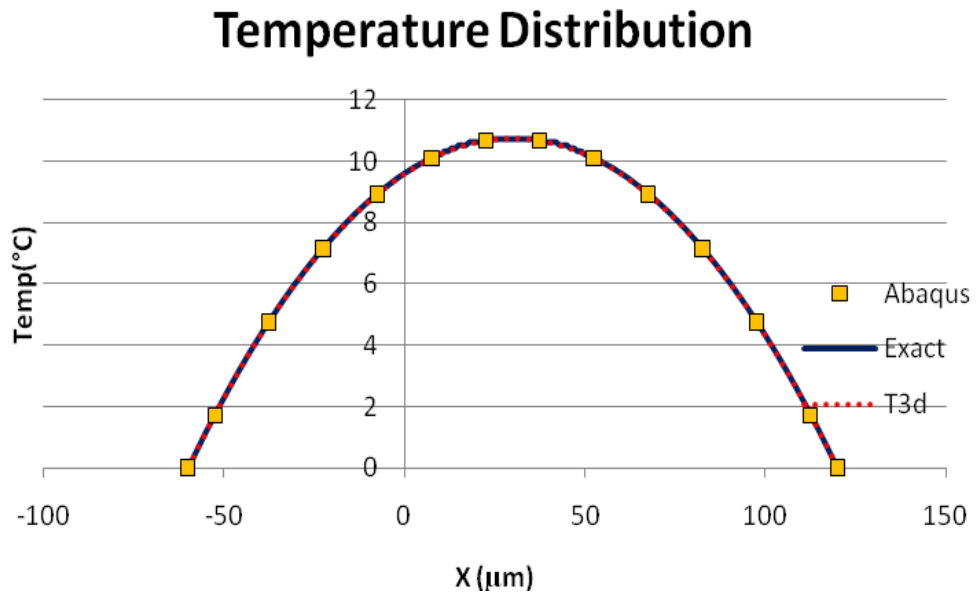


Figure 5.2: The temperature distribution of one wire simulation.

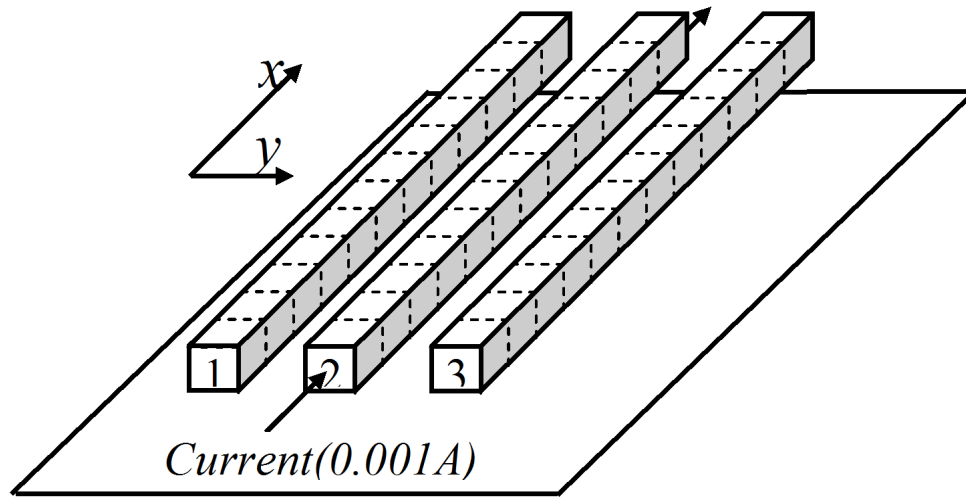


Figure 5.3: The layout of three-wire simulation

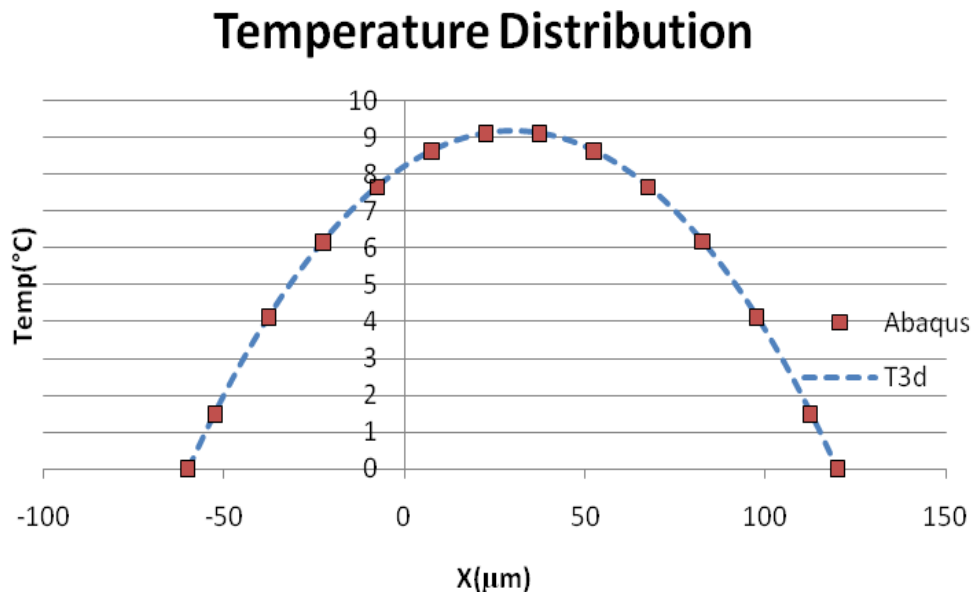


Figure 5.4: The temperature distribution of three-wire simulation.

Table 5.1: Material properties used in simulations adjusted by narrow-line effects [46] [65]

| | Material | Thermal Conductivity (W/m-K) |
|-----------------------|------------------|------------------------------|
| Wire (Row and Column) | Cu | 710 |
| Vias | Cu | 710 |
| Dielectric | SiO ₂ | 1.4 |

Table 5.2: Material properties used in simulations.

| | Material | Thermal Conductivity (W/m-K) |
|-----------------------|------------------|------------------------------|
| Wire (Row and Column) | Bulk-Cu | 401 |
| Vias | Bulk-Cu | 401 |
| Dielectric | SiO ₂ | 1.4 |

5.2 IC Interconnects Network

The IC interconnect modelling is a fundamental application of Therminator3D. The rapid and accurate simulations on IC interconnects by Therminator3D was originally demonstrated by Labun and Jagjitkumar [17]. In this section, I present two examples with Manhattan layouts. They are Joule heating simulations with and without a dielectric, and a fixed temperature boundary condition on one end of a wire.

A four-column by four-row, two-layer grid (Figure 5.5) was rendered as an RC network for Therminator3D, and written as a coupling file and a netlist file. Temperature and thermal flux boundary conditions were achieved using equivalent current sources and resistors at the end of the corresponding rows and columns (Figure 5.6). As shown in Figure 5.7, both electrical and thermal conductivities of wires are considered to be temperature dependent. The electrical and thermal conductivities of dielectric (matrix) are considered to temperature-independent. Each row and column was divided into 12 identical resistors. Each resistor coupled to those opposite

to it by the same G^{lat} value. The values of G^{lat} were calculated and calibrated by ABAQUS simulations. Each via was also represented by a resistor. For ABAQUS without dielectric, each resistor was modeled as a single, three-dimensional rectangular element (a “brick”). The coarsest mesh of a brick is consistent with an accurate FEA solution in order to minimize CPU time and memory. Dielectric fill required a more complex mesh in the finite element method. To simulate scenarios without vias in the presence of dielectric, the material type of via was simply changed to dielectric. In ABAQUS, I used a “tie” type of constraint without any space tolerance. The materials of wire and vias were copper and the dielectric was SiO_2 with properties shown in Table 5.1. The dimension of each interconnect is $10\mu m \times 10\mu m \times 120\mu m$ (WxDxL).

The selected mesh size in Figure 5.8 was to make a fair comparison between two simulations by ABAQUS and Therminator3D. More meshes in the ABAQUS’s model will increase the accuracy of simulations. However, it will also increase the consumption of computational resources. In Therminator3D, the inside temperature distribution of a resistor is calculated by equation (2.14), which is based on an analytical solution as opposed to the approximation used in FEA.

Two examples were executed: a passive thermal problem with vias and a Joule heating problem without vias.

The temperature distribution in the passive network was calculated by Therminator3D (Figure 5.8 (a) and (b)). The ABAQUS model with an automatic incrementation found the temperature contours shown in Figure 5.8 (c) and (d). Figure 5.9 shows the consistency of temperature solution along column 3, obtained by both Therminator3D and ABAQUS. The CPU time for these cases (Table 5.3) is the average of three simulation runs; note that due to the variation of actual user- and system- time from one run to another, the total time and memory on the same machine is somewhat variable for each result.

ABAQUS meshes the dielectric, and it significantly increases the number of nodes N , the CPU time, and memory requirements (Table 5.3). The network of Therminator3D does not

require more nodes to include dielectric heat conduction, but instead couples through the dielectric by updating T^{ref} on each resistor while it iterates the evaluations. Therminator3D's CPU time is dominated by the $O(N^3)$ symbolic solution. Iterative evaluations require $O(N)$ operations and incur negligible incremental CPU time.

The next example is to remove all vias and apply the electrical current (0.01 A) on column 3. The temperatures of endpoints of all interconnects are set to 0 °C. The resulting temperature distribution calculated by Therminator3D for this network is shown in Figure 5.10 (a) and (b). A similar model was established in ABAQUS with automatic incrementation and the temperature contours were plotted in Figure 5.10 (c) and (d). Figures 5.10 to 5.12 show the consistency of the temperature distribution, obtained by Therminator3D and ABAQUS. Overhead dominates ABAQUS CPU time for small number of elements, but for larger problems (such as the cases with dielectric) CPU time scales with the number of iterations.

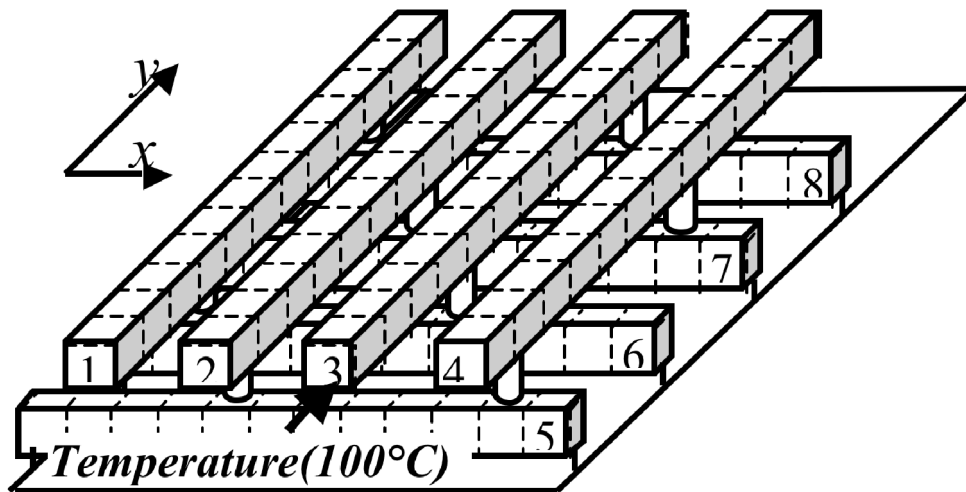


Figure 5.5: Four-by-four, two-layer grid with vias showing approximate segmentation into connected resistors. Temperature at each end and on substrate is set to $T = 0$ °C, except $T = 100$ °C is applied to one end of interconnect 3. Note that here both electrical and thermal conductivities of wires are assumed to be temperature dependent (i.e., non-linear analysis). The porosity of SiO_2 is considered to be 0 %.

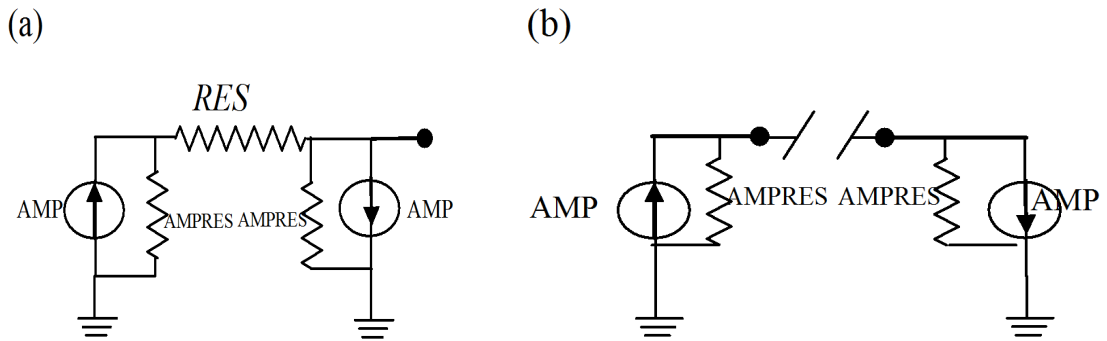


Figure 5.6: Boundary Conditions achieved by equivalent circuit source and resistors (a) Temperature boundary condition circuit schematic (b) Heat flux boundary condition circuit schematic.

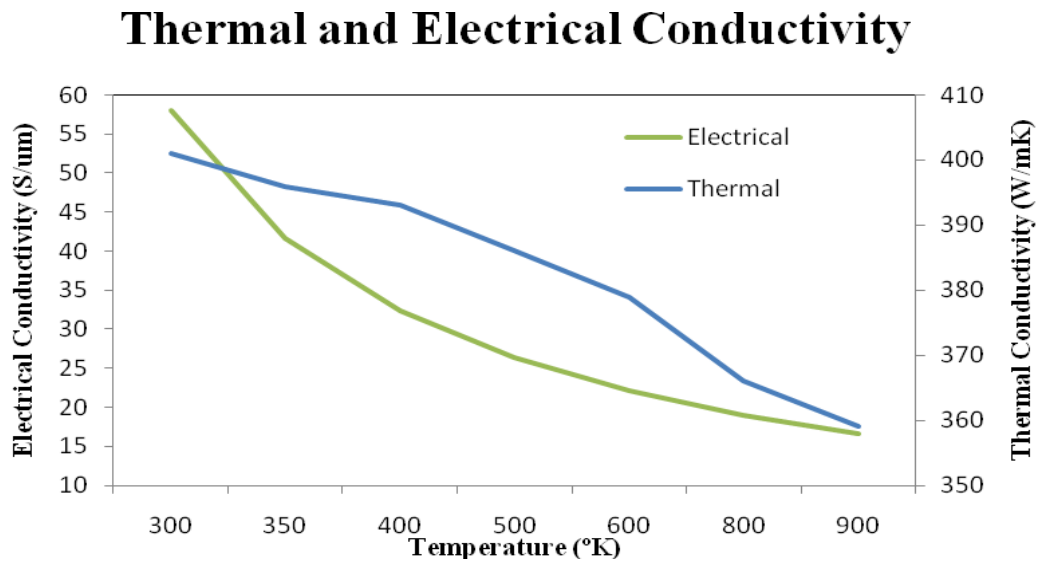


Figure 5.7: Temperature-dependent thermal and electrical conductivities of copper.

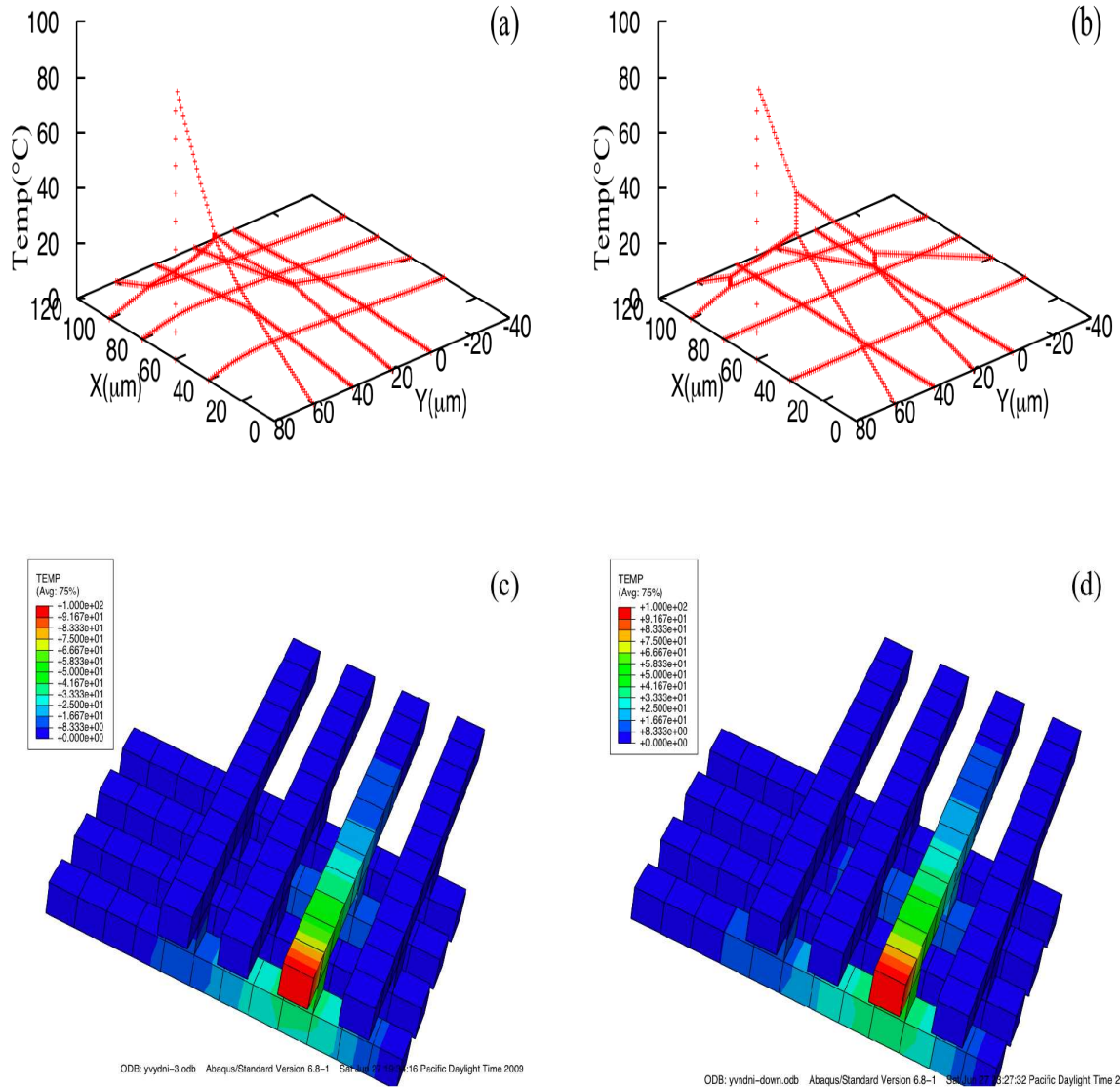


Figure 5.8: Interconnect temperature distribution for the network shown in Figure 5.5 computed by Therminator3D with (a) and without (b) dielectric, and by ABAQUS with (c) and without (d) dielectric ($T=100^{\circ}\text{C}$ applied to the end of column 3 at $(x,y)=(80,60)$); note: the dielectric material mesh around the wires is not shown in figures (c) and (d).

Table 5.3: Comparison of CPU time and memory required by Therminator3D and ABAQUS for Joule heat analysis with temperature-dependent electrical and thermal conductivities.

| | Dielectric | Number of Elements | CPU Time(sec) | Number of Iterations | Minimum Memory Required |
|-------------------------------|------------|------------------------------|---------------|----------------------|-------------------------|
| <i>T3D</i> Fig. 5.8(a) | <i>yes</i> | 96 + 8 (vias) (104 nodes) | 0.063 | 12 | 2.6 MB |
| <i>ABAQUS</i> Fig. 5.8(c) | | 741 (2212 nodes) | 12.0 | 7 | 24 MB |
| <i>T3D</i> Fig. 5.8(b) | <i>no</i> | 96 + 8 (vias) (104 nodes) | 0.054 | 11 | 2.5 MB |
| <i>ABAQUS</i> Fig. 5.8(d) | | 104 (480 nodes) | 1.1 | 7 | 18 MB |
| <i>T3D</i> Fig. 5.10(a) | <i>yes</i> | 96 (96 nodes) | 0.053 | 13 | 2.5 MB |
| <i>ABAQUS</i> Fig. 5.10(c) | | 741 (2212 nodes) | 19.8 | 13 | 24 MB |
| <i>T3D</i> Fig. 5.10(b) | <i>no</i> | 96 (96 nodes) | 0.049 | 13 | 2.5 MB |
| <i>ABAQUS</i> Fig. 5.10(d) | | 96 (416 nodes) | 1.1 | 9 | 18 MB |

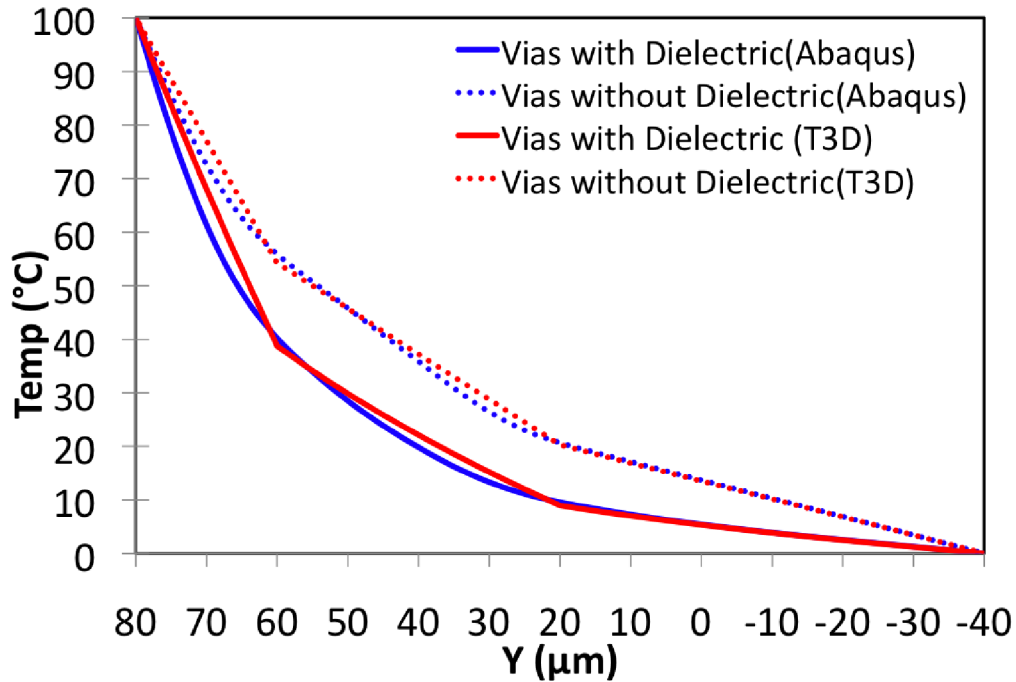


Figure 5.9: Comparison of column 3 temperature distribution in Figure 5.5, calculated by Therminator3D and ABAQUS.

5.3 Non-Crimp Fabric Network

In this section, I simulate non-crimp fabric network model which may be an interpreted IC interconnects model. The overall layout of non-crimp fabric is made by layers with stitches that fix the fabric shape. I can conveniently translate the whole non-crimp fabric network into an interconnect network. The yarn of NCF materials is analogous to the interconnect of IC circuits. The vias, which can be assigned different values in Therminator3D, express the contact behaviour between yarns in NCF. The dielectric in IC circuits is analogous to the resin material in NCF networks. Overlapping yarns are assumed to be in perfect contact without a gap. The resin material is analogous to the 0% porosity SiO_2 .

A dry biaxial NCF structure made of copper is considered. In Therminator3D, only longitudinal and overlap contact thermal conduction is assumed (i.e., $G^{lat} = 0$ for all rows and columns of the network). The latter assumption was to simplify the problem for comparison purposes with other FE models. The size and computational cost of Therminator3D analysis

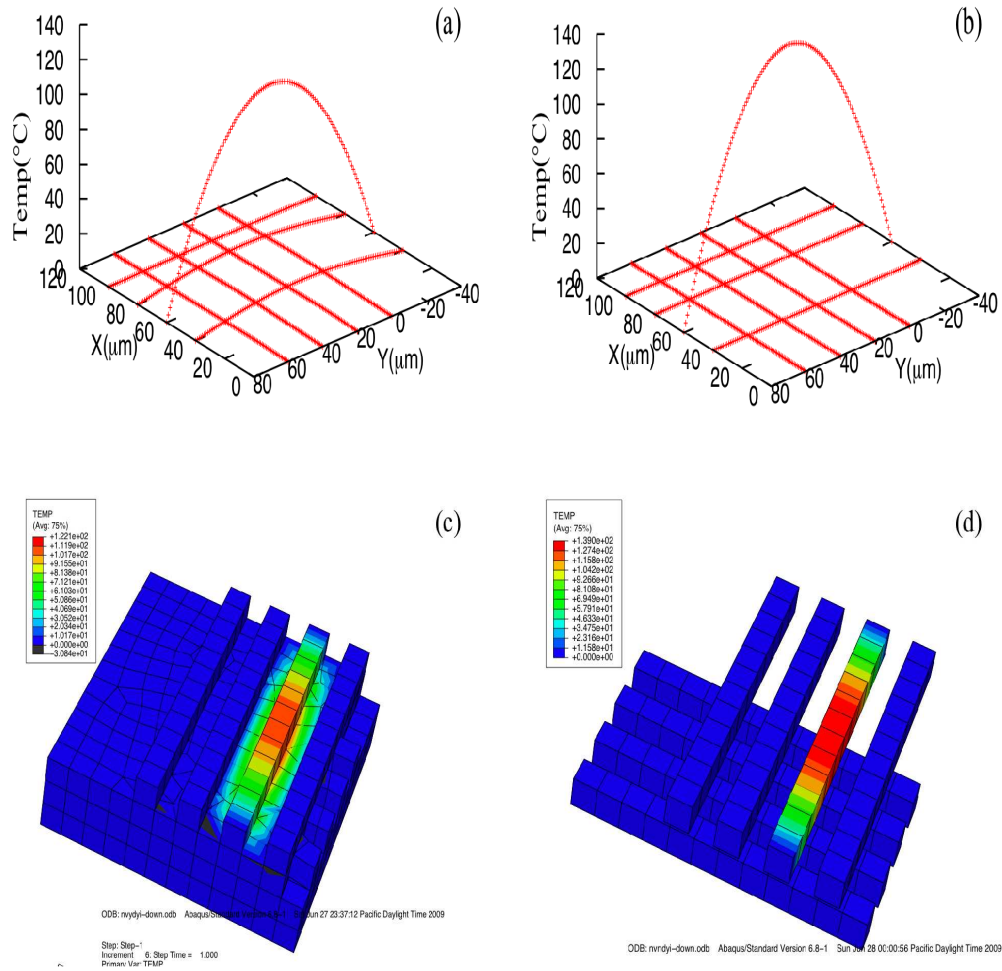


Figure 5.10: Interconnect temperature distribution for the network shown in Figure 5.5 with vias removed, computed by Therminator3D with (a) and without (b) dielectric, and by ABAQUS with (c) (partial cut-view) and without (d) dielectric ($I_{rms} = 0.01$ Amp through column 3). Notice that in the ABAQUS model, the dielectric material should be actually meshed.

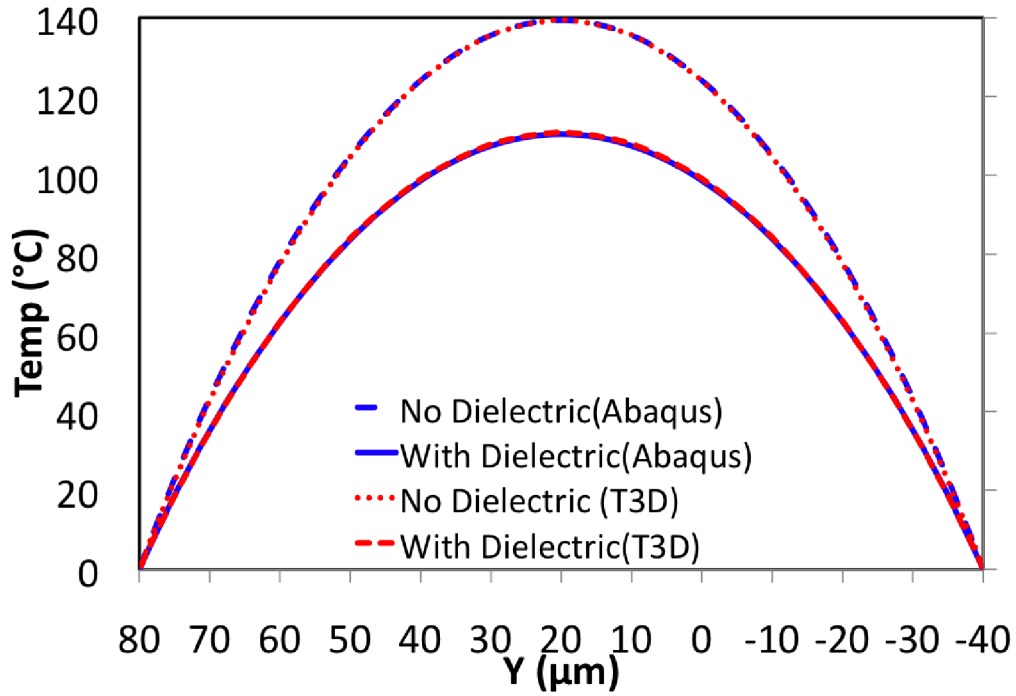


Figure 5.11: Comparison of column 3 temperatures shown in Figure 5.5 with vias removed, calculated by Therminator3D and ABAQUS.

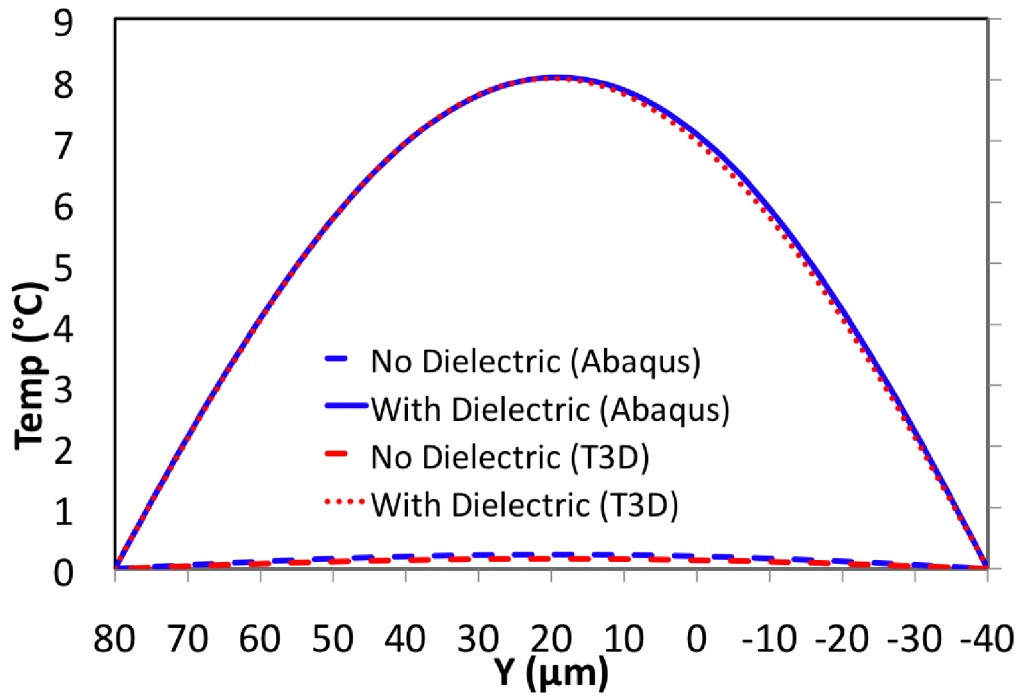


Figure 5.12: Comparison of column 4 temperature distribution in Figure 5.5 with vias removed, calculated by Therminator3D and ABAQUS.

was not significantly affected by the neglect of lateral thermal conduction [17]; note that the inclusion of G^{lat} would result in an unsymmetrical system matrices based on the two different orders of differential equations appearing in Equation 2.11. It is also assumed that there are no Joule self-heating and no heat loss into the environment (adiabatic condition). Vias, with relatively small dimensions compared to the interconnect ($G^{lat} = 0$), represent a perfect thermal contact between overlapping yarns. Nodal temperature (i.e., essential) and thermal flux (i.e., free) types of boundary conditions were achieved using equivalent current sources and resistors at the end of corresponding rows/columns.

The first test problem is shown in Figure 5.13, which consists of a four-by-four, two-layer grid. The thermal conductivity was assumed to be constant. Values of material properties used are given in Table 5.2. Each yarn is $10 \mu m \times 10 \mu m \times 100 \mu m$. The resulting temperature distribution in the network was calculated by Therminator3D and is shown in Figure 5.14(a). A similar model was established in the ABAQUS finite element package with automatic incrementation and the temperature contours were obtained (Figure 5.14(b)). Figure 5.15(a) shows the temperature variation along column 7, obtained by T3D and ABAQUS. Next, the procedure was repeated by allowing a variation of conductivity with temperature (similar to the example in Figure 5.5). Comparison of results for the new nonlinear case is shown in Figure 5.15(b). Table 5.4 also includes results for an unbalanced NCF where the thermal conductivity value of rows is doubled (for columns, it was unchanged).

Table 5.4 compares the CPU time required for these two examples using T3D and ABAQUS in an Apple MacBook. Each value shown is the average of three repeats of a computer experiment; note that due to the variation of actual user- and system- time from one repeat to another, the total time in the same machine can be non-repeatable. Values in parentheses refer to the CPU times normalized by the number of temperature nodes (DOF). The temperature trajectory for the temperature-independent thermal resistance case is found in a single T3D evaluation. As compared to ABAQUS results, the convergence of the self-consistent temperature calculation for the temperature dependent case was faster in T3D due to the linear time required for

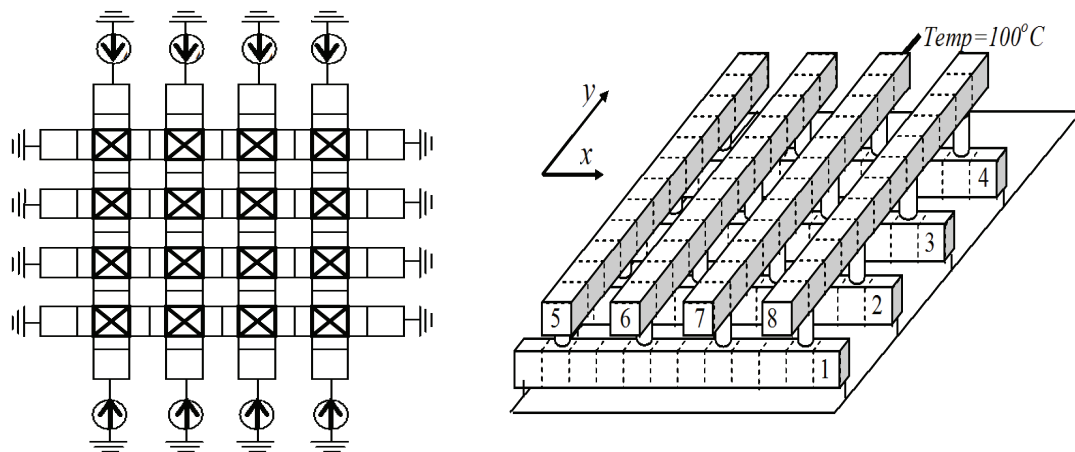


Figure 5.13: An NCF represented by a two-layer interconnect grid with vias showing approximate segmentation into connected resistors. All endpoint temperatures are set to $T = 0\text{ }^{\circ}\text{C}$ except $T = 100\text{ }^{\circ}\text{C}$ is applied to one end of interconnect/yarn 7. To mimic a dry fabric, the zero porosity of dielectric can be used in Therminator3D.

the evaluation of the symbolic solution. For example, the computation time was 0.056 second using T3D and 1.53 second using ABAQUS. The estimation time of T3D is 29 times faster than that of ABAQUS (80 elements). From Figure 5.15(a), I notice that in ABAQUS I require a large number of elements (640 elements) to achieve a temperature distribution almost identical to that of T3D with 80 elements (this would suggest that the convergence rate of solution during mesh refinements would be faster in T3D). For example in temperature independent case, the temperature calculated using Therminator3D was $36.1\text{ }^{\circ}\text{C}$, ABAQUS (80 elements) was $37.6\text{ }^{\circ}\text{C}$, and ABAQUS (640 elements) was $36.3\text{ }^{\circ}\text{C}$ on the point at coordinate $x=60\text{ }\mu\text{m}$ and $y=0\text{ }\mu\text{m}$. The temperature distribution calculated using T3D was close to that using ABAQUS (640 elements).

Finally, a fourth example was chosen to demonstrate the application of T3D for thermo-electrical analysis of fabrics (e.g., for E-textiles where electronic components are embedded into a fabric structure). The NCF geometry of four-by-four, two-layer grid was considered and an electric current (0.001 Amp) was applied to interconnect 7 (Figure 5.16). Each wire is $10\text{ }\mu\text{m} \times 10\text{ }\mu\text{m} \times 180\text{ }\mu\text{m}$. In this case, the Joule heat creates a body heat flux through-

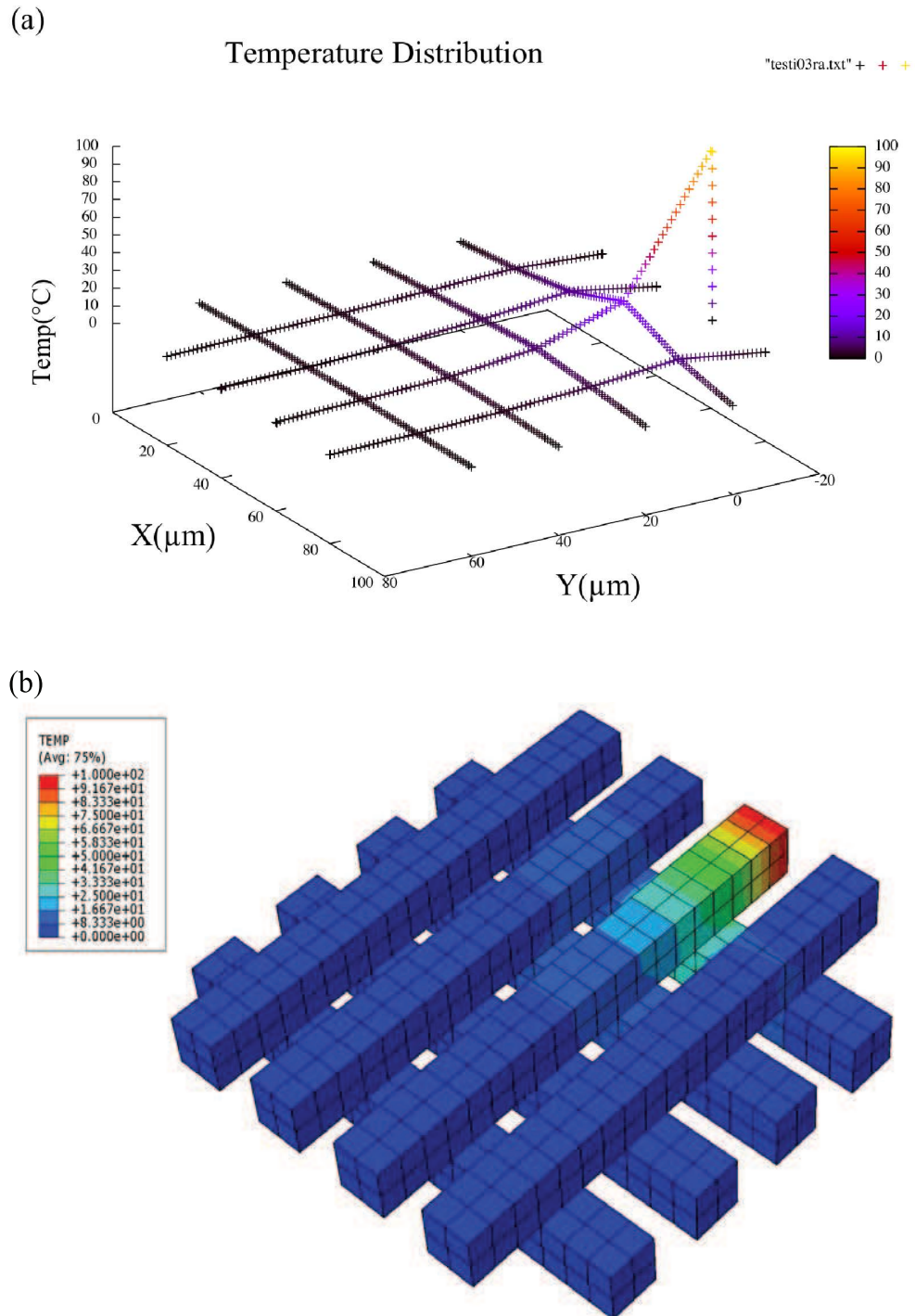


Figure 5.14: Interconnect temperature distribution for the network shown in Figure 5.13, computed by Therminator3D (a) by ABAQUS (b) ($T=100^{\circ}\text{C}$ applied to the end of column 7 at $(x,y)=(80,60)$).

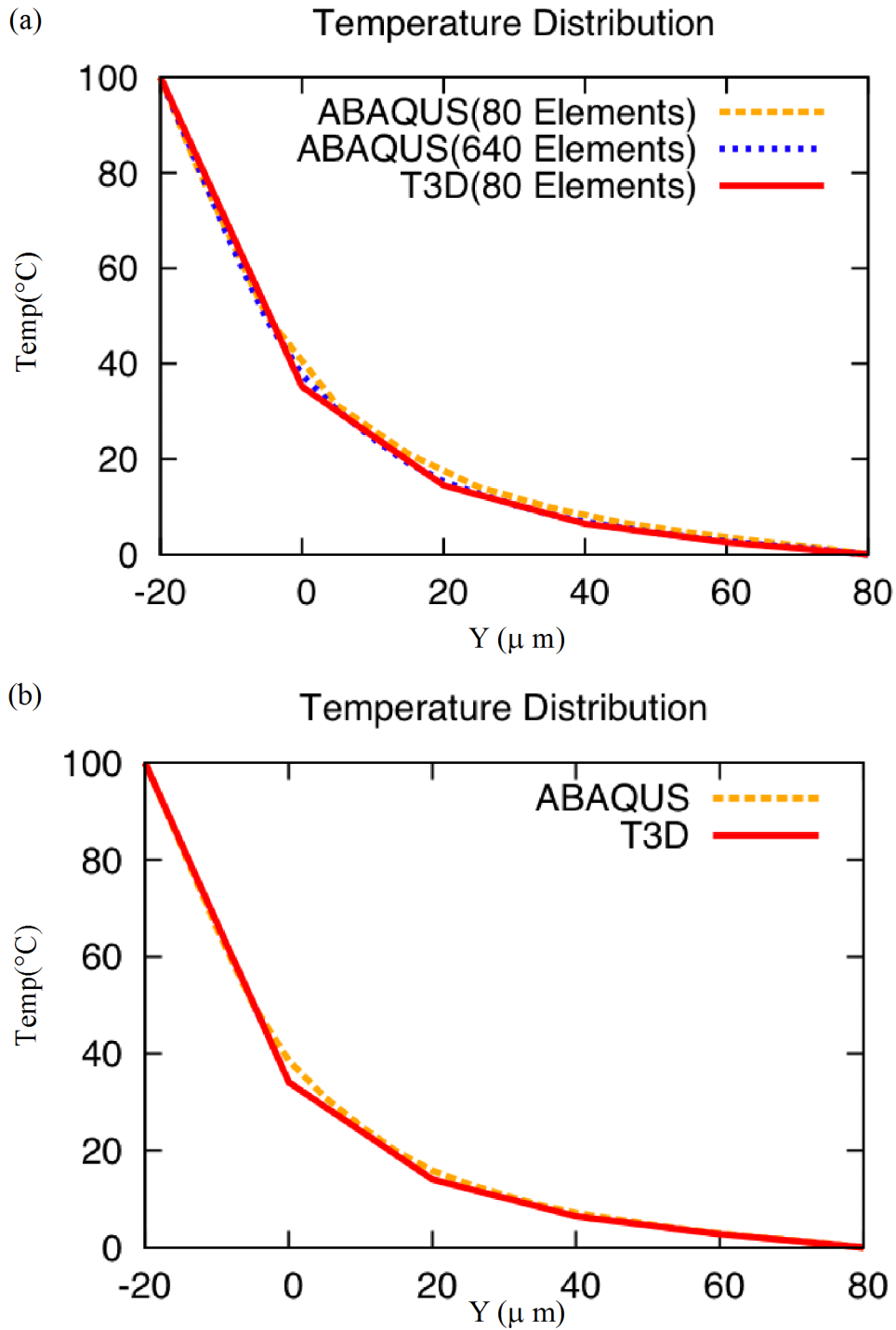


Figure 5.15: The row 3 temperature trajectory for the network in Figure 5.13, computed by T3D and ABAQUS with thermal resistance independent (a) and dependent (b) of temperature (results are for the balanced fabric case).

Table 5.4: Comparison of Therminator3D and ABAQUS CPU times for the heat analysis of a 4x4 metal non-crimp structure.

| | T3D | ABAQUS | ABAQUS |
|---|---------------------|--------------------|--------------------|
| No. of Elements | 80 | 80 | 640 |
| CPU Time (sec) for Temperature Independent Balanced NCF Example | 0.055 (6.88E-04) | 1.63 6.44E-03 | 3.03 (2.00E-03) |
| CPU Time (sec) for Temperature Dependent Balanced NCF Example | 0.056 (7.00E-04) | 1.53 (6.05E-03) | 2.93 (1.94E-03) |
| CPU Time (sec) for Temperature Dependent Unbalanced NCF Example | 0.057 (7.13E-04) | 1.66 (6.56E-03) | 2.96 (1.96E-03) |

out column 7. The result of the network calculation is shown in Figure 5.17 and the result of ABAQUS simulation is shown in Figure 5.18. Self-consistent thermo-electrical calculation with temperature-dependent thermal and electrical resistance required only 0.096 sec CPU time. Figure 5.19 shows the temperature comparison on all 8 wires. The temperature distribution lines of ABAQUS and Therminator3D along all 8 wires are reasonably matched.

5.4 Woven Fabric Composite Network

Woven fabric composite materials are composed of interlacing yarns with good mechanical properties, specially for impact applications. The exact shape of woven fibres is rather difficult to reproduce using CAD tools. Descriptions of the exact contact behaviours between fibres are also challenging. In Therminator3D, the shape of yarns can be represented by switching the coordinates of nodes in the NCF case and replacing new coupling data for the thermal and electrical capacitances. I have made a comparison of the two simulation (ABAQUS and Therminator3D) results in this section to show the potential of Therminater3D for thermal and electrical evaluations of woven materials.

The layout of the fabric considered is four by four dry plain weave wires (here, I also refer to the wires as yarns) with partial vias shown in Figure 5.20. The dimension of each yarn

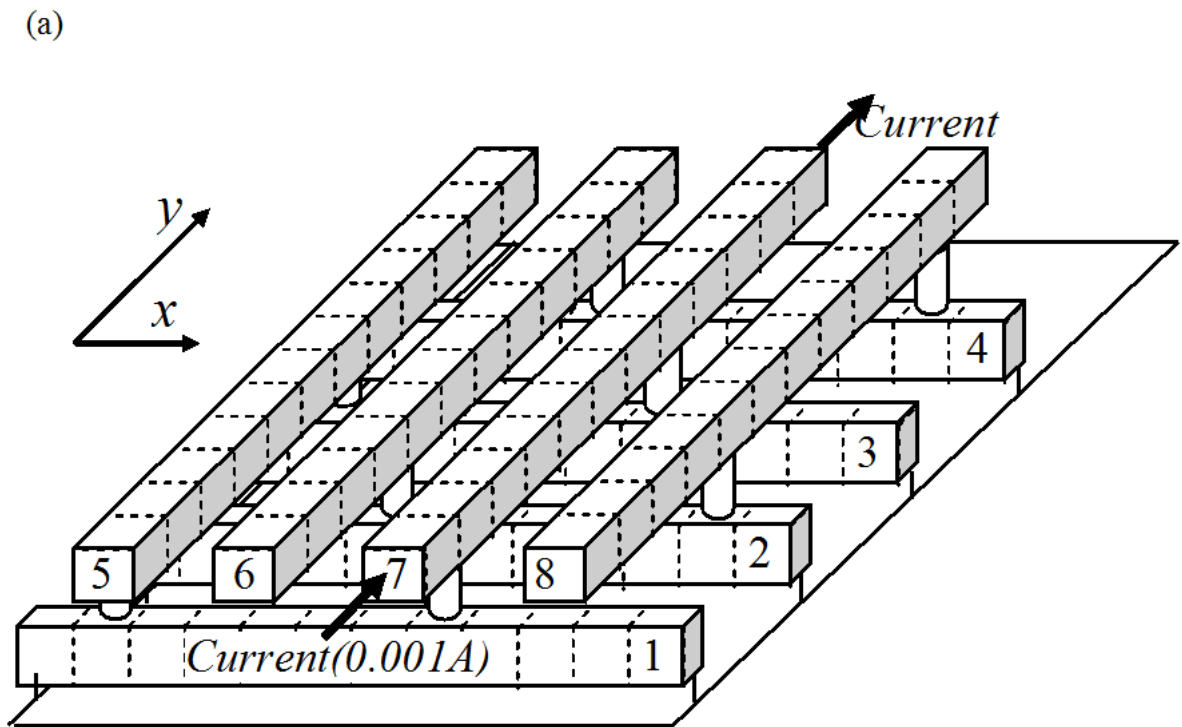


Figure 5.16: A two-layer interconnect grid layout with vias and Joule heat generated on interconnect 7.

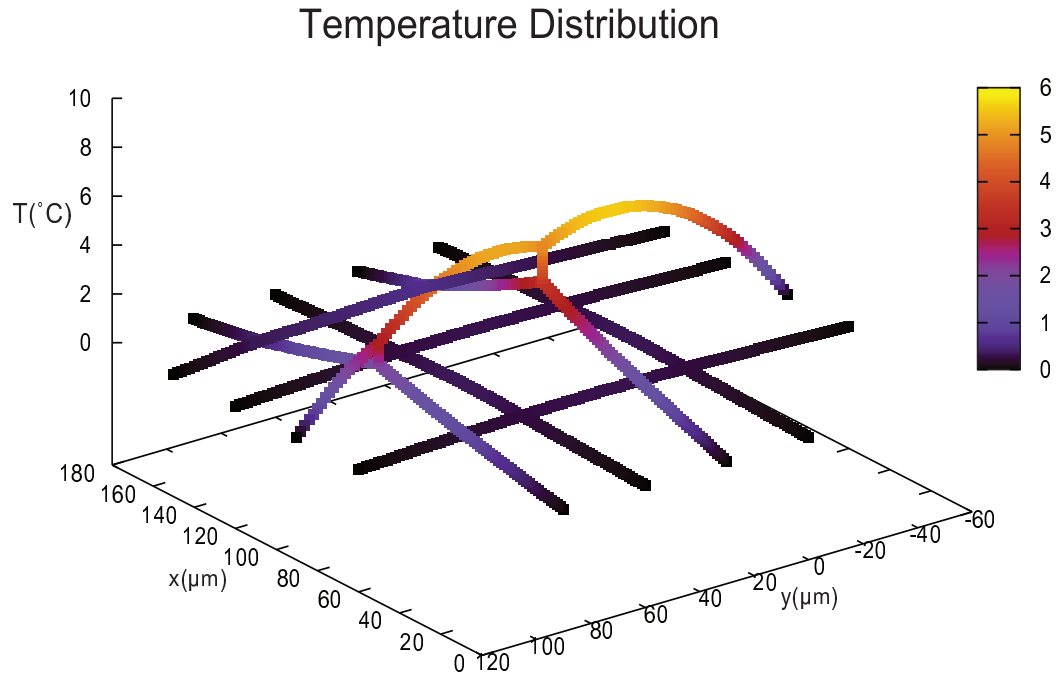


Figure 5.17: T3D implementation of NCF layout in Figure 5.16 .

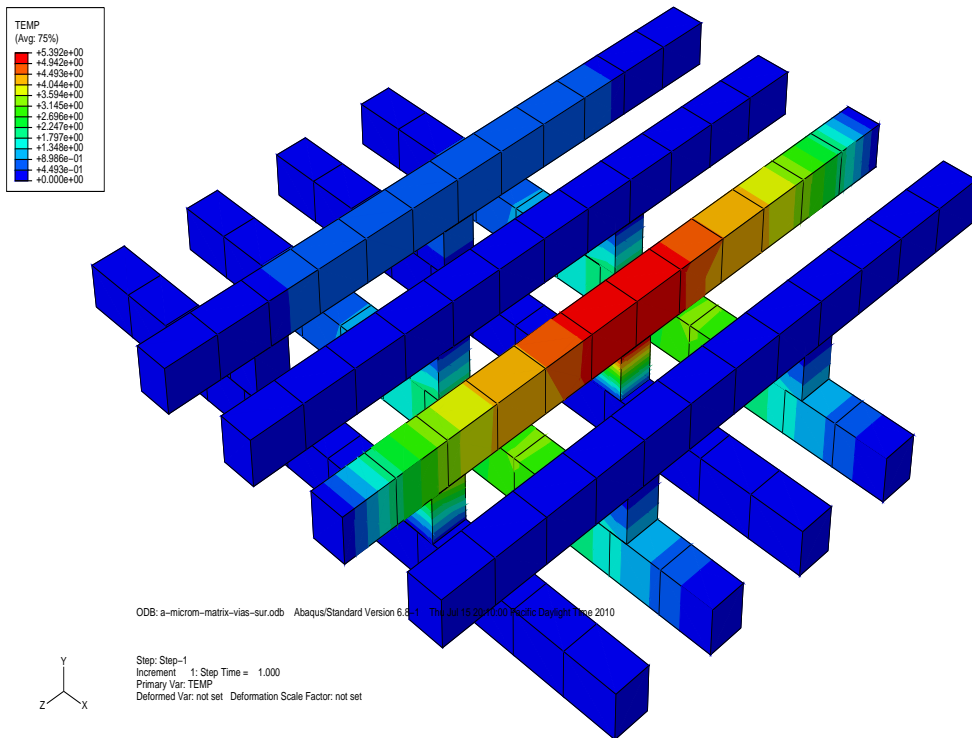


Figure 5.18: ABAQUS implementation of NCF layout in Figure 5.16 .

5.4. Woven Fabric Composite Network

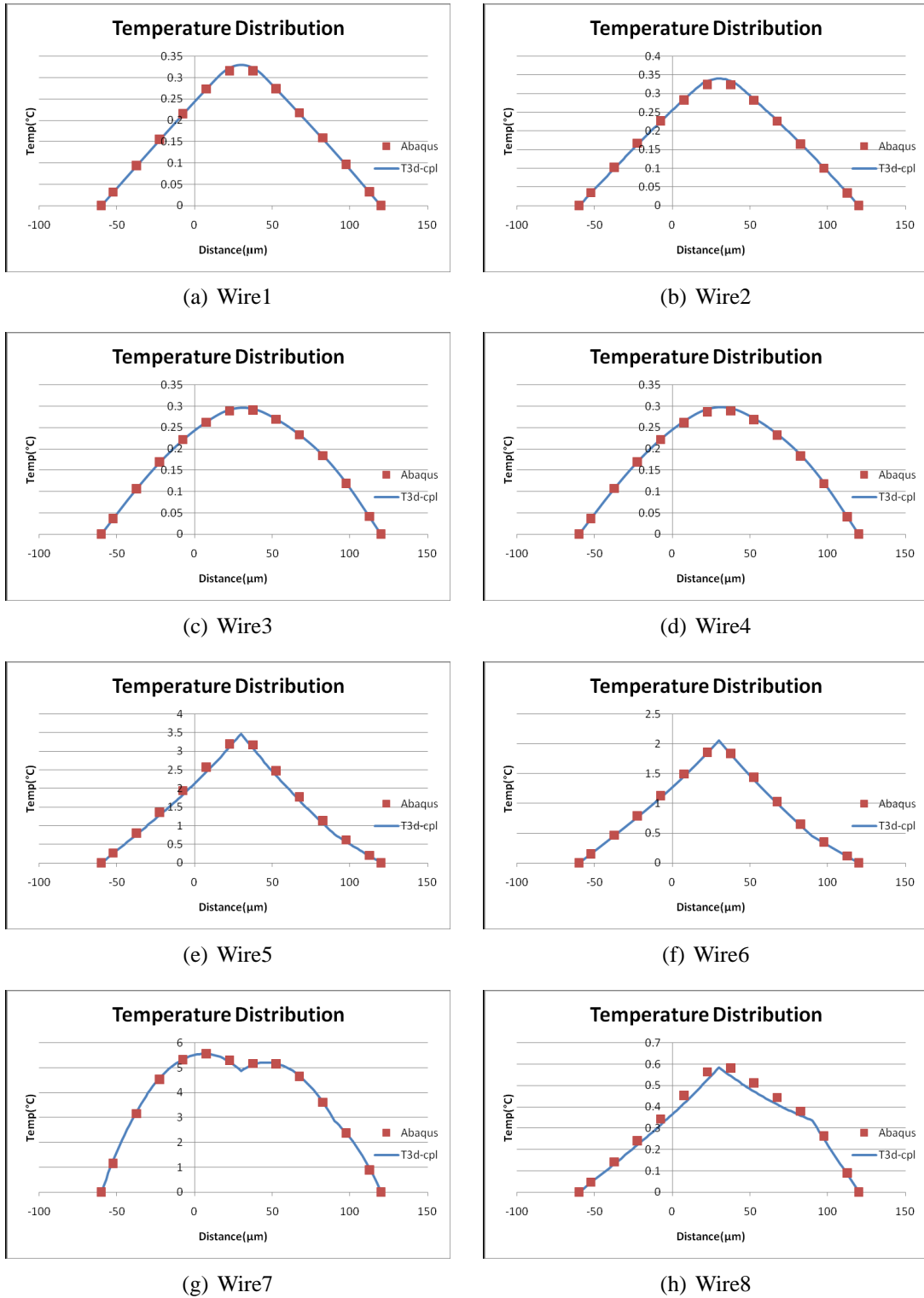


Figure 5.19: The comparison of all 8 wires between ABAQUS and Therminator3D with vias and heated wire 7

is $10\mu m \times 10\mu m \times 180\mu m$ (WxDxL). The material properties used are listed in Table 5.2. A current (0.001 AMP) was applied to yarn 5. The resulting temperature distributions of T3D and ABAQUS are shown in Figure 5.21 and 5.22, respectively.

To further evaluate differences between two simulations by ABAQUS and Therminator3D, I listed the temperature profiles of all 8 yarns in Figure 5.23. As a second test case, I applied the same current to yarn 7. Those temperature distributions on all 8 yarns have been shown in Figure 5.24. In the woven fabric case, since there is no simple method to compute the exact coupling data, I used a calibration with the results of ABAQUS to estimate the G^{lat} parameters (Figure 3.5). The Therminator3D results of all yarns are in a good agreement with the simulation of ABAQUS, except for yarn 7 in the first example (Figure 5.23) and for yarn 5 in the second example (Figure 5.24). The reason those yarns do not match well the temperature distribution lines of ABAQUS is the complexity of coupling behaviours estimated in Therminator3D. For example, the Therminator3D temperature of yarn 7 is colder than that of ABAQUS in the case of heated yarn 5 (Figure 5.23). In fact, in Therminator3D, there is no coupling data for yarns 5 and 7 to see each other. In future work, it is worth continuing to derive more comprehensive coupling formulas in order to obtain more accurate results from Therminator3D. In Table 5.5, I list the data of CPU time and memory required by Therminator3D and ABAQUS for the performed woven fabric simulations. The results clearly show that Therminator3D has higher speed and memory saving capabilities. The CPU time for the simulation of Therminator3D is 0.06 sec. The CPU time for the simulation of ABAQUS is 8.1 sec.

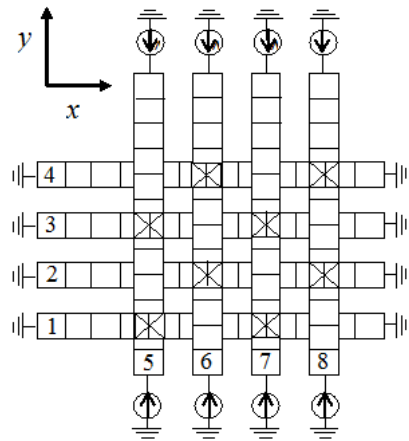


Figure 5.20: A woven fabric composites represented by a two-layer interconnect grid with vias showing approximate segmentation into connected resistors. The “X” indicate the yarn have vias presented and woven. All endpoint temperatures are set to $T = 0\text{ }^{\circ}\text{C}$.

Table 5.5: Comparison of CPU time and memory required by Terminator3D and ABAQUS on woven fabric materials. Cases for Joule heat analysis with temperature-independent electrical and thermal conductivities. A current of 0.001 AMP was applied to yarn 5

| | Dielectric | No. of Elements | CPU Time(sec) | Minimum Memory Required |
|---------------------|------------|--|---------------|-------------------------|
| T3D Fig. 5.21 | yes | 96 + 8 (Vias) +2 (Sky) (106 nodes) | 0.06 | 2.5 MB |
| ABAQUS Fig. 5.22 | | 12893 (3751 nodes) | 8.1 | 31 MB |

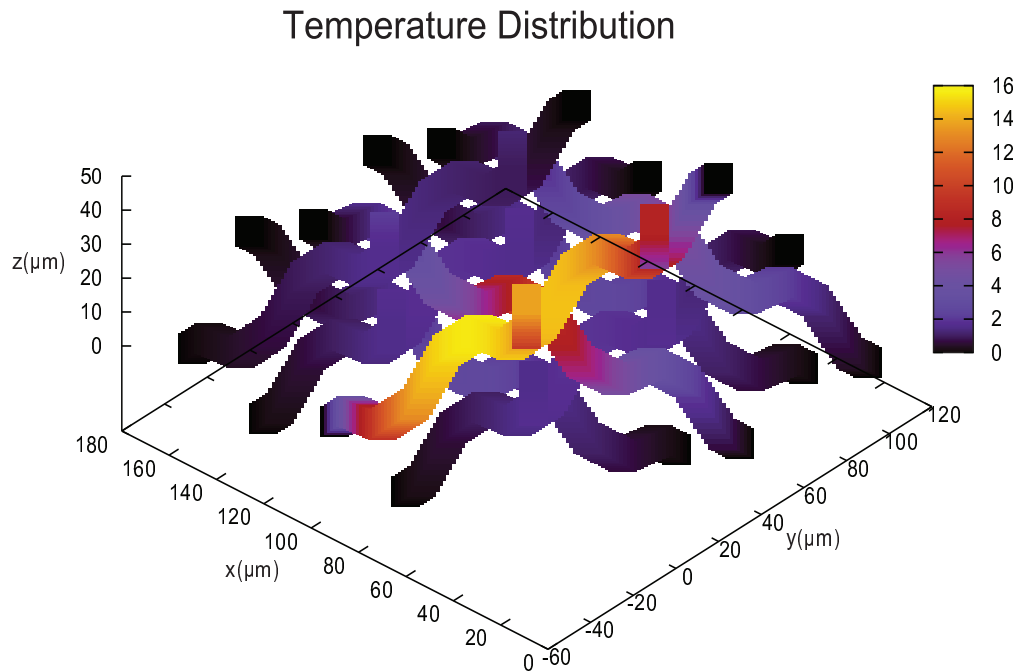


Figure 5.21: Yarn temperature distribution for the network shown in Figure 5.20, computed by Therminator3D.

5.5 Large-Scale Network Simulation

This research expects that Therminator3D has high capability to simulate large-scale networks. In this section, I use two examples to verify this. The first example shown in Figure 5.25 is a 20 (columns) by 20 (rows) network with vias. The dimension of each wire is $10 \times 10 \times 400 \mu m$ ($W \times D \times L$). The material properties are given in Table 5.2. The boundary condition is $0^\circ C$ temperature on substrate and a current of 0.001 AMP is applied to wire 3. This network has 1680 nodes including vias for Therminator3D and 45538 nodes for ABAQUS. The CPU time of simulation of Therminator3D was found to be 181.19 sec (including 179 seconds to form the symbolic solution and only 2 seconds for performing the numerical solution). The CPU time of simulation of ABAQUS was 391.70 sec. The symbolic solution in Therminator3D took most of the CPU time before entering iteration loops of numerical solution. The number of iterations in Therminate3D was 35 iterations (in ABAQUS, it was 2 iterations). However, the speed of

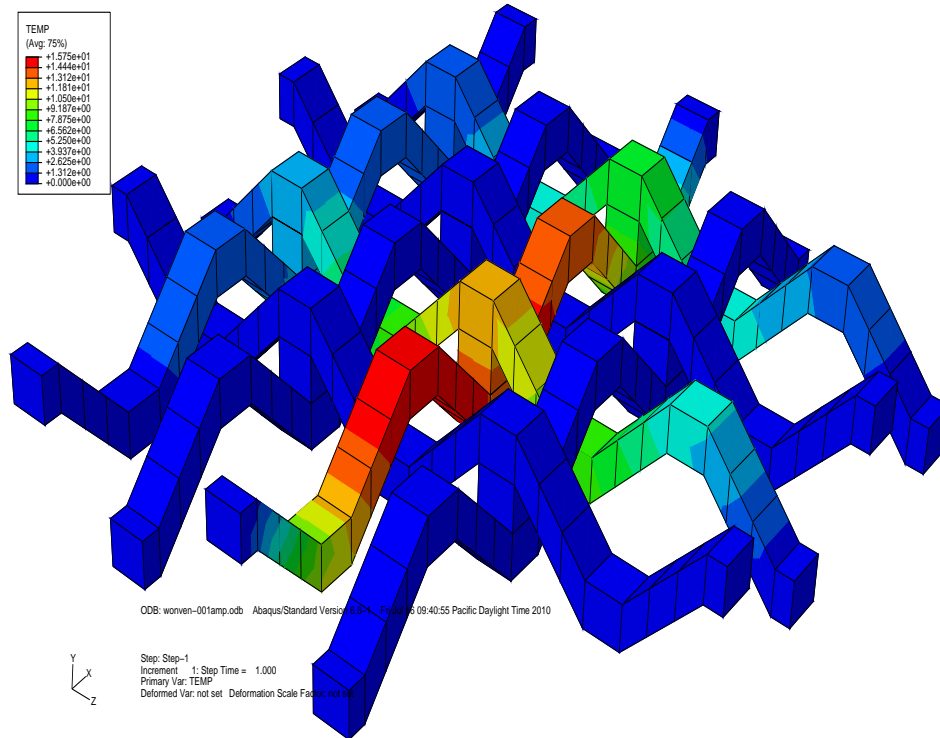


Figure 5.22: Yarn temperature distribution for the network shown in Figure 5.20, computed by ABAQUS.

iterations of Therminator3D was very fast, each iteration only took 0.0571 sec, compared to ABAQUS which took 185.85 sec.

The second example shown in Figure 5.26 is a 20 (columns) by 20 (rows) network without vias and a temperature of 0°C is applied to the ends of all wires and the substrate. It has 1680 nodes without vias for Therminator3D and 45538 nodes for ABAQUS. The CPU time of Therminator3D is 181.18 sec. The CPU time of ABAQUS is 325.40 seconds. When compared to the previous example, the CPU time of Therminator3D is not much affected by the presence or absence of vias. It also shows that Therminator3D's iterations only require $O(N)$ additional operations and do not correlate with CPU time.

Figure 5.27 shows the simulation results of Therminator3D program and Figure 5.28 shows the simulation results of ABAQUS program. From those two figures, the temperature distributions of T3D and ABAQUS are consistent. Table 5.6 shows that Therminator3D could reach the purpose of fast simulation on large scale networks. In these large-scale simulations, I found

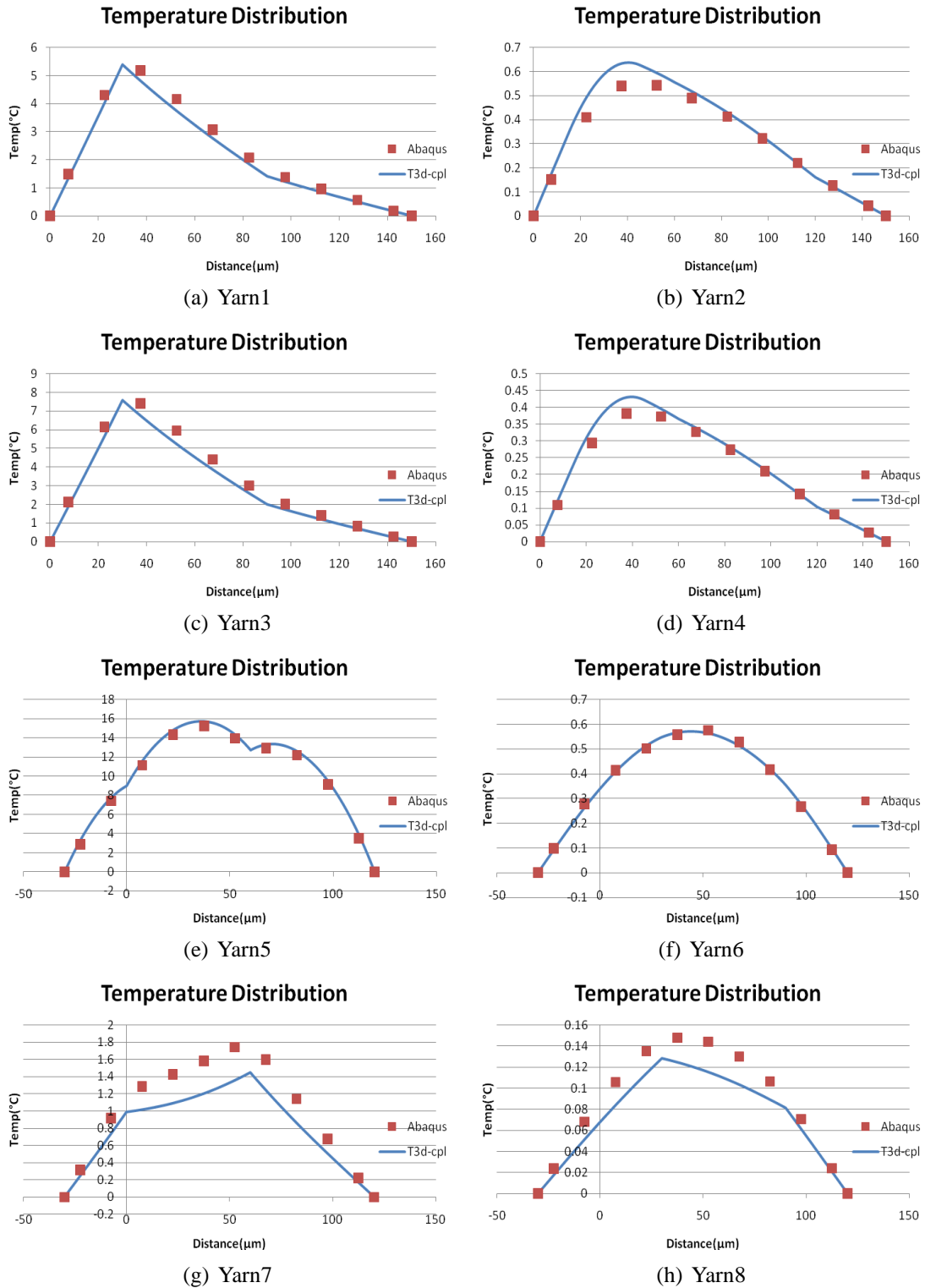


Figure 5.23: The comparison of all 8 yarns between ABAQUS and Therminator3D on woven case without vias and with heated yarn 5. (the dimension is changed to 10x10x180 (WxDxL) μm).

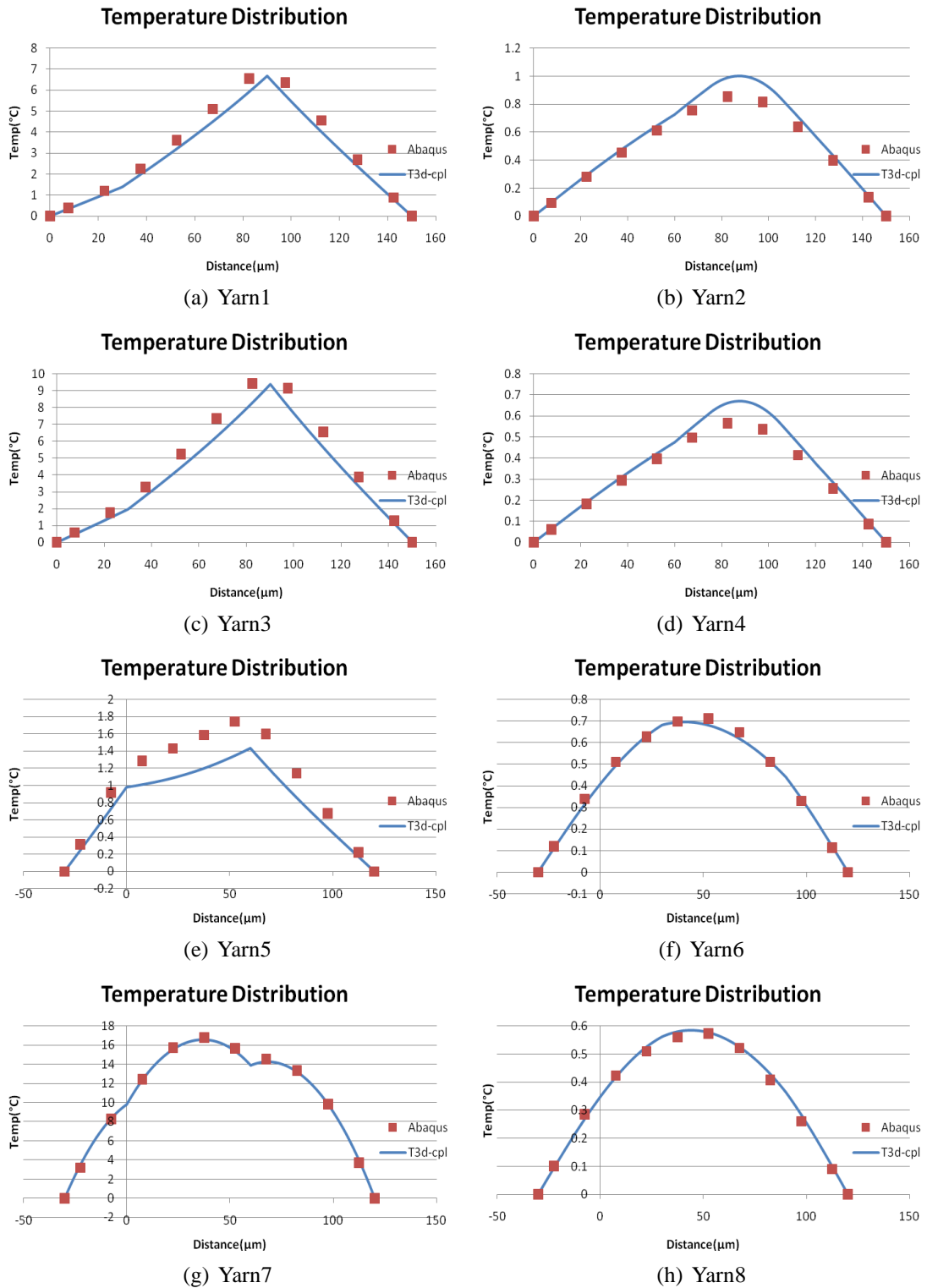


Figure 5.24: The comparison of all 8 yarns between ABAQUS and Therminator3D on woven case without vias and with heated yarn 7.

that the order of memory of the worst case (which has vias connected with columns and rows) to form the L and U matrices is near to N^3 . The reason such a large memory is required while the size of networks increased, is the solver of the Crout algorithm to form the linked-list hashtables of L and U matrices. However, the iteration time of numerical solution is hardly affected by the scale of network.

Finally, I include an additional simulation case of 18 (columns) by 18 (rows) with multi-boundary condition as shown in Figure 5.29. The dimensions of each wire is $10 \times 10 \times 400 \mu\text{m}$ (WxDxL) and its material properties are the same as those of previous large-scale networks. It is very straight forward to apply boundary conditions in Therminator3D. I use a set of currents, current resistors and one resistor to create a heat source and apply any node designated to the netlist file as shown in Figure 5.6. This shows the potential of Therminator3D program to demonstrate complicated boundary conditions on large-scale networks. The simulation time for the latter example was 195.3 seconds and the required CPU for iteration became 1.9 seconds.

Table 5.6: Comparison of CPU time required by Therminator3D and ABAQUS on Large Scale network. Cases for Joule heat analysis with temperature-independent electrical and thermal conductivities.

| | Dielectric | No. of Elements | CPU Time(sec) | Iterations |
|------------------------|------------|-----------------------------------|---|------------|
| T3D Fig. 5.27(a) | yes | 1680 + 400 (Vias) (1680 nodes) | 181.19 (179 seconds for symbolic solution, 2 seconds for numerical solution) | 35 |
| ABAQUS Fig. 5.28(a) | | 52263 (45538nodes) | 391.70 | 2 |
| T3D Fig. 5.27(b) | yes | 1680 (1680 nodes) | 181.18 | 35 |
| ABAQUS Fig. 5.28(b) | | 52263 (45538 nodes) | 325.40 | 2 |

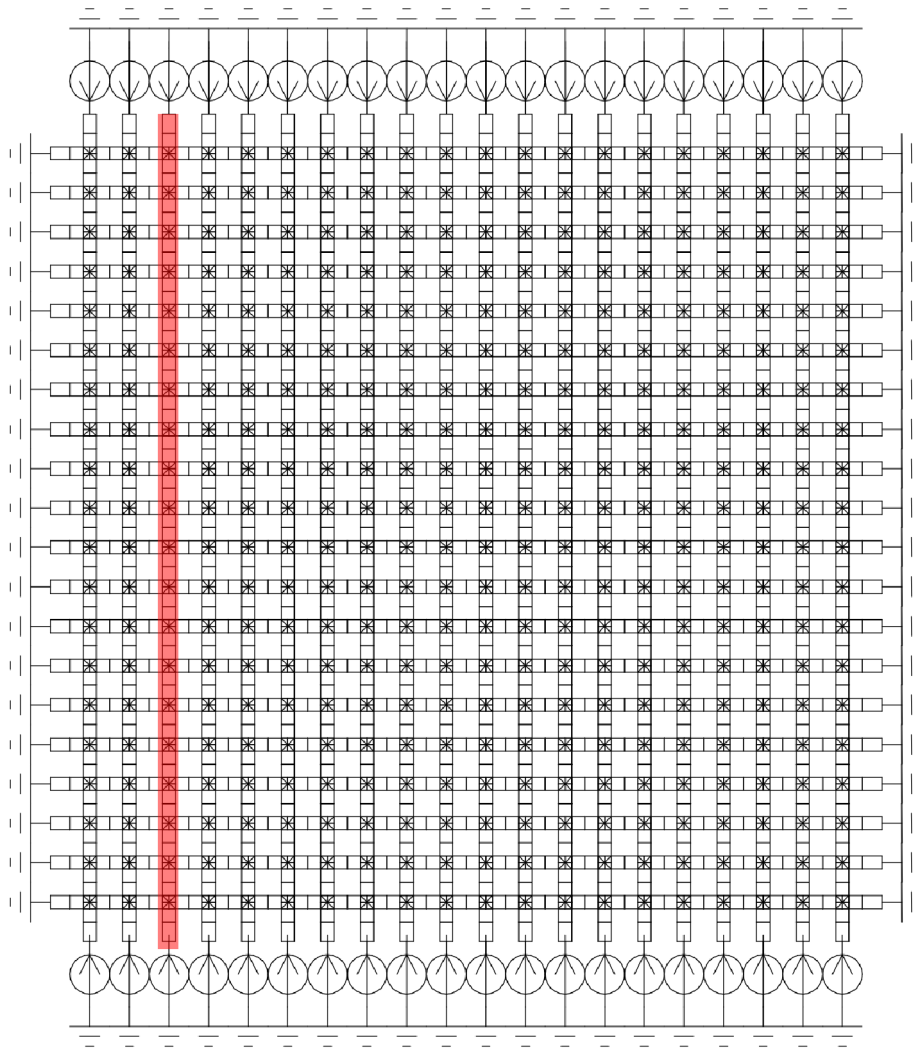


Figure 5.25: The layout of a 20 (columns) by 20 (rows) large scale network with vias (X) with a heated wire (red line). The temperature of substrate is 0°C . The porosity of SiO_2 is considered to be 0 %.

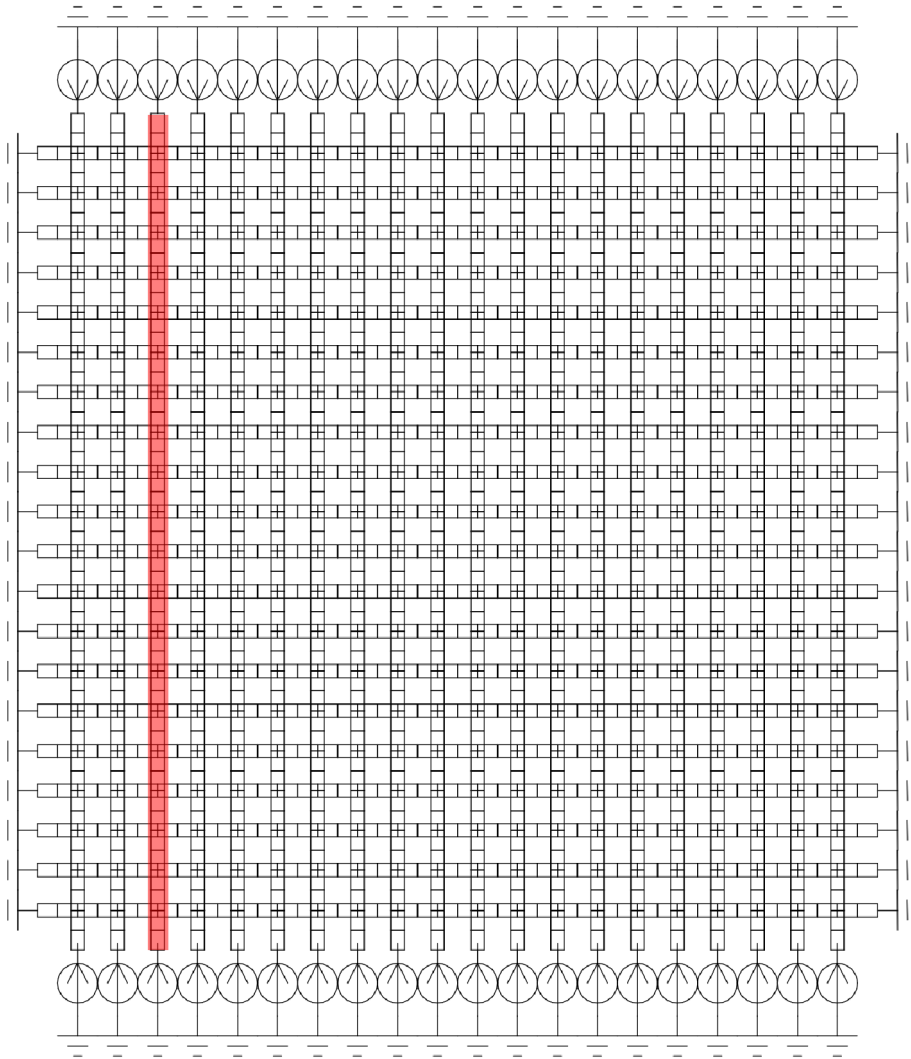


Figure 5.26: The layout of 20 (columns) by 20 (rows) large scale network without vias and with a heated wire. The boundary condition of temperature of 0°C is applied to both ends of all wires and the substrate. The porosity of SiO_2 is considered to be 0 %.

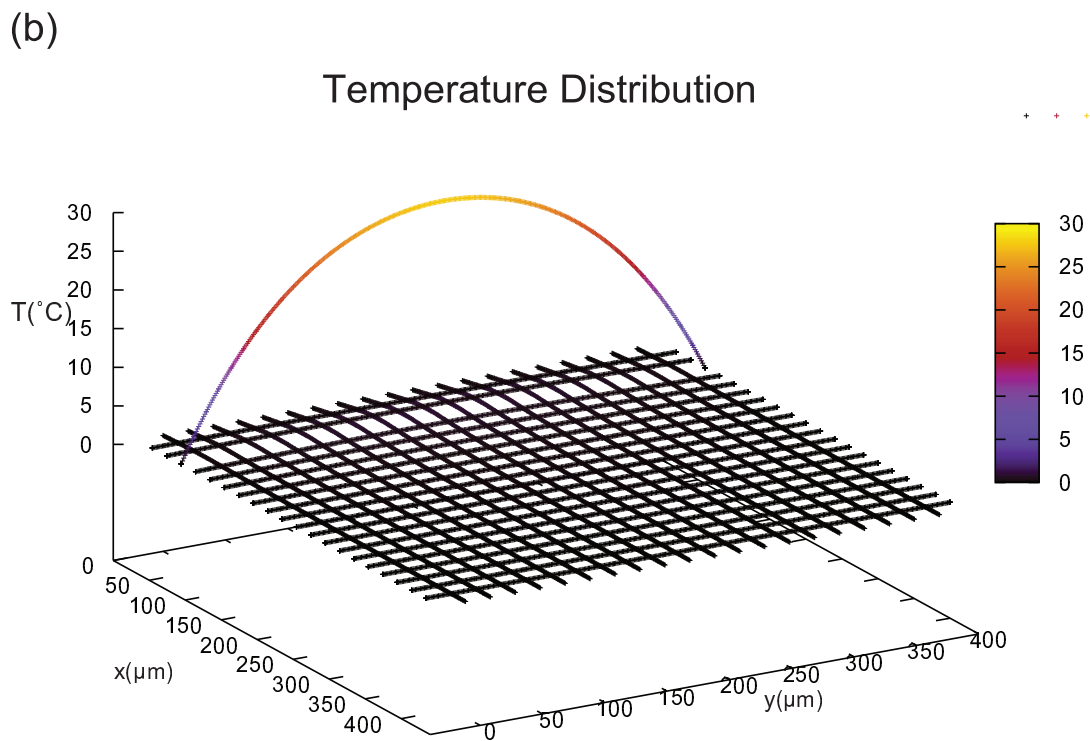
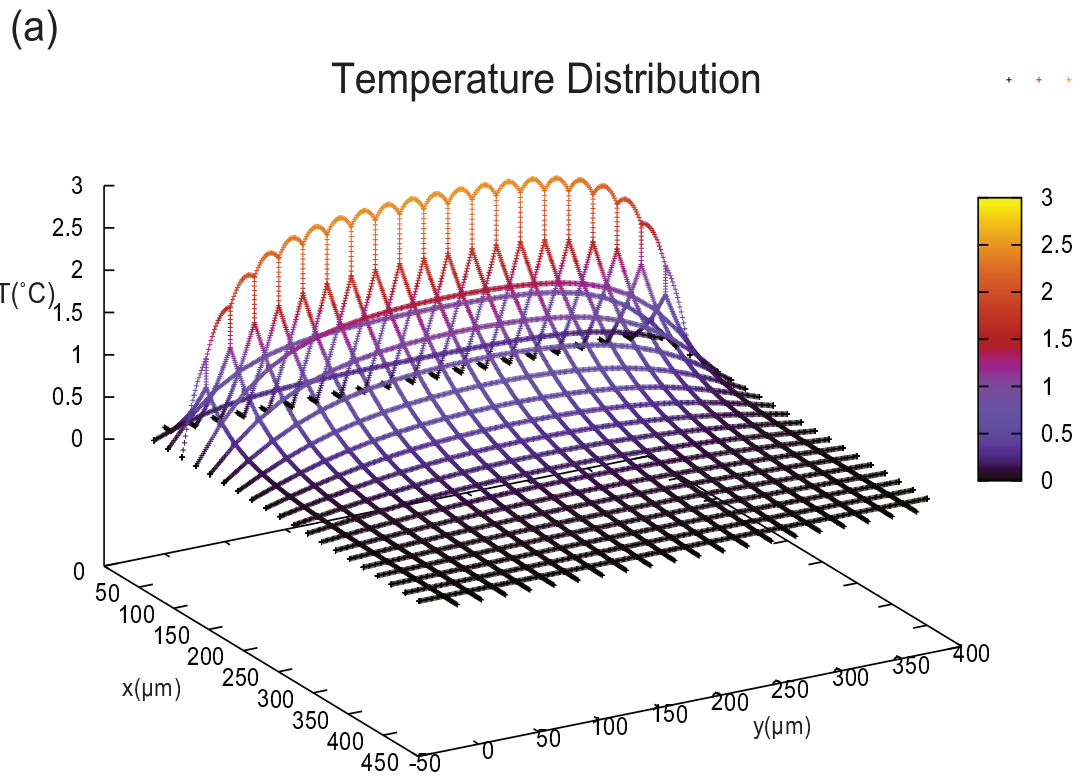
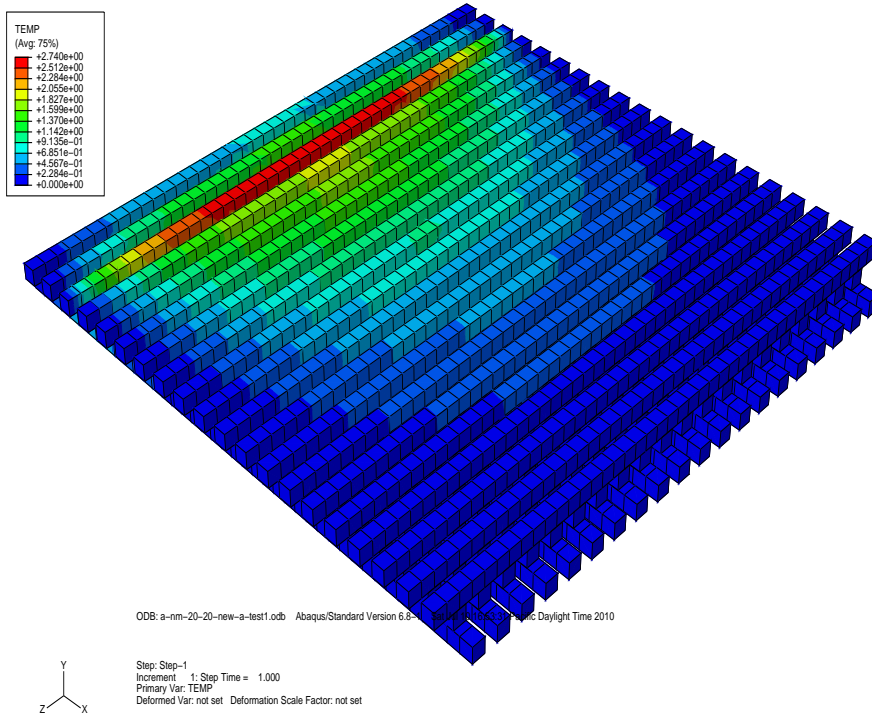


Figure 5.27: The simulation results of Therminator3D for a 20x20 net. (a) Layout as Figure 5.25. (b) Layout as Figure 5.26.

5.5. Large-Scale Network Simulation

(a)



(b)

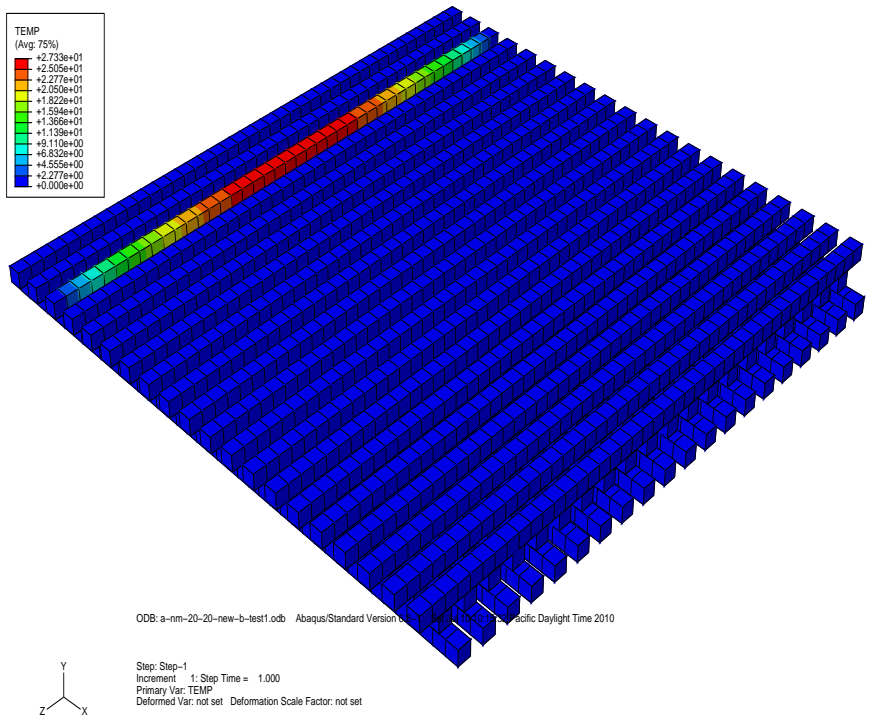


Figure 5.28: The simulation results of ABAQUS for a 20x20 net. (a) Layout as Figure 5.25. (b) Layout as Figure 5.26.

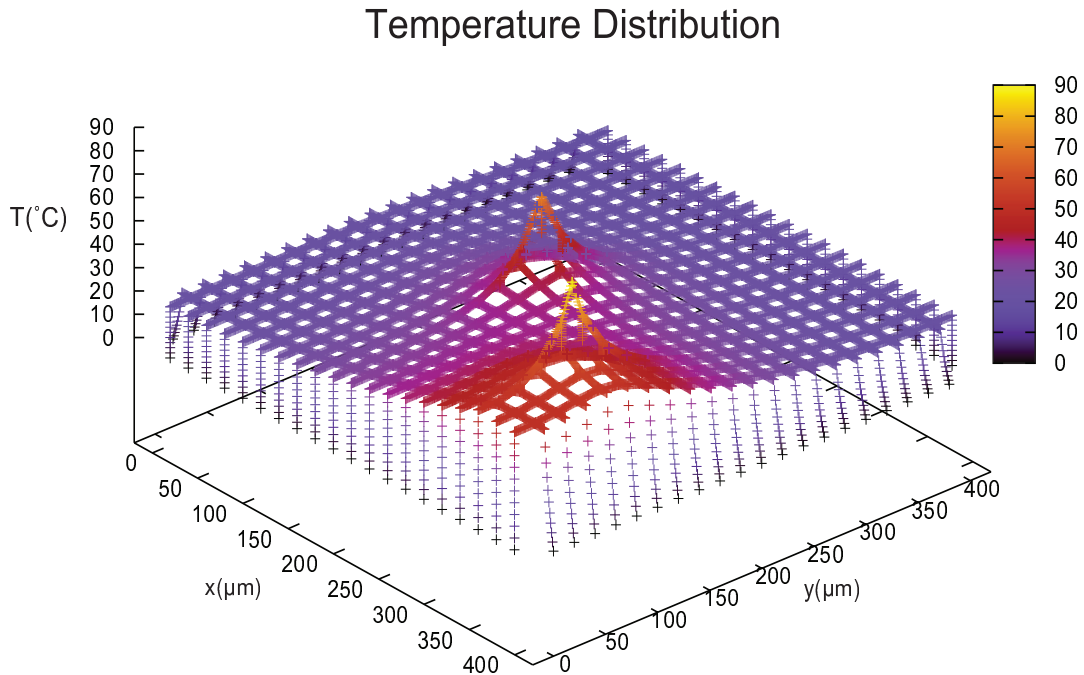


Figure 5.29: The multiple boundary condition simulation results by Therminator3D for a 18x18 net.

5.6 Evaluation of Effective Thermal Conductivity

Therminator3D program is also a tool which could rapidly perform sensitivity analysis on effective thermal conductivities of textile networks. Let us consider a three-factor and three-level design of experiment (DOE) to evaluate the effect of significant factors on the effective thermal conductivity of a typical woven fabric. Figure 5.30 is the cause-effect diagram to indicate these factors. Detailed steps of the conducted DOE are shown in Appendix D.

Similar parametric studies could be used for other mechanical properties of textiles. I could also use Therminator3D to find optimal textile materials on an specific design objective such as maximization of effective thermal conductivity. For maximizing the thermal conductivity of a given textile material, varying the degree of via contacts should be considered as a first attempt, without a need to change the fibre/matrix materials. As a result, different optimum products could be manufactured with minor changes in fabrication process. In fact, in my DOE

study, the vias effect (see Figure C.2 in Appendices D) proved to be the highest among the study variables (width of wires, vias, and porosity of matrix).

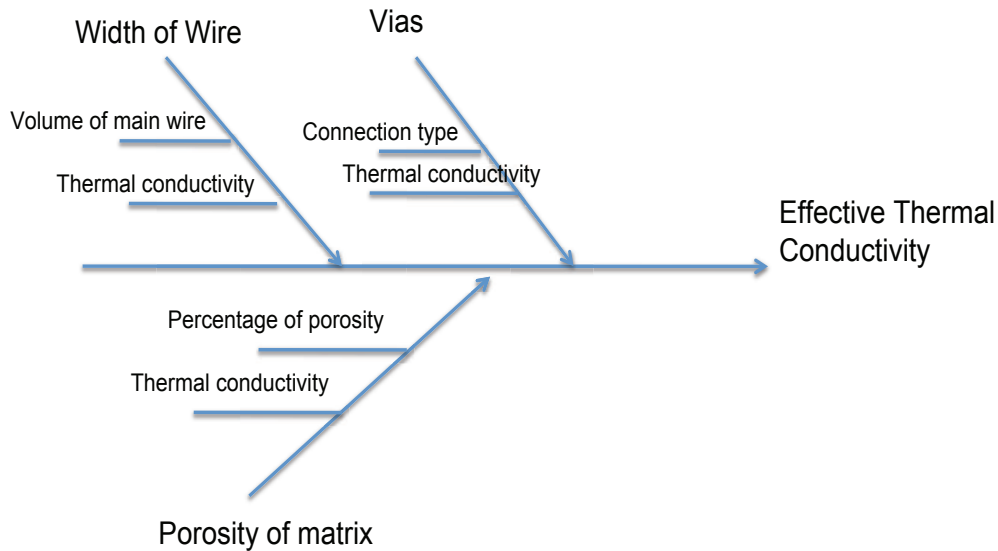


Figure 5.30: Cause-effect diagram used in the DOE study.

5.7 Summary

In summary, the symbolic solution procedure and the incorporation of analytical heat solution over each interconnect segment allows the net-based approach in Therminator3D to efficiently address the equivalent resistance circuits that incorporate the thermal transport of interconnects. From examples performed in this chapter, the speed and accuracy of Therminator3D are very satisfactory. The examples also showed that Therminator3D can solve large scale simulations in a short time and the consumed CPU time is not significantly affected by the iterations required for nonlinear problems. It is also able to deal with several boundary conditions problems. The analytical model and network structure mean Therminator3D uses fewer nodes, and thus less memory than FEA, while offering a competitive accuracy. In FEA, the dielectric material is actually included in the CAD model and meshed, whereas in Therminator3D no additional elements are used for the dielectric (matrix). Future studies are needed to use layout

5.7. Summary

extractors, such as Magic, to extract netlists and more accurate coupling input files, specially for woven networks.

Chapter 6

Conclusions

In this chapter, I summarize the main conclusions of the conducted research and present some future work directions for further development and improvement of the work.

6.1 Summary of Contributions

The new network-based temperature simulation program, Therminator3D, was successfully developed. This program employs a modified RC network which is developed from electromigration reliability verification concept. Performance of the proposed network-based simulation has been verified through several test cases. Therminator3D appeared to be a fast and accurate thermo-electrical simulation tool throughout this thesis. In the case of large network simulations, the memory need was large during symbolic solution procedure because of forming LU matrices by Crout algorithm. However, after the LU matrices are formed, the CPU-time usage of iterations to reach the thermal solution was found to be much less than traditional FEA tool. The main characteristics of Therminator3D can be summarized as follows.

1. Network-based approach in Therminator3D efficiently addresses the equivalent resistance circuits that incorporate the thermal transport of interconnects, and fibre yarns in the case of textiles.
2. Therminator3D can solve large interconnect/textile composite simulations in a short time and the consumed time is not significantly affected by the iterations required for nonlinear problems.

3. The analytical models and network structures mean that Therminator3D uses fewer nodes and thus less memory than FEA. In FEA, the dielectric/matrix material is actually included in the CAD model and meshed, whereas in Therminator3D no additional elements are used for the dielectric/matrix.
4. Therminator3D can be used as a fast and reliable simulation tool in optimal design of IC interconnect/textile networks at micro/meso scales.

There are assumptions applied to the applications of this study:

1. This research only calculated heat conduction behaviour. Heat convection and heat radiation are not considered in this study.
2. This research only simulated steady-state problems.
3. The temperature in each conductor varies only in the lengthwise direction.
4. The property of via represents the degree of contact between column and row. The applications in this research assumed that those contacts are perfectly connected with columns and rows, and without G^{lat} .

6.2 Future Work

The work represented in this thesis was a first step to improve the simulation of large scale network models using Therminator3D. I only illustrated the thermal and electrical problems on IC interconnects and textile materials. However, there is a good potential to develop several other mechanical simulations on material behaviours, such as strain-stress response which is normally obtained by FEA, and multi-physic problems which often require higher computational resources.

To achieve these future goals, there are four phases to follow:

1. Develop more advanced coupling formulas to include layout variables such as the angle of yarn, distance, effective properties, etc. Also consider coupling effects between more wires in complex layouts such as woven fabrics. Since the simple area model is not perfectly working in the woven structures, formulation of the coupling value with different curvilinear shapes should be calibrated by experiments and/or FEA results. The other option to improve the accuracy of coupling data is using a field solver to calculate the coupling data.
2. Modify an open-source layout extractor, such as Magic, to extract netlist input files with detailed thermal coupling data. In this research, netlist and coupling data were the key input information. Using a friendly and precise layout tool will improve accuracy of simulations and avoid unexpected convergence errors.
3. Modify the Therminator3D code to increase its speed even further. Therminator3D demonstrated a fast and accurate temperature estimation on large scale IC interconnects and textile composite networks. However, for the large scale problem, the Crout algorithm in symbolic solution increased the consumption of memory in forming LU matrices dramatically. One can employ a different decomposition algorithm, such as SuiteSparseQR Decomposition [66], to store the information of large scale networks which would decrease the convergence order from $O(N^3)$ to $O(N^{1.7})$.
4. Simulate different mechanical properties in textile composite materials and IC fields. There are very complicated and ultra-large structures which could be considered for mechanical stress analysis coupled with an interaction of the electrical behaviour of wires/-yarns.

Bibliography

- [1] “2007 itrs roadmap for semiconductors,interconnect table intc1, 2, <http://www.itrs.net/links/2007itrs/home2007.htm>,” 2007.
- [2] J. Black, “Electromigration;a brief survey and some recent results,” *Electron Devices, IEEE Transactions on*, vol. 16, no. 4, pp. 338 – 347, Apr 1969.
- [3] S. Sankaran, S. Arai, R. Augur, M. Beck, G. Biery, T. Bolom, G. Bonilla, O. Bravo, K. Chanda, M. Chae, F. Chen, L. Clevenger, S. Cohen, A. Cowley, P. Davis, J. Demarest, J. Doyle, C. Dimitrakopoulos, L. Economikos, D. Edelstein, M. Farooq, R. Filippi, J. Fitzsimmons, N. Fuller, S. M. Gates, S. E. Greco, A. Grill, S. Grunow, R. Hannon, K. Ida, D. Jung, E. Kaltalioglu, M. Kelling, T. Ko, K. Kumar, C. Labelle, H. Landis, M. Lane, W. Landers, M. Lee, W. Li, E. Liniger, X. Liu, J. R. Lloyd, W. Liu, N. Lustig, K. Malone, S. Marokkey, G. Matusiewicz, P. S. McLaughlin, P. V. McLaughlin, S. Mehta, I. Melville, K. Miyata, B. Moon, S. Nitta, D. Nguyen, L. Nicholson, D. Nielsen, P. Ong, K. Patel, V. Patel, W. Park, J. Pellerin, S. Ponoth, K. Petrarca, D. Rath, D. Restaino, S. Rhee, E. Ryan, H. Shoba, A. Simon, E. Simonyi, T. Shaw, T. Spooner, T. Standaert, J. Sucharitaves, C. Tian, H. Wendt, J. Werking, J. Widodo, L. Wiggins, R. Wisnieff, and T. Ivers, “A 45 nm CMOS node Cu/low-k/ ultra low-k PECVD SiCOH (k=2.4) BEOL technology,” in *Electron Devices Meeting, 2006. IEDM '06. International*, 11-13 2006, pp. 1 –4.
- [4] R. Fox, O. Hinsinger, E. Richard, E. Sabouret, T. Berger, C. Goldberg, A. Humbert, G. Imbert, P. Brun, E. Ollier, C. Maurice, M. Guillermet, C. Monget, V. Plantier, H. Bono,

- M. Zaleski, M. Mellier, J. Jacquemin, J. Flake, B. Sharma, L. Broussous, A. Farcy, V. Arnal, R. Gonella, S. Maubert, V. Girault, P. Vannier, D. Reber, A. Schussler, J. Mueller, and W. Besling, “High performance k=2.5 ULK backend solution using an improved TFHM architecture, extendible to the 45nm technology node,” in *Electron Devices Meeting, 2005. IEDM Technical Digest. IEEE International*, 5-5 2005, pp. 81 –84.
- [5] K. A. Dransfield, L. K. Jain, and Y.-W. Mai, “On the effects of stitching in CFRPs—I. mode I delamination toughness,” *Composites Science and Technology*, vol. 58, no. 6, pp. 815 – 827, 1998.
- [6] V. Sukharev, A. Kteyan, E. Zschech, and W. Nix, “Microstructure effect on EM-induced degradations in dual inlaid copper interconnects,” *Device and Materials Reliability, IEEE Transactions on*, vol. 9, no. 1, pp. 87 –97, march 2009.
- [7] W. Huang, M. R. Stan, K. Skadron, K. Sankaranarayanan, S. Ghosh, and S. Velusam, “Compact thermal modeling for temperature-aware design,” in *DAC '04: Proceedings of the 41st annual Design Automation Conference*, New York, NY, USA, 2004, pp. 878–883, ACM.
- [8] P. D. Franzon, W. R. Davis, M. B. Steer, S. Lipa, E. C. Oh, T. Thorolfsson, S. Melamed, S. Luniya, T. Doxsee, S. Berkeley, B. Shani, and K. Obermiller, “Design and CAD for 3D integrated circuits,” in *DAC '08: Proceedings of the 45th annual Design Automation Conference*, New York, NY, USA, 2008, pp. 668–673, ACM.
- [9] S. M. Alam, C. L. Gan, C. V. Thompson, and D. E. Troxel, “Reliability computer-aided design tool for full-chip electromigration analysis and comparison with different interconnect metallizations,” *Microelectronics Journal*, vol. 38, no. 4-5, pp. 463 – 473, 2007, Special Issue of the 6th International Symposium on Quality Electronic Design (ISQED) March 21-23 San Jose, CA.
- [10] S. M. Alam, D. E. Troxel, and C. V. Thompson, “Thermal aware cell-based full-chip

- electromigration reliability analysis,” in *GLSVLSI '05: Proceedings of the 15th ACM Great Lakes symposium on VLSI*, New York, NY, USA, 2005, pp. 26–31, ACM.
- [11] S. M. Alam, D. E. Troxel, and C. V. Thompson, “Layout-specific circuit evaluation in 3-D integrated circuits,” *Analog Integr. Circuits Signal Process.*, vol. 35, no. 2-3, pp. 199–206, 2003.
- [12] D. Walkey, T. Smy, D. Celo, T. MacElwee, and M. Maliepaard, “Compact, netlist-based representation of thermal transient coupling using controlled sources,” *Computer-Aided Design of Integrated Circuits and Systems, IEEE Transactions on*, vol. 23, no. 11, pp. 1593 – 1596, Nov. 2004.
- [13] D. Zweidinger, S.-G. Lee, and R. Fox, “Compact modeling of bjt self-heating in spice,” *Computer-Aided Design of Integrated Circuits and Systems, IEEE Transactions on*, vol. 12, no. 9, pp. 1368 –1375, Sep. 1993.
- [14] C.-S. Yun, P. Malberti, M. Ciappa, and W. Fichtner, “Thermal component model for electrothermal analysis of igbt module systems,” *Advanced Packaging, IEEE Transactions on*, vol. 24, no. 3, pp. 401 –406, Aug 2001.
- [15] V. Székely, A. Poppe, M. Rencz, A. Csendes, and A. Páhi, “Electro-thermal simulation: a realization by simultaneous iteration,” *Microelectronics Journal*, vol. 28, no. 3, pp. 247 – 262, 1997, Thermal Investigations of ICs and Microstructures.
- [16] Y.-L. Shen, “Analysis of Joule heating in multilevel interconnects,” *Journal of Vacuum Science and Technology B: Microelectronics and Nanometer Structures*, vol. 17, no. 5, pp. 2115–2121, 1999.
- [17] A. Labun and K. Jagjitkumar, “Rapid detailed temperature estimation for highly coupled IC interconnect,” *Computer-Aided Design of Integrated Circuits and Systems, IEEE Transactions on*, vol. 27, no. 10, pp. 1840 –1851, Oct. 2008.

- [18] G. A. Bibo, P. J. Hogg, and M. Kemp, “Mechanical characterisation of glass- and carbon-fibre-reinforced composites made with non-crimp fabrics,” *Composites Science and Technology*, vol. 57, no. 9-10, pp. 1221 – 1241, 1997.
- [19] S. Drapier and M. R. Wisnom, “A finite-element investigation of the interlaminar shear behaviour of non-crimp-fabric-based composites,” *Composites Science and Technology*, vol. 59, no. 16, pp. 2351 – 2362, 1999.
- [20] N. Tessitore and A. Riccio, “A novel fem model for biaxial non-crimp fabric composite materials under tension,” *Computers and Structures*, vol. 84, no. 19-20, pp. 1200 – 1207, 2006, Computational Models for Multilayered Structures and Composite Structures.
- [21] D. R. S. Hind and F. Robitaille, “Parametric unit cell modelling of the effective transverse thermal conductivity of carbon plain weave composites,” in *TEXCOMP-8 Int’l Conf. on Textile Composites*, 2006.
- [22] V. F. M. Nordlund, T.S. Lundström and A. Jakovics, “Application of permeability network model to non-crimp fabrics,” in *FPCM-7 International Conference on Flow Processes in Composites Materials*, 2004.
- [23] M. Nordlund, T. Lundstrm, V. Frishfelds, and A. Jakovics, “Permeability network model for non-crimp fabrics,” *Composites Part A: Applied Science and Manufacturing*, vol. 37, no. 6, pp. 826 – 835, 2006, Selected Contributions from the 7th International Conference on Flow Processes in Composite Materials held at University of Delaware, USA.
- [24] Q.-G. Ning and T.-W. Chou, “A closed-form solution of the transverse effective thermal conductivity of woven fabric composites,” *Journal of Composite Materials*, vol. 29, no. 17, pp. 2280–2294, 1995.
- [25] J. Xu and R. Wirtz, “In-plane effective thermal conductivity of plain-weave screen laminates,” *Components and Packaging Technologies, IEEE Transactions on*, vol. 25, no. 4, pp. 615 – 620, Dec. 2002.

- [26] X. Peng, X. Lu, and R. Balendra, “FE simulation of the blanking of electrically heated engineering materials,” *Journal of Materials Processing Technology*, vol. 145, no. 2, pp. 224 – 232, 2004, The Manufacturing Engineering Research Centre.
- [27] D. Tiwari, B. Basu, and K. Biswas, “Simulation of thermal and electric field evolution during spark plasma sintering,” *Ceramics International*, vol. 35, no. 2, pp. 699 – 708, 2009.
- [28] C. T.-W. Ishikawa, T., “Stiffness and strength behaviour of woven fabric composites,” *Journal of Materials Science*, vol. 17, no. 11, pp. 3211–3220, 1982, cited By (since 1996) 195.
- [29] X. Peng and J. Cao, “A continuum mechanics-based non-orthogonal constitutive model for woven composite fabrics,” *Composites Part A: Applied Science and Manufacturing*, vol. 36, no. 6, pp. 859 – 874, 2005.
- [30] L. Li, S. Kim, S. Song, T. Ku, W. Song, J. Kim, M. Chong, J. Park, and B. Kang, “Finite element modeling and simulation for bending analysis of multi-layer printed circuit boards using woven fiber composite,” *Journal of Materials Processing Technology*, vol. 201, no. 1-3, pp. 746 – 750, 2008, 10th International Conference on Advances in Materials and Processing Technologies - AMPT 2007.
- [31] J. Lienhard and J. Lienhard, *A Heat Transfer Textbook - 3rd ed.* Phlogiston Press: Cambridge, Massachusetts, 2008.
- [32] W. D. Callister, Jr., *Materials Science and Engineering: An Introduction, 7th Edition.* Jan. 2006.
- [33] C. Kittel, “Introduction to solid state physics,” 1995.
- [34] J. Clement, S. Riege, R. Cvijetic, and C. Thompson, “Methodology for electromigration

- critical threshold design rule evaluation,” *Computer-Aided Design of Integrated Circuits and Systems, IEEE Transactions on*, vol. 18, no. 5, pp. 576–581, May. 1999.
- [35] J. P. Hwang, “REX—a VLSI parasitic extraction tool for electromigration and signal analysis,” in *DAC '91: Proceedings of the 28th ACM/IEEE Design Automation Conference*, New York, NY, USA, 1991, pp. 717–722, ACM.
- [36] V. Peng, D. R. Donchin, and Y.-T. Yen, “Design methodology and CAD tools for the NVAX microprocessor,” in *ICCD '92: Proceedings of the 1991 IEEE International Conference on Computer Design on VLSI in Computer & Processors*, Washington, DC, USA, 1992, pp. 310–313, IEEE Computer Society.
- [37] C.-C. Teng, Y.-K. Cheng, E. Rosenbaum, and S.-M. Kang, “iTEM: a chip-level electromigration reliability diagnosis tool using electrothermal timing simulation,” in *Reliability Physics Symposium, 1996. 34th Annual Proceedings., IEEE International*, 30 1996, pp. 172–179.
- [38] P. Li, L. Pileggi, M. Asheghi, and R. Chandra, “IC thermal simulation and modeling via efficient multigrid-based approaches,” *Computer-Aided Design of Integrated Circuits and Systems, IEEE Transactions on*, vol. 25, no. 9, pp. 1763–1776, Sep. 2006.
- [39] P. Wilkerson, A. Raman, and M. Turowski, “Fast, automated thermal simulation of three-dimensional integrated circuits,” in *Thermal and Thermomechanical Phenomena in Electronic Systems, 2004. IThERM '04. The Ninth Intersociety Conference on*, 1-4 2004, pp. 706–713 Vol.1.
- [40] Y. Zhan and S. Sapatnekar, “A high efficiency full-chip thermal simulation algorithm,” in *Computer-Aided Design, 2005. ICCAD-2005. IEEE/ACM International Conference on*, 6-10 2005, pp. 635–638.
- [41] T.-Y. Wang and C. C.-P. Chen, “3-D Thermal-ADI: a linear-time chip level transient

- thermal simulator,” *Computer-Aided Design of Integrated Circuits and Systems, IEEE Transactions on*, vol. 21, no. 12, pp. 1434 – 1445, Dec. 2002.
- [42] A. Labun and J. Jensen, “One-dimensional estimation of interconnect temperatures,” in *Integrated Reliability Workshop Final Report, 2002. IEEE International*, 21-24 2002, pp. 155 – 158.
- [43] A. Labun and T. Reeve, “CLIMATE (chip-level intertwined metal and active temperature estimator),” in *Simulation of Semiconductor Processes and Devices, 2003. SISPAD 2003. International Conference on*, 3-5 2003, pp. 23 – 26.
- [44] T.-Y. Chiang and K. Saraswat, “Closed-form analytical thermal model for accurate temperature estimation of multilevel ULSI interconnects,” in *VLSI Circuits, 2003. Digest of Technical Papers. 2003 Symposium on*, 12-14 2003, pp. 275 – 278.
- [45] B.-Y. Tsui, C.-C. Yang, and K.-L. Fang, “Anisotropic thermal conductivity of nanoporous silica film,” *Electron Devices, IEEE Transactions on*, vol. 51, no. 1, pp. 20 – 27, Jan. 2004.
- [46] A. Labun, “Thermally-coupled IC interconnect networks,” in *Mixed-Signals, Sensors, and Systems Test Workshop, 2008. IMS3TW 2008. IEEE 14th International*, 18-20 2008, pp. 1 – 5.
- [47] W. H. Press, S. A. Teukolsky, W. T. Vetterling, and B. P. Flannery, *Numerical Recipes in C: The Art of Scientific Computing. Second Edition*. Cambridge University Press, 1992.
- [48] F. G. Gustavson, W. Liniger, and R. Willoughby, “Symbolic generation of an optimal Crout algorithm for sparse systems of linear equations,” *J. ACM*, vol. 17, no. 1, pp. 87–109, 1970.
- [49] A. Hefner and D. Blackburn, “Thermal component models for electrothermal network simulation,” *Components, Packaging, and Manufacturing Technology, Part A, IEEE Transactions on*, vol. 17, no. 3, pp. 413 – 424, Sep. 1994.

- [50] T. Kojima, Y. Nishibe, Y. Yamada, T. Ueta, K. Torii, S. Sasaki, and K. Hamada, “Novel electro-thermal coupling simulation technique for dynamic analysis of HV (Hybrid Vehicle) inverter,” in *Power Electronics Specialists Conference, 2006. PESC '06. 37th IEEE*, 18-22 2006, pp. 1 –5.
- [51] S. Wunsche, C. Clauss, P. Schwarz, and F. Winkler, “Electro-thermal circuit simulation using simulator coupling,” *Very Large Scale Integration (VLSI) Systems, IEEE Transactions on*, vol. 5, no. 3, pp. 277 –282, Sep. 1997.
- [52] D. R. Donchin, T. C. Fischer, T. F. Fox, V. Peng, R. P. Preston, and W. R. Wheeler, “The NVAX CPU chip: Design challenges, methods, and CAD tools,” 1992.
- [53] J. H. Mathews and K. D. Fink, *Numerical Methods Using MATLAB*. Simon & Schuster, 1998.
- [54] C. C. Dyer and P. S. S. Ip, *An Elementary Introduction to Scientific Computing*. Division of Physical Sciences, University of Toronto at Scarborough, 2000.
- [55] H. Kardestuncer and D. H. Norrie, Eds., *Finite element handbook*. New York, NY, USA: McGraw-Hill, Inc., 1987.
- [56] J. Farooqi and M. Sheikh, “Finite element modelling of thermal transport in ceramic matrix composites,” *Computational Materials Science*, vol. 37, no. 3, pp. 361 – 373, 2006.
- [57] W. J. Drugan and J. R. Willis, “A micromechanics-based nonlocal constitutive equation and estimates of representative volume element size for elastic composites,” *Journal of the Mechanics and Physics of Solids*, vol. 44, no. 4, pp. 497 – 524, 1996.
- [58] C. T. Sun and R. S. Vaidya, “Prediction of composite properties from a representative volume element,” *Composites Science and Technology*, vol. 56, no. 2, pp. 171 – 179, 1996.

- [59] Y. S. Song and J. R. Youn, “Evaluation of effective thermal conductivity for carbon nanotube/polymer composites using control volume finite element method,” *Carbon*, vol. 44, no. 4, pp. 710 – 717, 2006.
- [60] R. J. M. Smit, W. A. M. Brekelmans, and H. E. H. Meijer, “Prediction of the mechanical behavior of nonlinear heterogeneous systems by multi-level finite element modeling,” *Computer Methods in Applied Mechanics and Engineering*, vol. 155, no. 1-2, pp. 181 – 192, 1998.
- [61] K. Hibbitt and S. Inc., *ABAQUS Theory Manual*, Hibbitt, Karlsson and Sorenson Inc., 6.4 ed., 2004.
- [62] B.-J. Wang and S. Hilali, “Electrical-thermal modeling using ABAQUS,” in *1995 ABAQUS Users’ Conference, Paris*, 1995, pp. 771–785.
- [63] A. Z. J. Zhang and J. Groza, “The effect of specimen conductivity on current and temperature distribution in field activated sintering,” in *Proceedings of international conference, Part 4 Modelling, vol. Advances in power metallurgy and particulate materials Metal Power Industries*, 2003, pp. 88–89.
- [64] P. Potluri and V. Thammandra, “Influence of uniaxial and biaxial tension on meso-scale geometry and strain fields in a woven composite,” *Composite Structures*, vol. 77, no. 3, pp. 405 – 418, 2007.
- [65] W. Steinhoegl, G. Schindler, G. Steinlesberger, M. Traving, and M. Engelhardt, “Scaling laws for the resistivity increase of sub-100 nm interconnects,” in *Simulation of Semiconductor Processes and Devices, 2003. SISPAD 2003. International Conference on*, 3-5 2003, pp. 27 – 30.
- [66] T. A. Davis, “Users guide for SuiteSparseQR, a multifrontal multithreaded sparse QR factorization package,” 2008.

- [67] C.-S. Liao, A. Labun, and A. S. Milani, “A rapid method to compute the temperature distribution in non-crimp fabric composites,” in *17th International Conference on Composite Materials*, Edinburgh, UK, 2009.

Appendix A

The Input Parameters of Weave Program

There is a pre-processor program, called “Weave”, that was used instead of layout extraction tools. It created netlist file and coupling file of an interconnect layout for the examples I demonstrated in this thesis. The following technology parameters used in this program are shown as samples:

```
##### Technology parameters#####  
#  
# Vertical distance between rows and substrate in nm  
A=10  
# Row thickness in nm  
B=10  
# Vertical distance between rows and columns in nm  
C=10  
# Column thickness in nm  
D=10  
# zero-porosity isotropic dielectric coefficient of dielectric  
E=3.8  
# electric potential on voltage sources (V) or current on current sources  
# (A), depending on preceding (v) or (i) flag  
F=1  
# bulk thermal conductivity of interconnect W/nm-K  
# True value: G=7.1E-7
```

G=7.1E-7
Number of rows per net
K=2
Number of columns per net
L=2
Number of nets (1 or 2)
M=1
Number of resistors between vias on a row in net 1
N=4
number of resistors between vias on a row in net 2
n=4
% porosity of dielectric ($0 \leq O \leq 100$)
O=0
Number of resistors between vias on a column in net 1
P=4
Number of resistors between vias on a column in net 2
p=4
Temperature coefficient of resistance (%/K)
#Q=0.33
Q=0
bulk electrical resistivity of interconnect Ohm-nm
[From Steinhoegl, et al, 2003, Fig. 6, for T=300K]
R=22
Resistance of vias in ohms
S=2.2
zero-porosity thermal conductivity of dielectric W/nm-K
True value: T=1.4E-9

Appendix A. The Input Parameters of Weave Program

T=1.4E-9

Row pitch in nm (for rows on the same net!)

U=40

Column pitch in nm (for columns on the same net!)

V=40

Row width in nm

W=10

Column width in nm

X=10

Factor for thermal & electrical source resistances (i.e. source resistance = Y * via resistance)

Y=1000

Multiplier for longitudinal thermal resistance on row terminating resistors

Z=1.0E3

Appendix B

Modified Netlist and Coupling Data for Simulations

The netlist and coupling data of different simulation cases can be modified to apply different boundary conditions. Below an example is shown:

Original format of a netlist file: (for a four columns by four rows case)

Resistor node0 nodeL R # $x_{lowerleft}y_{lowerleft}x_{upperright}y_{upperright}LR^{long}$

Current_source node0 nodeL I_{rms}

RES4 36 3.300000 # 135 90 150 90 10.000000 211267.605634

AMP1 0 37 0.000000

RESAMP1 0 37 30000000.000000 # 25 -35 35 -25 0.001 0.0001

.....

RES2-39 2 39 300000000000.000000 # 25 -5 35 5 10.000000 192061.459667

How to apply the boundary conditions on the netlist file:

1. Keep the original values of R^{long} from the weave program, the simulation will keep the “Adiabatic” condition .
2. To set a heat flux condition, I input the value of current I_{rms} into the AMP set.
3. To make the temperature zero degree on one specific point, I simply apply a very small R^{long} (large G^{long}) on that point and connect it to the substrate.

4. To make a specific temperature BC, I use a set of regular resistor, current sources and very large current resistors. The large current resistor is to keep the current in the set (e.g., along a given wire). The format of this set is shown below for a 20-column by 20-row case with a fixed temperature boundary condition applied on node 1228.

```
AMP41 0 1681 1.000000
```

```
RESAMP40 0 1681 3000000000.000000 # 405 405 415 415 10.000000 192061459.667093
```

```
RES1681 1228 1681 2.200000 # 405 415 415 425 10.000000 140845.070423
```

```
AMP42 0 1228 -1.000000
```

```
RESAMP40 0 1228 3000000000.000000 # 415 415 425 425 10.000000 192061459.667093
```

Woven material application :

For woven material applications, I simply change the coupling data with actual location of the woven resistor.

Example of an original coupling data with the interconnects coupled to the ground substrate is shown below (the example is a four-column by four-row case):

(cap resistor {resistor|0(substrate)} c # Glat

```
CAP RES23 0 6750 # 0.000000067581395396
```

```
CAP RES24 0 6750 # 0.000000067581395396
```

```
CAP RES25 0 750 # 0.000000007509043933
```

```
CAP RES26 0 750 # 0.000000007509043933
```

```
CAP RES27 0 750 # 0.000000007509043933
```

```
CAP RES28 0 500 # 0.000000005006029289
```

.....

The modified coupling data for the woven material coupled to the ground and an upper level substrate (RES97 is the upper level substrate) is as follows (the following information is for the woven case in Figure 5.20)

```
CAP RES1 0 646.6666667 # 0.00000000647446455
```

Appendix B. Modified Netlist and Coupling Data for Simulations

CAP RES2 0 2833.333333 # 0.00000002836749930

CAP RES3 0 2833.333333 # 0.00000002836749930

CAP RES4 0 480 # 0.00000000480578812

CAP RES5 0 480 # 0.00000000480578812

.....

CAP RES1 RES97 2833.333333 # 0.00000002836749930

CAP RES2 RES97 646.6666667 # 0.00000000647446455

CAP RES3 RES97 646.6666667 # 0.00000000647446455

CAP RES4 RES97 2833.333333 # 0.00000002836749930

CAP RES5 RES97 2833.333333 # 0.00000002836749930

CAP RES6 RES97 480 # 0.00000000480578812

CAP RES7 RES97 480 # 0.00000000480578812

.....

Appendix C

Using DOE in the Evaluation of Effective Thermal Conductivity of the Fabric with T3D

The effective thermal conductivity of a bar with an uniform cross-section can be assessed by:

$$K_{eff} = \frac{qAx}{\Delta T}$$

K_{eff} is the effective thermal conductivity, q is heat flux, x is the length, and ΔT is the difference of temperature,

Previous studies show that K_{eff} increases as the ratio of yarn width to gap (pitch) spacing increases, and also increases as the yarn or resin materials conductivity increases [67].

In my DOE study using Therminator3D, the model simulated was two-column by two-row model as shown in Figure C.1. All parameters are the same as those shown in Table 5.2. The list of chosen factors and their levels is shown in Table C.1. The ANOVA analysis was performed in Minitab. From the effects plots, shown in Figure C.2 and C.3, I could easily identify the most effective factors by the slopes of the plots. In this study, the present of vias and the width of yarn (represents the inverse of gap between two parallel wires) seem to be key factors to modify the effective thermal conductivity of the fabric (Table C.2 and Figure C.2). The vias factor contributes 95% to the effective thermal conductivity variation while the width of yarn (wire) has 3.95% contribution. The porosity has only 0.00378941% contribution. Figure C.3 shows that there are no interaction effects between the parameters (The interaction between

vias and the yarn width is as low as 0.23%). The ANOVA model has a p-value $< 1.34E-07$. It means that the model has more than 99.9999% confidence.

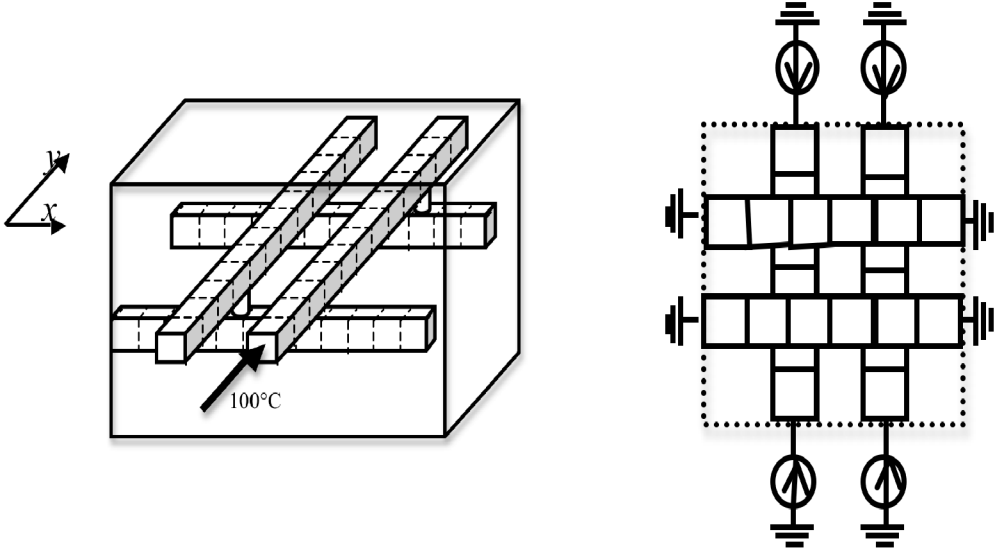


Figure C.1: The layout used in the DOE study.

Table C.1: Study factors and their levels.

| Experiment No. | Porosity | Width | Vias | K_{eff} |
|----------------|----------|-------|------|------------|
| 1 | 0 | 10 | yes | 5.59192439 |
| 2 | 0 | 10 | no | 3.45329090 |
| 3 | 90 | 10 | yes | 5.59163182 |
| 4 | 90 | 10 | no | 3.43795226 |
| 5 | 0 | 15 | yes | 6.15930938 |
| 6 | 0 | 15 | no | 3.81417690 |
| 7 | 90 | 15 | yes | 6.15908276 |
| 8 | 90 | 15 | no | 3.77329034 |

Table C.2: ANOVA results and effect estimates from minitab.

| Parameters | Effect Estimate | | Sum of Squares | Percent Contribution |
|--------------|-----------------|---------|----------------|----------------------|
| Width (A) | 0.457765004 | SSA | 0.419097597 | 3.94576573% |
| Porosity (B) | -0.014186096 | SSB | 0.000402491 | 0.00378941% |
| Vias (C) | 2.255809488 | SSC | 10.17735289 | 95.81885115% |
| AB | -0.006370492 | SSAB | 8.12E-05 | 0.00076417% |
| AC | 0.109652961 | SSAC | 0.024047544 | 0.22640544% |
| BC | 0.013926506 | SSBC | 0.000387895 | 0.00365200% |
| ABC | 0.006403465 | SSABC | 8.20E-05 | 0.00077211% |
| | | Sserror | 4.62E-14 | |
| | | SST | 10.62145159 | |

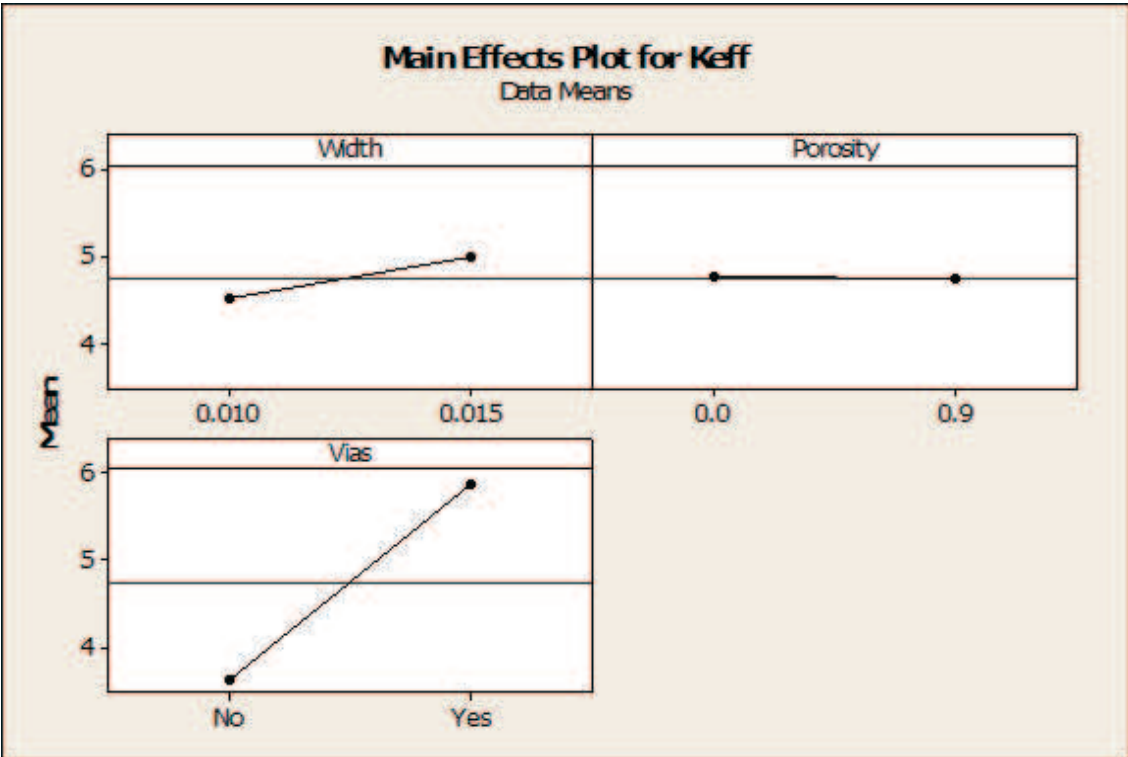


Figure C.2: Main effects plot for K_{eff} .

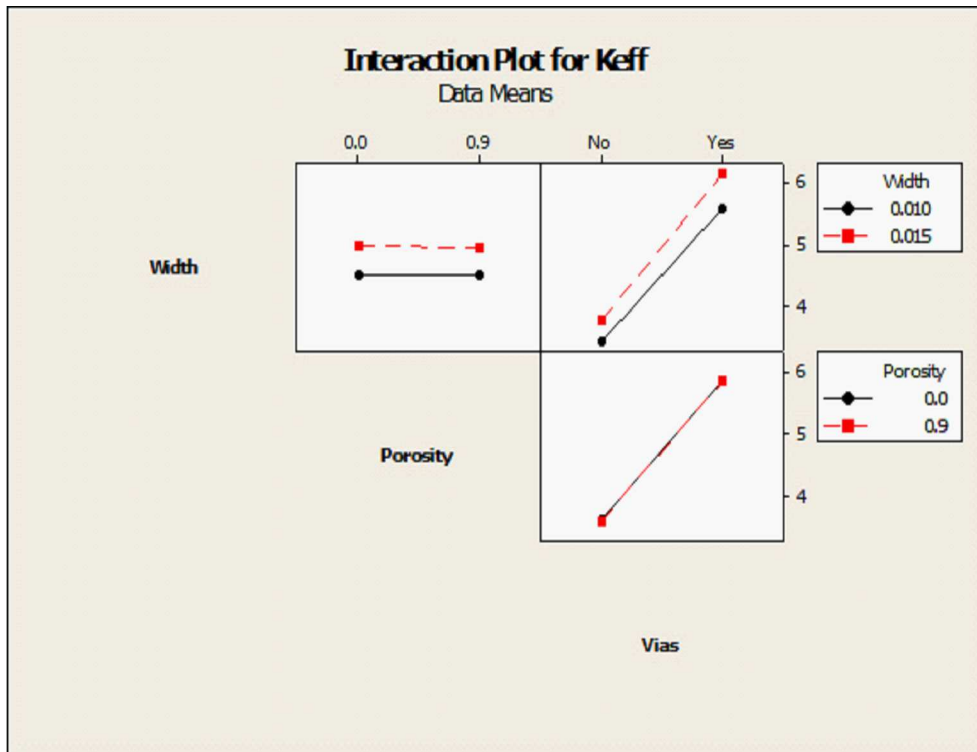


Figure C.3: Interaction effects plot for K_{eff} .